2021

Muscarinic Excitation of Dopamine Neurons in the Ventral Tegmental Area via Activation of a TRPC-like Cation Conductance

Yu Tzu Chen
Virginia Commonwealth University

Muscarinic excitation of dopamine neurons in the ventral tegmental area via activation of a TRPC-like cation conductance

A dissertation submitted in partial fulfillment of the requirements for the degree of Doctor of Philosophy in Neuroscience

By

Rita Yu-Tzu Chen

B.S. in Biology, University of Wisconsin-Madison, 2014

Director: Jose-Miguel Eltit, Ph.D.
Department of Physiology and Biophysics

Co-advisor: A. Rory McQuiston, Ph.D.
Department of Anatomy and Neurobiology

Virginia Commonwealth University
Richmond, Virginia
December 17, 2021

ACKNOWLEDGEMENTS

TABLE OF CONTENTS

LIST OF ABBREVIATIONS

2-AG	2-arachidonoylglycerol
2-APB	2-aminoethoxydiphenylborane
5-HT	5-hydroxytryptamine, serotonin
ACh	acetylcholine
ACSF	artificial cerebrospinal fluid
ADHD	attention-deficit hyperactivity disorder
AHP	afterhyperpolarization
AMPA	α-amino-3-hydroxy-5-methyl-4-isoxazolepropionic acid
AP	action potential
Atro	atropine
BAPTA	1,2-bis(2-aminophenoxy)ethane-N,N,N',N'-tetraacetic acid
Base	baseline
BK	large conductance calcium-activated potassium (channel)
BTP2	3,5-bis(trifluoromethyl)pyrazole, Pyr2, YM-58483
cAMP	cyclic adenosine monophosphate
Carb	carbachol
Cav	voltage-gated calcium (channel)
CIRB	calmodulin/IP$_3$-receptor-binding (domain)
CK2	casein kinase 2
CoV	coefficient of variation
CPA	cyclopiazonic acid
CPP	conditioned place preference
CRF	corticotropin-releasing factor
CaSR	calcium sensing receptor
DA	dopamine
DAG	diacylglycerol
DAT	dopamine transporter
DHPG	(S)-3,5-dihydroxyphenylglycine
DMSO	dimethyl sulfoxide
DTT	dithiothreitol
EPSC	excitatory postsynaptic current
ER	endoplasmic reticulum
ERG	ether-a-go-go-related gene (potassium channel)
FAR	(spike) frequency adaptation ratio

f-I	frequency-current (relationship)
FRET	fluorescence resonance energy transfer
GABA	γ-aminobutyric acid
GIRK	G protein-activated inwardly rectifying potassium (channel)
GPCR	G protein-coupled receptor
HCN	hyperpolarization-activated cyclic nucleotide-gated (channel)
ICSS	intracranial self-stimulation
IP$_3$	inositol 1,4,5-triphosphate
IPSC	inhibitory postsynaptic current
ISI	interspike interval
I-V	current-voltage (relationship)
KO	knockout
Kv	voltage-gated potassium (channel)
LDT	laterodorsal tegmental nucleus
LJP	liquid junction potential
mAChR	muscarinic acetylcholine receptor
mGluR	metabotropic glutamate receptor
mRNA	messenger ribonucleic acid
MSN	medium spiny neuron
MT	medial terminal nucleus of the accessory optic tract
NAc	nucleus accumbens
nAChR	nicotinic acetylcholine receptor
NALCN	sodium leak channel
Nav	voltage-gated sodium (channel)
NHERF	Na$^+$/H$^+$ exchanger regulatory factor
NK3	neurokinin-3 (receptor)
NMDAR	N-methyl-D-aspartate receptor
OAG	1-oleoyl-2-acetyl-sn-glycerol
OCD	obsessive-compulsive disorder
PIP$_2$	phosphatidylinositol 4,5-bisphosphate
PLA$_2$	phospholipase A2
PLC	phospholipase C
PKA	protein kinase A
PKC	protein kinase C
PPT	pedunculopontine tegmental nucleus
QX-314	N-(2,6-dimethylphenylcarbamoylmethyl)triethylammonium chloride
Ri	input resistance
ROCE	receptor-operated calcium entry

SD	standard deviation
SERCA	sarco–endoplasmic reticulum Ca^{2+}-ATPase
SFA	spike frequency adaptation
SFK	Src family kinase
sIPSC	spontaneous inhibitory postsynaptic current
SK	small conductance calcium-activated potassium (channel)
SNc	substantia nigra pars compacta
SNr	substantia nigra pars reticulata
SOCE	store-operated calcium entry
STIM	stromal interaction molecule
TEA	tetraethylammonium
TH	tyrosine hydroxylase
TRP	transient receptor potential (channel)
TTX	tetrodotoxin
$V_{1/2}$	half-activation voltage
VGAT	vesicular GABA transporter
Vm	membrane potential
VTA	ventral tegmental area
WT	wild type

ABSTRACT

Dopaminergic (DA) neurons in the ventral tegmental area (VTA) play a crucial role in reward and motivational behaviors, including the development of drug addictions. VTA DA neurons receive excitatory cholinergic inputs from the mesopontine tegmentum. Blockage of the M5 muscarinic receptor in DA neurons has been shown to attenuate drug-induced DA release and abuse-related behaviors, but the molecular mechanism is unknown. In this study, experiments were designed to identify the electrophysiological effects of muscarinic agonism in the modulation of action potential kinetics and firing patterns in VTA DA neurons of mice. Pharmacology of the muscarinic receptor-evoked current was also characterized. In the presence of tetrodotoxin (TTX), the cholinergic receptor agonist carbachol (Carb) depolarized membrane potential and decreased input resistance, effects that were completely inhibited by the muscarinic receptor antagonist atropine (Atro). This carbachol-induced depolarization caused an increase in spontaneous firing frequency without affecting firing regularity, frequency-current relationship, HCN sag ratio, or the kinetics of action potential shape. In addition, carbachol had no effects on spontaneous inhibitory postsynaptic currents (sIPSCs) in VTA DA neurons. In the voltage-clamp configuration, carbachol induced a non-desensitizing inward current and an increase in current fluctuations that were insensitive to TTX and Cs^+ but sensitive to tetraethylammonium (TEA), Cd^{2+}, and the TRPC channel blocker BTP2. Collectively, the current evidence suggests that activation of HCN channels, inhibition of potassium channels, and changes in inhibitory synaptic inputs do not participate in the muscarinic slow depolarization in VTA DA neurons, but points toward activation of a non-selective cation conductance mediated by TRPC channels.

INTRODUCTION

Cholinergic modulation of the midbrain dopamine system

The midbrain dopamine system: implications for reward and diseases

The survival of an individual or a species is dependent on motivated behaviors such as eating, mating, learning, and avoiding dangers. In mammals, midbrain dopamine (DA) neurons encode reward signals and modulate reinforcing behaviors. Such neural system effectively assigns reward value and orients the organism to beneficial stimuli, but it is also vulnerable to dysregulation in addiction disorders. Indeed, the synaptic levels of DA play a powerful and causative role in reinforcement to food and drugs. On one hand, mice with mutations that cause a hyperdopaminergic state showed higher food and water intake, increased sensitivity to the rewarding effect of cocaine, and enhanced motivation for reward (Pecina *et al.*, 2003; Bello *et al.*, 2011). On the other hand, mice with mutations or lesions that cause DA deficiency were hypoactive, did not eat food or drink water, and died by 4 weeks of age (Zhou & Palmiter, 1995; Palmiter, 2008). When maintained to adulthood with daily DA supplements, these DA-deficient mice were apathetic and failed to show normal social behavior, nesting behavior, and reward association learning (Szczypka *et al.*, 2001; Palmiter, 2008). The hypolocomotion, loss of motivation to feed, and the expression of learned behaviors could all be rescued by restoration of DA signaling (Zhou & Palmiter, 1995; Szczypka *et al.*, 2001; Robinson *et al.*, 2005; Palmiter, 2008). Likewise, lesions of midbrain DA neurons abolished cocaine self-administration, whereas lesions of noradrenergic neurons had no effects (Roberts *et al.*, 1977). Thus, these early studies established DA as the common neural substrate that drives the consumption of natural rewards and addictive drugs as well as permits the expression of

reward learning.

Midbrain DA neurons comprise two major cell populations with different projection targets: the nigrostriatal pathway that projects from the substantia nigra pars compacta (SNc) to the dorsal striatum and the mesolimbic pathway that projects from the ventral tegmental area (VTA) to the nucleus accumbens (NAc) in the ventral striatum (Mogenson *et al.*, 1980; Swanson, 1982). As a part of the motivation circuitry, VTA DA neurons also project to the prefrontal cortex via the mesocortical pathway and to limbic structures such as the amygdala and the hippocampus (Swanson, 1982). Traditionally, the nigrostriatal pathway is associated with voluntary motor control, action selection, and habitual behaviors (Vanderschuren *et al.*, 2005; Kravitz *et al.*, 2010; Howard *et al.*, 2017), while the mesocorticolimbic pathways are believed to be the hotspots for reward and reinforcement learning (Willuhn *et al.*, 2010; Pascoli *et al.*, 2015). Functional segregation among DA pathways was explored by behavioral experiments using dopamine receptor antagonists, which attenuated reward response at doses that did not compromise motor performance. Intracranial self-stimulation (ICSS) of the medial forebrain bundle is an operant procedure to assess the abuse potential of drugs (Negus & Miller, 2014). DA receptor antagonists shifted the ICSS frequency-rate curve in the direction that signifies abuse-limiting effects but did not alter responding rates at maximum frequency as motor-impairing treatments would (Franklin, 1978). Moreover, DA receptor antagonists did not immediately affect conditioned responses to rewarding stimuli, such as food or heroin but, instead, progressively reduced habitual responding over days (Wise & Raptis, 1986; McFarland & Ettenberg, 1995). These results suggest the DA pathways implicated in motor function, motivation for acute reward, and reinforcement of reward are dissociable.

However, the mesolimbic and nigrostriatal pathways in fact overlap in their projection targets and physiological functions, allowing them to complement each other in behavioral outputs

(Wise, 2009). In the DA-deficient mice, selective restoration of DA signaling in the dorsal striatum was sufficient to rescue feeding and locomotion (Szczypka *et al.*, 2001; Sotak *et al.*, 2005). Restoring DA signaling in the NAc did not induce feeding, although it restored exploratory behavior (Szczypka *et al.*, 2001). DA signaling in the NAc also regulates simple locomotor behaviors such as running (Zhu *et al.*, 2016). In the classic "reward prediction error" study, dopamine neurons of both SNc and VTA showed characteristic electrical signals to reward, reward-predicting stimuli, and reward omission; in fact, the responses were indistinguishable, and data from the two regions were pooled (Schultz, 1998). Later studies revealed that a dorsolateral-ventromedial gradient is a better representation of the functional heterogeneity of DA pathways (Burton *et al.*, 2015). The midbrain-striatum projections are arranged topographically: SNc projects to the dorsal striatum, the dorsolateral VTA projects to the lateral shell of the NAc, and the medial VTA projects to the medial shell and core of the NAc and the prefrontal cortex (Baik, 2020). Progressively from the dorsolateral to the ventromedial, there is a shift from more sensorimotor function to value encoding (Burton *et al.*, 2015). It is now accepted that the nigrostriatal and mesolimbic pathways are not distinct systems, although there are differences. The initiation and expression of goal-directed behaviors requires the integration of both DA circuits.

Due to the implication of midbrain DA system in motor function, reward, motivation, attention, and cognition, it is not surprising that DA is involved in many neurological disorders. The critical role of DA in motor control is exemplified by Parkinson's disease, a movement disorder caused be selective degeneration of DA neurons in the SNc (Raza *et al.*, 2019). The motor symptoms such as rigidity and the non-motor symptoms such as depression and cognitive impairments are attributed to the loss of DA signaling in the basal ganglia (Chaudhuri & Schapira, 2009; Raza *et al.*, 2019). DA neurotransmission is involved in all stages of drug addictions: acute reward, habit-forming, withdrawal, and relapse. Despite their diverse

molecular structures and pharmacological mechanisms, drugs of abuse converge on the reward circuitry to increase DA transmission (Nestler, 2005; Willuhn *et al.*, 2010). After repeated exposure to drugs, it is hypothesized that conditioned reinforcement and compulsive drug use involve a switch of control from the "hedonic" NAc to the "habitual" dorsal striatum (Vanderschuren *et al.*, 2005). The negative affective state of drug withdrawal has been partially attributed to decreased activities of the mesolimbic DA system (Koob & Volkow, 2010). Finally, DA neurons respond not just to reward, but also to reward-predicting conditioned stimuli. Increased DA neuron firing and DA release contribute to cue-evoked craving and reinstatement of drug-seeking behavior, causing relapse (Koob & Volkow, 2010; Willuhn *et al.*, 2010). Moreover, some subsets of DA neurons respond to aversive stimuli and mediate conditioned avoidance behavior (Ilango *et al.*, 2012). While the lethargic and negative affective state of major depression may reflect decreased DA transmission, some mesolimbic DA signals promote stress-induced anxiety and depression (Chaudhury *et al.*, 2013; Tye *et al.*, 2013). In addition, aberrant DA transmission is implicated in attention-deficit hyperactivity disorder (ADHD), obsessive-compulsive disorder (OCD), and schizophrenia (Del Campo *et al.*, 2011; Bokor & Anderson, 2014; McCutcheon *et al.*, 2019). Taken the diverse neuromodulatory roles of DA, understanding the physiological regulation of midbrain DA neurons would contribute to developing treatments for a variety of nervous system disorders.

There is great interest in the molecular basis of midbrain DA neuron firing patterns, which tightly control DA release in the striatum. At baseline, DA neurons are pacemakers that exhibit slow and irregular single-spike activity *in vivo* which sustains tonic DA levels in the striatum (Floresco *et al.*, 2003). Upon exposure to reward or reward-predicting stimuli, DA neurons increase excitability and switch from "tonic" firing to a high-frequency, "phasic" burst firing pattern (Schultz, 1998; Willuhn *et al.*, 2010). Both increases in single-spike frequency (Floresco *et al.*, 2003) and burst firing activity (Zweifel *et al.*, 2009) promote striatal DA release;

nevertheless, burst firing is more effective at doing so. In anesthetized rats, electrical stimulation that mimicked burst firing pattern caused a two-fold increase in striatal DA release compared to single-spiking of the same average frequency (Gonon, 1988). In a paradigm that applied trains of pulses, the evoked DA release increased exponentially with the frequency of pulses within each train (Gonon, 1988; Chergui *et al.*, 1994). The drastic increase in extracellular DA levels in the striatum acts as a form of information coding: to signal acute reward as well as trigger long-term neuroplastic changes that underlie reward conditioning (Koob & Volkow, 2010; Willuhn *et al.*, 2010). The firing activity of DA neurons – especially the transition from tonic firing to burst firing pattern – is regulated by excitatory and inhibitory synaptic inputs from various brain regions. Those include glutamatergic afferents from the prefrontal cortex and subthalamic nucleus, and mixed glutamatergic and cholinergic afferents from the mesopontine tegmentum (Kitai *et al.*, 1999; Paladini & Roeper, 2014).

The role of cholinergic inputs in dopamine release and reward behaviors

Acetylcholine (ACh) release from the mesopontine cholinergic nuclei directly regulates the firing activities of midbrain DA neurons. These nuclei are separated into two anatomically distinct cell groups, the pedunculopontine tegmental nucleus (PPT) and the laterodorsal tegmental nucleus (LDT), which provide the sole sources of cholinergic inputs to the midbrain DA system. The two nuclei are topographically organized, with the PPT mostly projects to SNc, whereas the LDT predominantly projects to VTA (Cornwall *et al.*, 1990; Oakman *et al.*, 1995). This innervation pattern suggests that the PPT and the LDT may preferentially modulate motor and reward behaviors, respectively. Both the PPT and the LDT are heterogenous nuclei comprising cholinergic, glutamatergic, and GABAergic neurons. Cholinergic cells make up ~25% and ~22% of the total neuronal populations in the PPT and LDT, respectively (Wang & Morales, 2009; Luquin *et al.*, 2018). Glutamatergic and GABAergic cells are more numerous,

each making up about one-third of the neurons in both nuclei (Wang & Morales, 2009; Luquin *et al.*, 2018). Subpopulations co-expressing cholinergic with glutamatergic or GABAergic markers are also present in both nuclei, but they together are minorities that comprise <10% of the total populations (Wang & Morales, 2009; Luquin *et al.*, 2018). The lack of cells with mixed markers suggests that co-release of ACh with glutamate or GABA from the cholinergic neurons is unlikely, although an electrophysiological study showed that PPT glutamatergic and cholinergic afferents converge on the same DA neuron (Futami *et al.*, 1995). Subpopulations of DA neurons may also be selectively targeted by the mesopontine cholinergic projections. It was found that LDT cholinergic neurons predominantly synapse onto mesoaccumbal DA neurons but scarcely onto mesocortical DA neurons (Omelchenko & Sesack, 2006). There is also recent evidence that LDT cholinergic afferents preferentially activate lateral VTA DA neurons and D1-expressing medium spiny neurons (MSNs) in the NAc core and shell (Coimbra *et al.*, 2021). Thus, a major role of the LDT-VTA-NAc circuitry in reward and motivational behaviors has been proposed.

The direct cholinergic inputs excite midbrain DA neurons via activation of both nicotinic (nAChRs) and muscarinic (mAChRs) receptors. While nAChRs are ligand-gated ion channels that increase cation conductance, the effects of mAChRs on cell excitability depend on the subtype. mAChRs subtypes coupled to the Gq pathway (M1, M3, and M5) are generally excitatory while others coupled to the Gi pathway (M2 and M4) are generally inhibitory. Notably, midbrain DA neurons express primarily the M5 mAChR subtype. In SNc and VTA dopaminergic cell bodies of rats, mRNA for the M5 receptor was the only mAChR subtype detected and was highly co-expressed with the D2 receptor (99% of cells) (Vilaro *et al.*, 1990; Weiner *et al.*, 1990). Pharmacological probes and antibodies against the M5 receptor protein showed comparable results (Reever *et al.*, 1997; Garzon & Pickel, 2013). Among the five mAChR subtypes, M5 has the lowest expression levels and the most restricted pattern

throughout the brain and peripheral tissues (Weiner *et al.*, 1990; Levey, 1993). This unique expression pattern predicts that M5 is a locus for selective modulation of DA neurons involved in abuse-related behaviors, making it an attractive pharmacological target for drug addiction.

Activation of cholinergic receptors on midbrain DA neurons causes DA release in the striatum, and mAChRs generate a larger, more sustained response than nAChRs. In anesthetized rats, electrically stimulated Ach release from the LDT elicited a time-dependent triphasic response as measured by DA levels in the NAc (Forster & Blaha, 2000). Immediately after LDT stimulation, there was an increase of accumbal DA that is dependent on nAChRs and ionotropic glutamatergic receptors, followed by a decrease in DA levels that is dependent on the M2 and M4 autoreceptors on the LDT cholinergic neurons. The third phase was a M5 mAChR-mediated large, slow DA increase that lasted for more than 60 min after stimulation (Forster *et al.*, 2002). This triphasic response shows that the M5 receptor quantitatively mediates most of the cholinergic-stimulated DA release. Another *in vivo* study in mice demonstrated that muscarinic inputs contribute to 60-70% of accumbal DA release after electrical stimulation of the LDT, while nicotinic inputs account for about 40% (Lester *et al.*, 2008; Lester *et al.*, 2010b). Importantly, a related study showed that intra-VTA injection of mAChR antagonists was able to reverse cocaine-induced accumbal DA elevation back to baseline levels (Lester *et al.*, 2010a). In the striatum, M5 mAChRs located on the DA axon terminals also modulate DA release. In agreement with the excitatory action of M5, two studies showed that activation of axonal M5 mAChRs promotes DA release (Zhang *et al.*, 2002; Shin *et al.*, 2015). Another study, however, reported the opposite: a reduction of DA release (Foster *et al.*, 2014). Nonetheless, these studies demonstrated that striatal DA release, especially in the context of psychostimulant-induced elevation, is largely mediated by mAChRs on the DA neurons.

It is well-established that cholinergic activation in the midbrain promotes DA-driven behaviors. As predicted by their anatomical segregation, optogenetic activation of PPT terminals in the SNc selectively increased locomotion, whereas activation of LDT terminals in the VTA selectively increased reward responses (Xiao *et al.*, 2016). Rats self-administrated and showed conditioned place preference (CPP) for direct VTA infusions of the cholinergic agonist carbachol (Ikemoto & Wise, 2002). Lesion of LDT, but not PPT, cholinergic neurons significantly prolonged latencies to initiate cocaine self-administration (Steidl *et al.*, 2014; Steidl *et al.*, 2015). Intra-VTA infusions of cholinergic antagonists also reduced cocaine- and morphine-induced locomotion and reward effects (Rezayof *et al.*, 2007; Steidl & Yeomans, 2009; Solecki *et al.*, 2013). Taken together, these results suggested that activation of cholinergic receptors in the VTA is crucial for the development of addiction-related behaviors. The causal role of VTA cholinergic signaling in drug-induced reward conditioning was demonstrated by *in vivo* microdialysis (You *et al.*, 2008): in cocaine-withdrawn rats, cue-evoked drug-seeking correlated with a robust increase of ACh release in the VTA. Drug-seeking behavior was increased by intra-VTA administration of a cholinesterase inhibitor that increased ACh levels, attenuated by a nicotinic antagonist, and completely blocked by a muscarinic antagonist. Notably, the stronger effects of muscarinic blockage on inhibiting drug seeking correlates with the larger contribution of muscarinic inputs in inducing NAc DA release.

In vivo genetic and pharmacological studies confirmed the importance of M5 signaling in DA-mediated behaviors. M5 receptor knockout (KO) completely abolished the largest, slowest phase of cholinergic-stimulated striatal DA release described above (Forster *et al.*, 2002). In behavioral assays, M5 KO mice exhibited significantly reduced cocaine- and morphine-induced locomotion, CPP, self-administration, and withdrawal (Basile *et al.*, 2002; Fink-Jensen *et al.*, 2003; Thomsen *et al.*, 2005; Steidl & Yeomans, 2009). Systemic administration of ML375, a novel M5-selective negative allosteric modulator, also attenuated self-administration of

cocaine, ethanol, and opioids at doses that did not significantly affect locomotion (Berizzi *et al.*, 2018; Gunter *et al.*, 2018; Gould *et al.*, 2019). Moreover, intra-VTA administration of an ML375 analogue reversed the pro-depressive and anxiogenic effects of cholinergic excess in this brain region (Nunes *et al.*, 2020). In summary, mAChRs expressed on the VTA DA neurons mediate a constellation of behaviors driven by dopaminergic neurotransmission, including locomotion, acute reward, drug-seeking, drug withdrawal, anxiety, and depression. However, while evidence provided by biochemical and behavioral studies is strong, information on how mAChRs modulate DA neuron firing is lacking. The next section discusses the electrophysiological mechanisms downstream of cholinergic signaling in midbrain DA neurons.

Cholinergic signaling and regulation of dopamine neuron firing

mAChRs are G protein-coupled receptors (GPCR) that rely on intracellular signaling transduction and modification of ion channel activity to alter neuronal firing. Therefore, the opening or closing of one or multiple ion channels must underlie the increased excitability mediated by mAChRs in midbrain DA neurons. As previously mentioned, the M5 receptor follows the pattern for the odd-numbered mAChR subtypes – M1, M3, and M5 are coupled to the Gq pathway, which results in activation of phospholipase C-β (PLCβ), phosphatidylinositol 4,5-bisphosphate (PIP$_2$) hydrolysis, increase in diacylglycerol (DAG), Ca^{2+} store release, and activation of protein kinase C (PKC) (Brown, 2018). Lacey *et al.* (1990) were among the first to demonstrate muscarinic actions in midbrain DA neurons were mediated by M1-like receptors. In acute slice preparations, bath perfusion of muscarine induced an TTX- and Cs$^+$-insensitive inward current, which corresponded with depolarization of membrane potential and an increase in pacemaking frequency. These excitatory effects were attenuated by the M1-like mAChR antagonist pirenzepine. Burst firing or depolarization block was not observed with the muscarine treatment. Interestingly, the muscarinic excitation was accompanied by a decrease

in membrane conductance between −50 and −65 mV but an increase in conductance between −40 and −50 mV. In addition, although muscarine reduced the amplitude of afterhyperpolarization (AHP), this effect was reversed by the injection of hyperpolarizing current. Accordingly, Lacey *et al.* suggested that mAChRs in midbrain DA neurons act by decreasing a potassium conductance, but an additional "leak-like" conductance is also involved.

The theory that potassium conductance was involved in muscarinic excitation of midbrain DA neurons was further elaborated by Kitai and colleagues, as deduced from mesopontine afferent modulation of DA neuron firing activities (Kitai *et al.*, 1999). At the time, it was established that activation of NMDA receptors is the major mechanism of burst generation in DA neurons. The conversion of *in vivo* firing patterns to *in vitro* pacemaking was ascribed to deafferentation of excitatory inputs, such as from the PPT. It was also evident that other mechanisms are involved in burst generation. Notably, inhibition of small conductance calcium-activated potassium (SK) channels induces bursting and facilitates NMDA-induced bursting. Along with the results from Lacey *et al.* showing decreased membrane conductance, Kitai and colleagues proposed that mAChRs in DA neurons suppress SK current and act in conjunction with glutamatergic inputs to increase excitation. In support of this hypothesis, an *in vivo* study by Lodge and Grace (2006) showed that the absence of mesopontine inputs resembled the effects of SK channel activation: pharmacological inhibition of the LDT abolished NMDA-induced bursting and caused regularization of tonic firing pattern in VTA DA neurons, suggesting mAChRs may tonically inhibit SK current. However, when other studies identified the critical role of β2-containing nAChRs in burst firing in DA neurons, a new theory emerged that nAChRs are responsible for the cholinergic control of firing mode switch (Maskos, 2008; Faure *et al.*, 2014).

Chen and coworkers provided the first evidence that a specific ion channel mechanism underlies muscarinic excitation of DA neurons. Using acute slice preparations, they showed that carbachol increased the pacemaking frequency in the majority of VTA DA neurons and induced burst firing in 20% of the cells (Zhang *et al.*, 2005). Those actions were due to combined activation of nAChRs and mAChRs. In the presence of TTX, carbachol elicited membrane potential oscillations that had similar time course to carbachol-induced burst cycles. The oscillations were sensitive to Cd^{2+} and nifedipine, implicating L-type Ca^{2+} channels. In subsequent studies, they showed that carbachol caused a modest increase of L-type Ca^{2+} current via PKC activation (Liu & Chen, 2008). In summary, works by the Chen Lab demonstrated that PKC-dependent activation of L-type Ca^{2+} channels is involved in the cholinergic switch of tonic to burst firing in DA neurons. Nonetheless, their results also showed that L-type Ca^{2+} current was not the only conductance modulated by mAChRs, as carbachol still induced a slow depolarization and an increase in pacemaking frequency in the presence of Cd^{2+}, nifedipine, or PKC inhibitors.

A more recent study by Foster et al., (2014) supported the receptor specificity and the involvement of Gq signaling in M5 mAchR-mediated excitation of DA neurons. In their experiments using acute slice preparation, the non-selective mAChR agonist oxotremorine-M induced a TTX-insensitive inward current that coincided with Ca^{2+} store release in SNc DA neurons – effects that were consistent with Gq activation. In spontaneously firing cells, oxotremorine-M caused an increase in pacemaking frequency and a slight broadening of AP width. These effects were potentiated by a M5-selective positive allosteric modulator and were absent in M5 KO mice. Although these results confirmed that the M5 mAChR mediates most, if not all, of the excitatory effects in DA neurons, the ionic mechanisms were not explored. Taken together, the evidence hitherto showed that (1) nAChRs and mAChRs both and independently contribute to cholinergic excitation of midbrain DA neurons, (2) mAChRs

induce membrane potential depolarization and an increase in firing frequency, and (3) mAChRs likely contribute to the tonic-burst firing mode switch. However, the results across studies were nebulous and complex – no consensus has been reached on the precise electrophysiological effects of mAChR activation, and it is likely that more than one ion channel mechanism is involved. This gap in the knowledge calls for a more thorough characterization of the electrical mechanisms underlying muscarinic excitation of midbrain DA neurons. The next section reviews ion channel mechanisms in the regulation of midbrain DA neuron excitability, especially in the context of modulation by Gq signaling.

Ion channel regulation of midbrain dopamine neuron activity

Ionotropic receptors (glutamatergic, GABAergic, and nicotinic receptors)

The *in vitro* pacemaking and *in vivo* bursting of midbrain DA neurons are generated by different sets of ion channels. As previously discussed, DA neurons *in vivo* exhibit two distinct firing patterns: a low-frequency tonic background activity (1-8 Hz) and transient high-frequency bursting (>15 Hz) (Roeper, 2013; Paladini & Roeper, 2014). A common criterion to define bursts is a minimum of three spikes, starting with an interspike interval (ISI) <80 ms and ending with a pause ISI >160 ms (Paladini & Roeper, 2014). The generation of burst firing requires synaptic inputs and can be modulated by multiple neurotransmitter systems. This can be achieved by activation of post-synaptic ionotropic glutamate receptors, GPCR-mediated reductions in AHP, or activation of other cationic channels (Johnson & Wu, 2004; Blythe *et al.*, 2007). In contrast, when synaptic inputs are absent, as in neuronal cultures or acute brain slices, DA neurons are incapable of bursting but retain the intrinsic ion channel mechanisms to maintain a highly regular, low-frequency pacemaking activity (Grace & Onn, 1989; Khaliq & Bean, 2010; Roeper, 2013).

The current "dual control model" states that the ionic conductance in DA neurons *in vivo* exists in a dynamic equilibrium between excitatory (i.e., glutamatergic) and inhibitory (i.e., GABAergic) inputs: bursts can be generated by either increasing NMDA receptor (NMDAR) or decreasing GABA$_A$ receptor (GABA$_A$R) stimulation (Paladini & Roeper, 2014). Accordingly, the application of intra-midbrain NMDA to anesthetized animals results in bursting of DA neurons (Zhang *et al.*, 1994), while NMDAR antagonists or selective KO of NMDAR in DA neurons disrupted bursting (Zweifel *et al.*, 2009). Activation of AMPA/kainate receptors produced similar effects: increased tonic firing frequency and burst firing (Zhang *et al.*, 1994). In this context, the modulation of fast inhibitory inputs via GABA$_A$R is also proposed to be a major mechanism of firing mode switch. These mechanisms allow DA neurons to quickly switch between tonic and burst firing modes in response to behaviorally salient events.

Nicotinic acetylcholine receptors (nAChRs) provide another major source of excitation and firing pattern control of midbrain DA neurons. In general, opening of nAChRs increases excitation by conducting non-selective cationic current (Picciotto *et al.*, 2012). Several characteristics of nAChRs further allow for exquisite spatial and temporal modulation of neuronal behaviors. First, the biophysical properties of nAChRs differ among subunit compositions. Neuronal nAChRs comprise 5 subunits that can be either a heteromeric combination of α and β subunits or homomeric with the α7 subunit (Faure *et al.*, 2014). Midbrain DA neurons are enriched in the α4, α5, α6, β2, and β3 subunits (Klink *et al.*, 2001; Faure *et al.*, 2014). The heteromeric α4β2-containing (a third subunit is possible) nAChRs have high affinity for Ach and play a major role in drug reinforcement, especially nicotine (Faure *et al.*, 2014). The low-affinity, homomeric α7-nAChRs are also present in a minority of VTA DA neurons, while they are rare in SNc DA neurons (Klink *et al.*, 2001; Wooltorton *et al.*, 2003; Faure *et al.*, 2014). In acute brain slices, bath perfusion of nicotine (10 µM) caused a 7.7 mV

depolarization and increased pacemaking frequency of SNc DA neurons (Matsubayashi *et al.*, 2003). In the voltage-clamp configuration holding at −60 mV, bath perfusion of nicotine (10 µM) induced an inward current with the saturation peak amplitude of −28.3 pA (Matsubayashi *et al.*, 2003). Most of the current was inhibited by the $\alpha4\beta2$ subtype-selective antagonist DHβE. Similarly, Ach-induced nAChR currents in VTA DA neurons were greatly reduced in $\alpha4$ KO and completely absent in $\beta2$ KO mice (Klink *et al.*, 2001). Those studies indicated that $\alpha4\beta2$ is the predominant functional subtype in midbrain DA neurons.

Second, nAChRs undergo desensitization with prolonged exposure to agonists; the propensity to desensitize also differs among nAChR subtypes (Faure *et al.*, 2014). After an initial activated, conducting state upon agonist binding, nAChRs change into a desensitized conformational state in which the channels are closed while the agonist is still bound to the nAChRs (Brunzell *et al.*, 2014). Heteromeric nAChRs are the high-affinity, slow-desensitizing subtypes, whereas the homomeric $\alpha7$-nAChRs are the low-affinity, fast-desensitizing (Brunzell *et al.*, 2014). Due to their high affinity to agonists, $\alpha4\beta2$-containing nAChRs are more readily desensitized compared to $\alpha7$-nAChRs when exposed to the same low concentration of agonists. Midbrain DA neurons depolarize and increase firing frequency acutely when exposed to low concentrations of nicotine (80-500 nM) in the brain slice preparation. This response is completely desensitized within a few minutes (Pidoplichko *et al.*, 1997; Wooltorton *et al.*, 2003; Pidoplichko *et al.*, 2004). In contrast, $\alpha7$-nAChRs are more resistant to desensitization by agonists of similar concentrations due to their low affinity (Wooltorton *et al.*, 2003). $\alpha7$-nAChRs are preferentially localized on the glutamatergic terminals that synapse onto DA neurons (Jones & Wonnacott, 2004). While the native nAChRs on DA neurons are desensitized, nAChR agonists can excite DA neurons by enhancing glutamatergic EPSCs (Pidoplichko *et al.*, 2004). Interestingly, the same treatment transiently enhanced but depressed IPSCs in VTA DA neurons after several minutes (Pidoplichko *et al.*, 2004). This suggested nAChRs on GABAergic

neurons that synapse onto DA neurons exhibit a similar time course of desensitization and ultimately contribute to disinhibition of DA neurons. Finally, the effects of nAChR activation depend on its location on the neuron (Picciotto *et al.*, 2012). nAChRs on the dendrites and soma of DA neurons serve as excitatory postsynaptic inputs that regulate firing activity, while nAChRs on the axonal terminals in the striatum regulate DA release (Exley *et al.*, 2008; Exley *et al.*, 2012).

Activation of nAChRs in DA neurons, especially in synergy with other synaptic inputs, is involved in cholinergic induction of burst firing. A direct role of nAChRs in burst generation was shown by Zhang *et al.* (2005): burst firing was induced in a subset of VTA DA neurons in brain slices via activation of $\alpha 4\beta 2$ nAChRs alone. However, because burst firing is usually absent *in vitro*, the majority of studies were done by observing *in vivo* KO phenotypes or administrating nAChR agonists to anesthetized animals. It was established that the $\beta 2$ subunit has the most critical role permitting burst firing. The *in vivo* firing pattern of VTA DA neurons from $\beta 2$ KO mice resembled *in vitro* pacemaking: having reduced firing rates and lacking spontaneous bursting (Mameli-Engvall *et al.*, 2006). Single KO of the α subunits showed no differences in spontaneous activity *in vivo* (Exley *et al.*, 2011; Morel *et al.*, 2014). However, only $\alpha 4$ KO and $\beta 2$ KO abolished nicotine-induced bursting, corroborating $\alpha 4\beta 2$ as the main nAChR mediating drug reinforcement (Mameli-Engvall *et al.*, 2006; Exley *et al.*, 2011). Interestingly, spontaneous bursting and nicotine-induced bursting of DA neurons only occurred when $\beta 2$ was present on both VTA DA and GABA neurons; this highlighted the importance of simultaneous inhibitory inputs (Tolu *et al.*, 2013). Together, these results were crucial to the development of the hypothesis that cholinergic inputs play a permissive role in burst firing. The nicotinic effect appears to be a network mechanism that primes DA neurons for the glutamatergic drives and the GABAergic pauses.

Voltage-gated sodium and calcium channels

Midbrain DA neurons are particularly susceptible to depolarization block, which restricts their maximum tonic firing frequency. Upon moderate excitation, there is a gradual shortening of AP amplitude, broadening of AP width, increase in AP threshold, and decrease in AHP amplitude that eventually leads to failure of AP generation (Richards *et al.*, 1997; Tucker *et al.*, 2012). Voltage-gated sodium (Nav) channels are involved in both AP initiation and depolarization block. The alterations in AP shape associated with decreased Nav channel availability can be induced by either a +250 pA current injection or addition of NMDAR conductance using dynamic clamp (Tucker *et al.*, 2012). Mechanistically, depolarization block results from accumulative inactivation of Nav channels. Treatment with a low concentration of tetrodotoxin (TTX, 10 nM), which causes partial inhibition of Nav channels, recapitulated the alterations in AP shape and increased susceptibility to depolarization block (Tucker *et al.*, 2012). Conversely, addition of somatic Nav channel conductance via dynamic clamp reversed the alternations in AP shape and prevented depolarization block (Tucker *et al.*, 2012). Moreover, somatic Nav channel conductance contributes to the slow depolarization during ISI and is linearly proportional to pacemaking frequency (Tucker *et al.*, 2012). *In situ* hybridization (Gonzalez-Cabrera *et al.*, 2017) and immunohistochemical studies (Yang *et al.*, 2019) showed that midbrain DA neurons predominantly express the Nav1.2 subunit. Compared to the more abundant Nav1.6 in the adult brain, Nav1.2 activates at more depolarized potentials and inactivates faster; these properties may explain the high AP threshold and susceptibility to depolarization block in DA neurons. Therefore, even though the AP is initiated in the axonal initial segment, somatic Nav channels, likely Nav1.2, control the balance between pacemaking frequency and depolarization block in midbrain DA neurons.

The mechanism of pacemaking generation in SNc DA neurons depends largely on the activity

of voltage-gated calcium (Cav) channels. Midbrain DA neurons express the Cav1.2 and Cav1.3 subtypes of L-type calcium channels; in both SNc and VTA Cav1.3 is expressed at higher levels (Takada *et al.*, 2001; Rajadhyaksha *et al.*, 2004; Chan *et al.*, 2007). Compared to Cav1.2, Cav1.3 has a lower activation threshold ($V_{1/2}$ = −40.4 mV) (Lipscombe *et al.*, 2004). Current flowing through Cav1.3 channels is activated at subthreshold voltages during the ISI and helps drive membrane potential to the spike threshold (Puopolo *et al.*, 2007; Putzier *et al.*, 2009). In the presence of TTX, this subthreshold calcium current produces slow membrane potential oscillations that can reach 15 mV in SNc DA neurons (Kang & Kitai, 1993; Zhang *et al.*, 2005; Chan *et al.*, 2007). The slow oscillations occur at membrane potentials between −50 and −38 mV and can be eliminated by the non-selective calcium channel blocker Cd^{2+} (100-400 μM) or dihydropyridine blockers (Kang & Kitai, 1993; Zhang *et al.*, 2005). In comparison, VTA DA neurons show very small (<5 mV) or no Ca^{2+}-mediated membrane potential oscillations in TTX and rely on additional mechanisms to drive pacemaking (Chan *et al.*, 2007; Khaliq & Bean, 2010). It is noteworthy that the repolarization and hyperpolarization phase of the oscillations requires a TEA- and apamin-sensitive Ca^{2+}-activated potassium conductance, indicating SK channel activities (Kang & Kitai, 1993; Ping & Shepard, 1996). Therefore, the activities of Cav channels and SK channels are definitely linked to attain pacemaking and regulate firing patterns in these neurons (Johnson & Wu, 2004).

Activation of Cav channels is also involved in burst generation in midbrain DA neurons. Studies showed that L-type calcium channel activators induced burst firing of VTA DA neurons in brain slices (Johnson & Wu, 2004; Zhang *et al.*, 2005; Liu *et al.*, 2014). The burst firing consists of a rhythmic cycle of two or more spikes with high frequency followed by a post-burst hyperpolarization; the average frequency of burst cycles was around 0.06-0.12 Hz (8-17 seconds per cycle) (Liu *et al.*, 2014). Dynamic clamp experiments showed that adding a virtual Cav1.3 conductance did not produce burst firing on its own, but it increased the frequency of

burst firing induced by a virtual NMDA receptor conductance. Like the generation of pacemaking, the amplification of bursting frequency required the specific voltage dependence ($V_{1/2}$) of Cav1.3 rather than the Ca^{2+} entry (Putzier *et al.*, 2009). SNc and VTA DA neurons also highly express the Cav3.1 isoform of T-type calcium channels (Poetschke *et al.*, 2015; Tracy *et al.*, 2018). T-type Cav channels have a low activation threshold ($V_{1/2}$ = −59.6 mV) and inactivate at depolarized potentials, making them ideally situated to regulate firing pattern (Tracy *et al.*, 2018). In subsets of SNc and VTA DA neurons, a period of hyperpolarization could relieve inactivation of Cav3.1 channels and produce rebound burst firing (Evans *et al.*, 2017; Tracy *et al.*, 2018). These rebound-ready DA neurons also showed higher tonic firing frequency and larger HCN voltage sag, suggesting an interplay between T-type Cav channels and HCN channels to promote excitation (Evans *et al.*, 2017). Together, the subthreshold calcium current through both L-type and T-type Cav channels enables membrane potential oscillations, which underlie the rhythmic pacemaking activity as well as rebound burst firing in midbrain DA neurons.

HCN channels

Hyperpolarization-activated cyclic nucleotide-gated (HCN) channels are voltage-gated non-selective cation channels that provide a depolarizing current in response to membrane hyperpolarization (Chu & Zhen, 2010). Midbrain DA neurons exhibit very prominent HCN currents and HCN-mediated "voltage sag", with the average amplitudes larger in the SNc compared to the VTA (Masi *et al.*, 2015; Krashia *et al.*, 2017). This unusually large HCN activation is an important feature to identify DA neurons. Virtually all SNc DA neurons and 98% of TH-positive VTA DA neurons exhibit HCN activity (Wanat *et al.*, 2008; Chu & Zhen, 2010; Roeper, 2013), except a subpopulation of DA neurons in the ventromedial VTA that lack HCN channel expression (Roeper, 2013; Masi *et al.*, 2015). On the contrary, GABAergic interneurons

of the VTA in mice exhibit very little or no HCN activity (Chieng *et al.*, 2011). The HCN channel is a major regulator of membrane potential in DA neurons. The 4 HCN subunits vary considerable in their gating kinetics and cAMP sensitivity (Chu & Zhen, 2010). Midbrain DA neurons express the HCN2, HCN3, and HCN4 subunits, which are highly sensitive to cAMP and have a slow activation time constant ranging from 0.5 to 5 s at −120 to −80 mV (Franz *et al.*, 2000). The slow activation kinetics suggest that HCN channels would remain active and depolarize the average membrane potential in pacemaking cells. Indeed, pharmacological blockage of HCN channels in SNc DA neurons resulted in a strong hyperpolarization of 11.8 mV and cessation of firing (Gambardella *et al.*, 2012). When the membrane potential change was compensated by current injection, pacemaking activity was recovered (Gambardella *et al.*, 2012). This suggested that HCN channels do not participate in the generation of pacemaking in DA neurons. HCN channels also regulate the shape of AHP (Neuhoff *et al.*, 2002; Okamoto *et al.*, 2006; Wanat *et al.*, 2008). After a single AP or a burst, DA neurons exhibit a prolonged AHP that often exceeds −70 mV. The hyperpolarization activates HCN channels, which drive the membrane potential back to the AP threshold. Therefore, enhancement of HCN activity will reduce the amplitude and duration of AHP, speed up pacemaking frequency, decrease rebound latency and, thus, increase the overall excitability of DA neurons.

HCN channels are directly gated by cAMP and are sensitive to many intracellular factors such as PIP_2 and protein kinases downstream of GPCRs (Chu & Zhen, 2010). It is predicted that Gs-coupled GPCRs would enhance HCN currents by stimulating adenylyl cyclase activity and cAMP production, while Gi-coupled GPCRs would have the opposite effect via inhibition of adenylyl cyclase and the reduction of cAMP levels. In addition, HCN channels are inhibited by PKC activation downstream of Gq signaling. Serotonin and dopamine inhibit HCN channels and decrease excitability in DA neurons via activation of $5-HT_2$ (Gq-coupled) and D_2 (Gi-coupled) receptors, respectively (Liu *et al.*, 2003; Gambardella *et al.*, 2012). However,

regulation of HCN by PKC is complex, perhaps due to different PKC isoforms. The neuropeptide corticotropin-releasing factor (CRF) enhanced HCN currents and increased the pacemaking frequency of VTA DA neurons via a PLC/PKC-dependent mechanism (Wanat *et al.*, 2008). Activation of the Gq-coupled α1-adrenoceptor also resulted in increased HCN currents and pacemaking frequency of DA neurons (Gambardella *et al.*, 2012; Goertz *et al.*, 2015). The signaling mechanisms responsible for this norepinephrine-induced effect are unknown. In summary, many neurotransmitters activate signaling pathways that have HCN channels as effectors, resulting in the modulation of DA neuron electrical activity.

Calcium-activated potassium channels (SK and BK channels)

One feature of midbrain DA neurons is a large and prolonged AHP. Following each action potential, the AHP on average has an amplitude of −22.1 mV, hyperpolarizes to −63.6 mV, and takes 330 ms to return to resting levels (Shepard & Bunney, 1991; Richards *et al.*, 1997; Wanat *et al.*, 2008). The AHP has a fast and a medium/slow component. In midbrain DA neurons, the medium/slow phase of AHP – the most hyperpolarized point – is mediated by the SK channel (Shepard & Bunney, 1991; Ping & Shepard, 1996). SK channels in central neurons are coded by the SK1-3 (KCa2.1-KCa2.3) genes (Stocker, 2004; Faber & Sah, 2007). Midbrain DA neurons express SK2 and SK3, with SK3 being the predominant subunit (Wolfart *et al.*, 2001; Deignan *et al.*, 2012). Although structurally similar to the voltage-gated potassium channels, SK channels are voltage-insensitive due to the loss of positive charges on the S4 voltage sensor domain (Stocker, 2004). Instead, SK channels are gated only by intracellular Ca^{2+} that enter the cells through Cav channels upon depolarization. The opening of SK mediates potassium conductance that hyperpolarizes the membrane to below baseline potentials, both allowing the recovery of other voltage-gated channels from inactivation and maintaining the rhythm of the pacemaking activity. SK channels are highly sensitive to Ca^{2+} with a K_d of 300 to 700 nM

(Stocker, 2004). The high affinity of Ca^{2+} allows SK channels to be regulated by a variety of Ca^{2+} sources, including Cav channels, NMDAR, nAChR, and GPCR-mediated store release (Faber & Sah, 2007). Among the Cav channel subtypes, SK activities in midbrain DA neurons are tightly coupled to T-type and N-type, while L-type channels are thought to play a much lesser role (Wolfart & Roeper, 2002; de Vrind *et al.*, 2016; Estep *et al.*, 2016).

Because the AHP determines the timing of the next AP, the SK channel is a potent regulator of both AP shape and firing pattern in midbrain DA neurons. Notably, inhibition of SK activity is involved in the generation of *in vivo* burst firing and *in vitro* electrical changes associated with burst firing. Negative modulation of SK in anesthetized animals increased firing rates and converted regular spiking to bursting, while activation of SK decreased both firing rates and burst firing (Herrik *et al.*, 2010). Correspondingly, the selective SK channel blocker apamin (100-300 nM) increased the pacemaking frequency and decreased firing regularity of DA neurons in brain slices, as quantified by both a decrease in the average ISI and an increase of the CoV of the ISI from 0.05 to 0.30 (Wolfart *et al.*, 2001; Deignan *et al.*, 2012). A detailed analysis using genetic KO mice revealed differential regulation by the subunits: SK2 regularizes firing pattern, while SK3 decreases firing frequency (Deignan *et al.*, 2012). In a current step protocol, apamin significantly reduced the kinetics of AHP, increased the slope of frequency-current (f-I) relationship, and increased the spike frequency adaptation (SFA) ratio (Shepard & Bunney, 1991; Vandecasteele *et al.*, 2011). Both AHP kinetics (amplitude and duration) and the AHP current were negatively correlated with the SFA ratio (Vandecasteele *et al.*, 2011). These results confirmed that SK activities regularize firing pattern and make the neurons less adapting by mediating a larger AHP. Therefore, inhibition of SK channels will produce the opposite effects, increasing adaptation and shifting the firing to a burst-like pattern.

In midbrain DA neurons, GPCRs are known to modulate SK channel activities. Transient

activation of group I mGluRs and mAChRs causes opening of SK channels through Gq-mediated Ca^{2+} store release (Fiorillo & Williams, 1998, 2000; Kramer & Williams, 2016). With sustained activation, the SK-mediated hyperpolarization is replaced by a more commonly reported depolarizing response (Fiorillo & Williams, 1998, 2000); this biphasic response may be a common effect of Gq signaling in DA neurons. Besides activation by Ca^{2+}, SK channels are PIP$_2$-sensitive and possess multiple phosphorylation sites, which allow modulation by protein kinases. Activation of the α1-adrenoceptor increased tonic firing frequency and burst firing of midbrain DA neurons partly due to inhibition of SK channels (Goertz *et al.*, 2015). In the hippocampal CA1 pyramidal neurons, the M1 mAChR inhibits SK channels via a PKC-(Buchanan *et al.*, 2010) or casein kinase 2 (CK2)-dependent mechanism (Giessel & Sabatini, 2010). However, knowledge on Gq-mediated protein kinase regulation of SK channels in DA neurons is lacking. It is unknown whether the Gq-coupled α1-adrenoceptor signals through the same mechanisms. On the other hand, activation of the Gi-coupled GABA$_B$ receptors was shown to suppress SK currents in SNc DA neurons via inhibition of adenylyl cyclase and PKA (Estep *et al.*, 2016). The interesting implication of this study is that transient GABAergic inputs can increase DA neuron excitability: co-activation of GABA$_A$ and GABA$_B$ receptors, the latter inhibit SK channels, could promote a pause-burst pattern of firing.

The fast phase of AHP, which corresponds to AP repolarization, is mediated by large conductance Ca^{2+}-activated potassium (BK) channels and some voltage-gated potassium channels (Maylie *et al.*, 2004; Faber & Sah, 2007). BK channels are encoded by a single gene, KCa1.1. Unlike the voltage-insensitive SK channels, BK channels open in response to depolarization and an increase in intracellular Ca^{2+}, which acts allosterically to shift the activation voltage (Su *et al.*, 2010; Vandael *et al.*, 2010). In pacemaker cells, BK channels are often coupled to L-type Cav1.3 channels and effectively control the fast AP repolarization and firing frequency (Vandael *et al.*, 2010). In SNc DA neurons, BK channels account for 38% of the

depolarization-induced potassium current (Kimm *et al.*, 2015). Pharmacological blockage of BK channels increased pacemaking frequency and widened AP, but had no effects on the slope of f-I relationship and paradoxically deepened the AHP (Kimm *et al.*, 2015). It was proposed that this paradoxical increase in AHP arose from recruitment of the slower-activating Kv2 channels when the fast BK-mediated repolarization was absent. Due to its Ca^{2+} sensitivity, BK channels can theoretically be modulated by Gq-coupled GPCRs. For example, α1-adrenoceptors decreased GABAergic inputs to VTA DA neurons via PKC-dependent activation of BK channels (Velasquez-Martinez *et al.*, 2015). However, no studies have demonstrated GPCR modulation of BK channels in midbrain DA neurons.

Kv7 (KCNQ) channels

Kv7 (KCNQ) channels are voltage-gated potassium channels that are regulated by GPCRs. Muscarinic inhibition of the Kv7 channels was the first discovered GPCR-mediated regulation of ion channels and was termed the "M-current" (Delmas & Brown, 2005). Activation of Gq-coupled mAChRs depletes membrane PIP_2, a necessary co-factor, and thus closes the channels (Delmas & Brown, 2005). PKC, a downstream effector of Gq signaling, also directly phosphorylates and inhibits Kv7 channels (Delmas & Brown, 2005). The result is a decrease in potassium conductance that reduces outward current and depolarizes membrane potential. The M1, M3, and M5 mAChRs inhibit Kv7 current with equal efficacy in a heterologous expression system (Guo & Schofield, 2003). In addition to mAChRs, other GPCRs including 5-HT_2, P2Y, substance P, mGluR, and opioid receptors also inhibit Kv7 channels (Greene & Hoshi, 2017). However, despite the prominent expression and functional consequences of Kv7 activity, there are no studies describing a GPCR-mediated modulation of Kv7 channels in midbrain DA neurons. Several unique biophysical properties of Kv7 channels make them potent regulators of neuronal excitability; Kv7 channels have a very negative activation

threshold around −60 mV, do not inactivate, and exhibit slow activation and deactivation kinetics (Selyanko *et al.*, 2000). These properties suggest that Kv7 channels maintain a low level of activity when the neuron is quiescent or firing tonically. Upon excitation, a train of burst firing will strongly activate the Kv7 channels as a negative feedback mechanism to hyperpolarize the neuron. Furthermore, Kv7 channels mediate the medium/slow phase of AHP (Stocker, 2004; Koyama & Appel, 2006; Mateos-Aparicio *et al.*, 2014; Greene & Hoshi, 2017). The presence of Kv7 currents also rises AP threshold and decreases input resistance (Mateos-Aparicio *et al.*, 2014). Conversely, inhibition of Kv7 channels may excite the neuron by depolarizing membrane potential, shortening the AHP, promoting burst firing, and enhancing excitatory synaptic integration.

The Kv7 channel is an important regulator of firing pattern in midbrain DA neurons. Out of the five Kv7 subunits, VTA DA neurons mainly express Kv7.4 (KCNQ4) – a rare subunit whose expression is restricted to the midbrain and the auditory pathway – with minor expression of Kv7.2, 7.3, and 7.5 (Hansen *et al.*, 2006; Li *et al.*, 2017). In contrast, SNc DA neurons mainly express Kv7.2 and 7.3, with minority subpopulations expressing 7.4 and 7.5 (Li *et al.*, 2017). Conflicting effects of Kv7 channel blockage on DA neuron excitability have been reported. One study showed that inhibition of Kv7 channels increased pacemaking frequency and promoted *in vivo* burst firing (Sotty *et al.*, 2009), while another reported no effects on *in vivo* firing pattern or *in vitro* recordings of membrane potential (Drion *et al.*, 2010). Similarly, one study showed that pharmacological blockage of Kv7 channels reduced the fast and slow component of AHP without changes in AP amplitude, duration, and threshold (Koyama & Appel, 2006), while another reported no effects on AP shape with the same treatment (Hansen *et al.*, 2006). The gating properties of Kv7 may provide an explanation for the inconsistent effects of channel blockage. The Kv7.4 homomeric channels and the Kv7.2/7.3 heteromeric channels both have a rather depolarized $V_{1/2}$ of around −18 mV (Selyanko *et al.*, 2000) and slow gating kinetics.

Therefore, the Kv7 channels may not be substantially activated during the pacemaking activity of DA neurons. Indeed, the excitatory effect of Kv7 inhibition became more apparent during high-frequency firing induced by depolarizing current injection or SK channel inhibition, when a larger population of Kv7 channels would be open (Hansen *et al.*, 2006; Drion *et al.*, 2010). This suggests that Kv7 inhibition will work synergistically with other excitatory inputs to promote excitation in DA neurons.

Other voltage-gated potassium channels

Midbrain DA neurons (on the somatodendritic compartments) express voltage-gated potassium channels including Kv4.3, which constitutes the "A-type" channels, Kv1.3, Kv2.1, Kv3.2, Kv3.3, which constitute the delayed rectifiers (Dufour *et al.*, 2014), and Kv11, the ether-a-go-go-related gene (ERG) potassium channels (Ji *et al.*, 2012). In general, inhibition of Kv channels decreases potassium conductance and increases intrinsic excitability. Kv2 channels account for 36% of the depolarization-induced potassium current in SNc DA neurons (Kimm *et al.*, 2015). Pharmacological inhibition of Kv2 channels caused an increase in pacemaking frequency in brain slices, a widening of AP, and a reduction of AHP (Kimm *et al.*, 2015). When fast firing was evoked by a depolarizing current step, Kv2 inhibition significantly increased the slope of f-I relationship and the propensity to enter depolarization block (Kimm *et al.*, 2015). Blockage of ERG Kv channels also increased spontaneous pacemaking frequency, f-I relationship, and the propensity to enter depolarization block of midbrain DA neurons in brain slices, but it had no effects on SFA and AHP (Ji *et al.*, 2012). Therefore, the general actions of Kv channels are to oppose the inward currents during spiking and slow pacemaking frequency.

The spontaneous firing of midbrain DA neurons is limited to low frequencies partially due to the prominent A-type current, which exerts a powerful control on intrinsic excitability. Those

potassium channels are named after their sensitivity to 4-aminopyridine (4-AP) but are resistant to TEA (Liss *et al.*, 2001; Khaliq & Bean, 2008; Xue *et al.*, 2020). The fast-inactivating A-type current is the dominant depolarization-induced potassium current in midbrain DA neurons (Liss *et al.*, 2001). Having a low activation threshold, A-type channels activate and inactivate at subthreshold voltages, providing a large outward current that significantly prolongs the ISI and delays spiking (Khaliq & Bean, 2008). In midbrain DA neurons, the main mediator of A-type potassium current is Kv4.3. The levels of Kv4.3 expression and A-type current density are inversely correlated with the pacemaking frequency of SNc DA neurons and are sufficient to explain the variation in spontaneous firing rates among DA neurons (Liss *et al.*, 2001). A recent study demonstrated endocannabinoid-mediated inhibition of A-type current, linking Gq signaling to modulation of DA neuron excitability (Gantz & Bean, 2017). Upon activation of Gq-coupled GPCRs, the endocannabinoid 2-arachidonoylglycerol (2-AG) is generated from its precursor DAG via diacylglycerol lipase activity (Katona & Freund, 2012). Activation of mGluRs, neurotensin, and orexin receptors effectively inhibited A-type current in SNc DA neurons via 2-AG generation. This resulted in an increase in pacemaking frequency and the slope of f-I relationship independent of cannabinoid receptors, suggesting a direct effect of 2-AG on the ion channels. Alternatively, Gq signaling may also inhibit A-type current in DA neurons via activation of PLC/PKCδ, as in the case of GHS-R1a, a G protein-coupled receptor of the hormone ghrelin (Xue *et al.*, 2020). There is very limited information of Gq-mediated inhibition of Kv channels other than Kv7 and A-type channels, though inhibition by Ca^{2+}-calmodulin or PIP_2 depletion were proposed mechanisms (Brown, 2018).

GIRK channels

G protein-activated inwardly rectifying potassium channels (GIRK, also known as Kir3) belong to a family of seven G protein-gated, PIP_2-sensitive potassium channels (Luscher & Slesinger,

2010). The outward current through GIRK channels is enough to strongly hyperpolarize the neurons and decreases excitability (Luscher & Slesinger, 2010). SNc DA neurons express the GIRK2a and GIRK2c isoforms which form homomeric channels (Inanobe et al., 1999), whereas VTA DA neurons express GIRK2c and GIRK3 (Cruz et al., 2004). GIRK channels are activated by stimulation of Gi/o-coupled GPCRs, whose G$\beta\gamma$ subunit directly gates the channel by strengthening the interaction between the channel and PIP$_2$ (Luscher & Slesinger, 2010). The most studied Gi-coupled GPCRs in midbrain DA neurons are the GABA$_B$ receptor and the D2 receptor; the latter acts as an autoreceptor (Ford, 2014). In addition to axonal release, DA neurons mediate Ca^{2+}-dependent release of DA from the somatodendritic compartment (Beckstead et al., 2004; Rice & Patel, 2015). The somatodendritic release of DA activates D2 receptors on the neuron itself and on neighboring neurons, hyperpolarizing the DA neurons and causing a cessation of activity (Beckstead et al., 2004; Dragicevic et al., 2014; Philippart & Khaliq, 2018). The extracellular level of DA in the midbrain, as well as the basal activity of GIRK channels, contribute to regulation of membrane potential and firing rates of DA neurons (Luscher & Slesinger, 2010; Ford, 2014). While GIRK conductance is the major component of D2 autoreceptor-mediated outward current (Beckstead et al., 2004), D2 autoreceptors also decrease excitability by modulating Kv1 (Fulton et al., 2011), HCN (Gambardella et al., 2012), and NALCN (Philippart & Khaliq, 2018).

In contrast to Gi/o-mediated activation of GIRK channels, Gq signaling was proposed to be a universal inhibitor of GIRK channels in midbrain DA neurons as well as other cell types. Early studies using heterologous expression systems implicated the Gα subunit, PLC, intracellular Ca^{2+}, and PKC in Gq-mediated inhibition of GIRK current, although the results were conflicting across studies (Hill & Peralta, 2001; Lei et al., 2001; Mao et al., 2004). So far, the mechanisms responsible for Gq-mediated inhibition of GIRK channels in midbrain DA neurons are equally puzzling. Substance P suppressed GABA$_B$-mediated outward current through activation of the

neurokinin-3 (NK3) receptor, which is Gq-coupled; this effect was shown to be dependent on PLC, intracellular Ca^{2+}, and PKC (Xia *et al.*, 2010). Intriguingly, a newer study demonstrated that intracellular Ca^{2+} can directly and transiently inhibit D2- and $GABA_B$-mediated GIRK current on a 1-second time scale. While the rise in free Ca^{2+} could be induced by either activation of group I mGluRs or direct store release, the inhibition of GIRK was not dependent on PLC, PKC, PLA_2, or calmodulin (Kramer & Williams, 2016). Finally, inhibition of GIRK by Gq-coupled mAChRs has been observed in other systems (Hill & Peralta, 2001), but it is unknown whether this pathway occurs in midbrain DA neurons.

Sodium leak channel (NALCN)

As pacemaker cells, midbrain DA neurons have a considerably more depolarized membrane potential compared to neurons that are quiescent at rest. When the pacemaker activity is silenced by TTX treatment, a "resting membrane potential" around −56 mV is revealed (Khaliq & Bean, 2010). Such value is much more depolarized than the equilibrium potential of potassium (E_K ~−90 mV), suggesting the existence of other resting conductances that are TTX-resistant. A "leak" non-selective cationic channel, the sodium leak channel (NALCN), was found to be crucial in pacemaking activity including that of midbrain DA neurons (Ren, 2011). NALCN is structurally related to the Nav and Cav channels but is believed to be voltage-insensitive and non-inactivating (Ren, 2011). However, a recent study using heterologous expression systems revealed voltage-dependent gating and selectivity for monovalent over divalent cations (Chua *et al.*, 2020). Inhibition of leak sodium current in VTA DA neurons resulted in an average hyperpolarization of 11 mV (Khaliq & Bean, 2010). This implied that NALCN provides a persistent Na^+ current in VTA DA neurons that brings the membrane potential close to AP threshold, permitting pacemaking. In contrast, NALCN currents are smaller in SNc DA neurons, whose pacemaking is driven mainly by subthreshold Ca^{2+}

oscillations. In addition to being TTX-resistant, NALCN is insensitive to Cs^+ (permeable), TEA (10 mM, impermeable), and Cav channel blockers such as nifedipine (Philippart & Khaliq, 2018; Chua *et al.*, 2020; Kschonsak *et al.*, 2020).

Besides being a background conductance, NALCN activity is modulated by GPCRs. NALCN forms a channel complex with UNC79, UNC80, and FAM155A, which are auxiliary subunits necessary for its functional expression (Lu *et al.*, 2009; Chua *et al.*, 2020; Kschonsak *et al.*, 2020). UNC80 is required for GPCR regulation of NALCN by acting as a scaffold protein for Src family kinases (SFKs) (Ren, 2011). Two neuropeptides – neurotensin and substance P – increased DA neuron excitability by evoking a slow NALCN-mediated cation current (Lu *et al.*, 2009). Although both are coupled to Gq-related pathways, the neurotensin receptor 1/2 and the substance P receptor activate NALCN via an SFK-dependent, G protein-independent pathway (Lu *et al.*, 2009). Conversely, NALCN is inhibited by 2 mM of extracellular Ca^{2+} and Gi-coupled GPCRs in SNc DA neurons (Philippart & Khaliq, 2018). It has been suggested that the action of Ca^{2+} is exerted through activation of the calcium sensing receptor (CaSR), a Gq-coupled GPCR that inhibits NALCN (Ren, 2011). The CaSR-NALCN coupling allows direct transduction of extracellular Ca^{2+} concentrations to neuronal excitability, though whether this is the mechanism in DA neurons has not been tested. The Gi-coupled D_2 autoreceptors and $GABA_B$ receptors inhibited NALCN and decreased pacemaking frequency via a G protein-dependent mechanism (Philippart & Khaliq, 2018). This Gi-mediated pathway provides another mechanism, in addition to activation of GIRK channels, how D2 and $GABA_B$ receptors potently suppress DA neuron activity. These studies demonstrated NALCN as an important regulator of DA neuron excitability in both spontaneous activity and integration of synaptic inputs.

TRPC channels as effectors of GPCR signaling

Biophysical properties of TRPC channels

Transient receptor potential (TRP) channels were discovered and named in 1975 after a *Drosophila* mutant whose retinal photoreceptor cells only exhibited transient depolarization to bright light instead of the sustained response in the wild type (WT) (Minke, 2010). Based on sequence homology, 28 mammalian TRP channels were subsequently cloned and grouped into 6 subfamilies: TRPC (canonical), TRPV (vanilloid), TRPM (melastatin), TRPA (ankyrin), TRPML (mucolipin), and TRPP (polycystin) (Nilius & Owsianik, 2011; Zheng, 2013). TRP channels are nested within the voltage-gated ion channel superfamily and possess many properties reminiscent of voltage-gated potassium channels (Yu & Catterall, 2004). TRP subunits assemble into either homo- or heterotetrameric channels (Zheng, 2013; Cao, 2020). Each subunit has 6 transmembrane α-helices (Yu & Catterall, 2004; Nilius & Owsianik, 2011; Chen *et al.*, 2020), with the S1-S4 helices forming the voltage sensor-like domain (VSLD) (Cao, 2020). In general, the voltage sensitivity of TRP channels is very low, making them unresponsive to voltage in the physiological range (Yu & Catterall, 2004; Zheng, 2013). The lack of voltage sensitivity is attributed to the loss of positively charged residues on the S4 helix (Yu & Catterall, 2004; Zheng, 2013; Cao, 2020). The S5 and S6 helices form the pore domain, which contains the ion conduction pathway and the selectivity filter (Zheng, 2013; Cao, 2020). Perplexingly, the selectivity filters of most TRP channels lack conserved sequence or structural characteristics that explain their ion selectivity (Cao, 2020). The cytosolic N- and C-termini form large intracellular domains which serve as interaction sites for many factors and proteins that regulate their expression and function (Nilius & Owsianik, 2011; Cao, 2020).

The TRPC subfamily contains 7 members that can be separated into four subgroups based on

their sequence and functional similarity: TRPC1, TRPC2, TRPC4/5, and TRPC3/6/7 (Clapham *et al.*, 2001; Chen *et al.*, 2020). TRPC2 is a pseudogene in humans and is mostly restricted to the vomeronasal organ and sperm cells in rodents (Clapham *et al.*, 2001; Nilius & Owsianik, 2011). TRPC3/6/7 are highly similar, sharing ~75% of sequence identities (Clapham *et al.*, 2001). TRPC4 and TRPC1 are 65% and 45% identical to TRPC5, respectively (Zholos, 2014). When forming heteromeric channels, TRPC subunits appear to preferentially assemble with members of the same subgroup. Systemic studies using rat brain synaptosomes and various heterologous expression systems found that TRPC2 does not interact with any other TRPC subunit; TRPC1/4/5 co-assemble, and TRPC3/6/7 co-assemble, but cross-interactions between the two subgroups do not occur (Goel *et al.*, 2002; Hofmann *et al.*, 2002). The results were corroborated by functional experiments showing that a dominant-negative TRPC6 subunit suppressed TRPC3- and TRPC6-mediated current but not TRPC4- or TRPC5-mediated current in HEK293 cells (Hofmann *et al.*, 2002). The preferential intra-subgroup assembly is not a hard-set rule, however. TRPC1 has been shown to form heteromeric channels with TRPC3 and TRPC7 in heterologous expression systems, astrocytes, and human salivary gland epithelial cells (Lintschinger *et al.*, 2000; Liu *et al.*, 2005; Zagranichnaya *et al.*, 2005; Belkacemi *et al.*, 2017). Inter-subgroup heteromers of three different subunits (i.e., containing TRPC1, TRPC4/5, and TRPC3/6/7) may exist in heterologous expression systems and embryonic brains but not adult brains (Strubing *et al.*, 2003; Storch *et al.*, 2012). The assembly of TRPC4/5 with TRPC3/6 requires the presence of TRPC1 (Strubing *et al.*, 2003). Associations of TRPC3 with TRPC4 in vascular endothelial cells (Poteser *et al.*, 2006) and TRPC4 with TRPC6 in HEK293 cells (Yuan *et al.*, 2007) were also reported. Therefore, the subunit composition of TRPC channels varies widely across systems, though there appears to be preferential association between members of the same subgroup.

Understanding the electrophysiological properties of TRP channels is difficult and complex.

Besides their non-selective ionic conductance, the permeabilities and I-V relationships of TRPC channels can be vary incredibly with different systems and subunit compositions. Nonetheless, some patterns can still be found. TRPC channels conduct a non-selective cation current. The permeability ratios of Na^+, K^+, and Cs^+ of most TRP channels including TRPC are approximately 1:1:1 (Inoue *et al.*, 2001; McKemy *et al.*, 2002; Feng, 2017). TRPC channels are also highly permeable to divalent ions including Ca^{2+}. The Ca^{2+}/Na^+ permeability ratios (P_{Ca}/P_{Na}) range from moderately Ca^{2+}-biased (~10:1) to no selectivity (1:1) (Feng, 2017). Despite the relatively high P_{Ca}/P_{Na}, Ca^{2+} current is very small compared to monovalent cationic current, even in solutions where Ca^{2+} is the only permeant cation (Strubing *et al.*, 2001; Estacion *et al.*, 2006). Due to their non-selective nature, TRPC channels typically have a reversal potential around 0 mV with physiological ion concentrations (Freichel *et al.*, 2014; Feng, 2017). Though considered to be mostly voltage-insensitive, TRPC channels do exhibit variable rectifications in their I-V relationships. In general, TRPC1, TRPC3 and TRPC7 channels show roughly linear I-V relationships (Zitt *et al.*, 1996; Lintschinger *et al.*, 2000; Liu *et al.*, 2005; Poteser *et al.*, 2006; Sun *et al.*, 2017), TRPC4, TRPC5, and TRPC6 channels exhibit the distinct "N-shaped" doubly rectifying I-V relationships (Schaefer *et al.*, 2000; Jung *et al.*, 2003; Obukhov & Nowycky, 2005; Storch *et al.*, 2012; Kim *et al.*, 2014), whereas it is common for heteromeric channels to be outwardly rectifying (Strubing *et al.*, 2001, 2003; Storch *et al.*, 2012; Kim *et al.*, 2014).

Mechanisms of TRPC channel activation by Gq signaling

Activation of TRPC channels by Gq-coupled GPCRs is well-documented in both neuronal and non-neuronal cells. The literature consensus is that all TRPC subunits are activated downstream of PLC and are intricately involved in Ca^{2+} signaling (Clapham *et al.*, 2001; Chen *et al.*, 2020; Wang *et al.*, 2020). However, just like the biophysical properties of TRPC channels, elucidating the precise mechanisms of activation has been a complex and difficult subject. To

understand the historical classification of TRPC subtypes based on mechanisms of activation, a brief discussion of the experimental methods for measuring TRP channel activity is unavoidable. One major mechanism, termed store-operated calcium entry (SOCE), refers to the Ca^{2+} influx upon ER store depletion. The classic protocol for measuring SOCE consists of pretreating cells with a SERCA inhibitor such as thapsigargin or cyclopiazonic acid (CPA) in the absence of extracellular Ca^{2+} in order to deplete the ER store (Bird *et al.*, 2008). Upon re-addition of extracellular Ca^{2+}, non-selective cation entry through TRPC channels can be quantified by fluorescence Ca^{2+} imaging or patch-clamp technique (Schaefer *et al.*, 2000; He *et al.*, 2005; Bird *et al.*, 2008). Since SOCE can occur without stimulating plasma membrane receptors, receptor-operated calcium entry (ROCE) is the counterpart mechanism that relies on G protein signaling. The most commonly used agonist to evoke Gq signaling is carbachol which targets the muscarinic receptors. Agonists of the histamine H1 receptor (i.e., histamine) and P2Y receptors (i.e., ATP) are also used (Schaefer *et al.*, 2000). Additional ways to stimulate components of the Gq pathway include GTPγS infusion and the membrane-permeable DAG analogue OAG (Schaefer *et al.*, 2000; Jung *et al.*, 2003; Storch *et al.*, 2012). Although SOCE and ROCE are independent mechanisms that can be dissected using experimental manipulations, it should be noted that both processes occur upon activation of Gq-coupled GPCRs.

Since the proposal that TRPC channels constitute a major component of SOCE, TRPC1 and other TRPC members have been intensely studied as store-operated channels (Chen *et al.*, 2020; Wang *et al.*, 2020). SOCE was first described by Putney in 1986 as a ubiquitous cellular mechanism to restore Ca^{2+} homeostasis (Putney, 1986). The physiological triggers for SOCE include activation of Gq-coupled GPCRs, which generate inositol 1,4,5-triphosphate (IP_3) and DAG from PIP_2 via PLC activity. IP_3 then acts on the cognate IP_3 receptor to release free Ca^{2+} from the ER. This store depletion activates the ER Ca^{2+}-sensing protein stromal interaction molecule (STIM1 and STIM2), which directly interacts with the plasma membrane Ca^{2+}-

selective ion channel Orai (Orai1, Orai2, Orai3) to induce Ca^{2+} entry and replenish the ER store (Nesin & Tsiokas, 2014; Majewski & Kuznicki, 2015; Ambudkar *et al.*, 2017). SOCE was first described in mast and T cells (Nesin & Tsiokas, 2014; Ambudkar *et al.*, 2017). The inward current associated with SOCE in the immune cells has low conductance, is highly Ca^{2+}-selective, and was discovered to be Orai1-mediated (Ambudkar *et al.*, 2017). However, TRPC channels contribute to SOCE in a variety of other cell types, including neurons, skeletal muscles, smooth muscles, epithelial secretory cells, and endothelial cells (Majewski & Kuznicki, 2015; Ambudkar *et al.*, 2017). TRPC1 physically interacts with both STIM1 and Orai1, which are necessary for its activation, though the exact mechanism remains controversial (Nesin & Tsiokas, 2014; Ambudkar *et al.*, 2017). The current evidence supports a model in which TRPC1 is stored in intracellular vesicles in resting conditions. Upon store depletion, Ca^{2+} entry through Orai1 recruits TRPC1 to the plasma membrane where it is gated by STIM1 via electrostatic interactions (Cheng *et al.*, 2011). TRPC1-STIM1 and Orai1-STIM1 are located in close proximity but form distinct channel complexes (Cheng *et al.*, 2011). STIM1 also mediates the assembly of TRPC1 with other TRPC subunits to form store-operated channels of various properties (Yuan *et al.*, 2007). As the result, SOCE current recorded in TRPC1-expressing cells is a combination of TRPC1- and Orai1-mediated current, which has higher conductance and is non-selective cationic. Therefore, SOCE in neurons may regulate excitability by mediating postsynaptic current and initiating Ca^{2+}-dependent signaling pathways (Hartmann *et al.*, 2014; Dou *et al.*, 2018).

Receptor-operated activation of TRPC channels involves complex membrane lipid signaling. Both the substrate and the products of PLC contribute to ROCE. $PI(4,5)P_2$ (simplified as PIP_2 unless otherwise specified) exerts dual effects, which explain why early studies obtained paradoxical results. On one hand, direct application of PIP_2 to the cytoplasmic side of inside-out patches enhanced the opening of TRPC3, 5, 6, and 7 (Lemonnier *et al.*, 2008; Trebak *et al.*,

2009). On the other hand, intracellular infusion of PIP_2 in whole-cell recording mode inhibited TRPC4 and TRPC5 (Otsuguro *et al.*, 2008; Trebak *et al.*, 2009). Those results suggested that multiple PIP_2 binding sites are likely. PIP_2 may act as a direct ligand or serve as a necessary co-factor that support channel function. At the same time, PIP_2 bound at a different site may exert tonic inhibition on the channel. Indeed, it was shown that PIP_2 inhibition of TRPC4 depends on linkage of the C-terminal calmodulin/IP_3-receptor-binding (CIRB) domain to actin cytoskeleton via the scaffold protein Na^+/H^+ exchanger regulatory factor (NHERF) (Otsuguro *et al.*, 2008). This cytoskeletal complex likely stabilizes TRPC4 in the inactive conformation. Depletion of PIP_2 is necessary to relieve the channel from inactivation, but is not sufficient for full activation without other components of the PLC pathway (Otsuguro *et al.*, 2008). This model also explains the results from the inside-out patches, where the inhibitory NHERF-cytoskeleton complex is lost and thus the activating effects of PIP_2 predominates. Consistently, a newer study using FRET to measure PIP_2 and DAG dynamics concurrently with TRPC6/7 current showed that both channel activation and inactivation were correlated with PIP_2 reduction, while only channel activation was correlated with DAG production (Itsuki *et al.*, 2014). Importantly, the other phosphoinositides including $PI(3,4)P_2$, $PI(3,5)P_2$, $PI(3,4,5)P_3$ and IP_6 had little or no effects on TRPC4 and TRPC5 (Otsuguro *et al.*, 2008; Trebak *et al.*, 2009), indicating specific recognition of PIP_2 by the channel protein rather than non-specific electrostatic interactions with the charged lipids.

Activation of TRPC channels by DAG, one major product of PLC activity, is considered the primary mechanism underlying ROCE (Chen *et al.*, 2020; Wang *et al.*, 2020). Despite DAG acting as the agonist in this classical ligand-gated process, the exact DAG binding site remained elusive. Only recently, a study of TRPC5 cryo-EM structure identified a putative DAG binding pocket near the pore loop (Song *et al.*, 2021). The DAG in this pocket is displaced by pharmacological inhibitors, suggesting this site is responsible for the direct channel activation.

However, OAG-induced current does not fully recapitulate the magnitude and kinetics of receptor-stimulated current (Albert & Large, 2003), suggesting there are additional mechanisms. Whether all TRPC members are activated by DAG has also been a controversial topic. The traditional view is that the TRPC1/4/5 subgroup are activated by ER store depletion, while TRPC3/6/7 are activated by receptor stimulation. This concept was consolidated by a series of studies in the 1990s through the early 2000s showing TRPC1, 3, 4, and 5 were activated by thapsigargin treatment, but TRPC6 and 7 were not (Wang *et al.*, 2020). Meanwhile, the TRPC3/6/7 subgroup was found to be directly activated by DAGs, which did not appear to activate TRPC4/5 (Wang *et al.*, 2020). The concept was contested by a number of studies showing that TRPC3/7-containing channels are sensitive to both DAGs and store depletion (Kiselyov *et al.*, 1998; Zagranichnaya *et al.*, 2005), while some TRPC4/5-containing channels are activated by Gq-coupled GPCRs but not store depletion (Schaefer *et al.*, 2000; Strubing *et al.*, 2001). A recent study discovered that co-expression with Gq-coupled GPCRs and depletion of PIP_2 confer DAG sensitivity to TRPC4/5 by causing dissociation of NHERF1/2 from the channel protein (Storch *et al.*, 2017). These results not only explained why application of DAGs alone fails to induce TRPC4/5 current, but also highlighted NHERF as a dynamic regulator of lipid gating by both DAG and PIP_2. Thus, DAG sensitivity appears to be a common feature of all TRPC subunits. The distinction between "store-operated" and "receptor-operated" channels is functional but not genetic. While all TRPC subunits are capable of forming store-operated or receptor-operated channels, studies suggested a model in which a single cell maintains separate pools of TRPC channels coupled to the SOCE and ROCE pathways (Vazquez *et al.*, 2003; Zagranichnaya *et al.*, 2005). SOCE and ROCE channels exhibit different properties and are independently regulated, although both pools would be activated by the physiological receptor agonists.

A dynamic mechanism involving the IP_3 receptor and calmodulin, as well as Ca^{2+} itself,

constitute other components of the PLC pathway that regulate TRPC channel activation. TRPC5 is the only TRPC member that is constitutively active (Schaefer *et al.*, 2000; Jeon *et al.*, 2012) and directly activated by Ca^{2+} [EC_{50} = 635 nM at membrane potential (Vm) = −80 mV; (Gross *et al.*, 2009)]. Upon store depletion or receptor stimulation, TRPC channels can be directly activated by the IP_3-bound IP_3 receptor. As previously discussed, all TRPC subtypes possess a C-terminal CIRB domain where calmodulin and IP_3 receptor share a mutually exclusive binding site (Tang *et al.*, 2001). Calmodulin binds to the CIRB domain constitutively and suppresses the basal activity of the channel (Zhang *et al.*, 2001). This calmodulin-TRPC interaction partially accounts for the inhibitory effects of Ca^{2+} on all TRPC subtypes (Wang *et al.*, 2020). The binding of calmodulin to TRPC is Ca^{2+}-dependent; the affinity differs for each TRPC subtype (K_d ranging from 10 nM for mTRPC2 to 290 nM for mTRPC6), suggesting their sensitivity to Ca^{2+}-mediated inhibition varies (Tang *et al.*, 2001). Interestingly, an active IP_3 receptor competes for the CIRB domain and displaces calmodulin, relieving the channel from inhibition (Zhang *et al.*, 2001). All three mammalian IP_3 receptors can bind to the CIRB domain via a conserved C-terminal domain (Tang *et al.*, 2001). IP_3 alone does not affect TRPC channels and its actions is dependent on IP_3 receptors. Direct application of IP_3 to inside-out patches had no effects on TRPC3/6/7 channel opening (Lemonnier *et al.*, 2008), while another study showed that the activating effect of IP_3 requires the presence of active IP_3 receptors (Kiselyov *et al.*, 1998). Therefore, direct channel activation by IP_3 receptors is another PLC-mediated mechanism that may explain why DAG alone does not recapitulate all features of TRPC activation (Albert & Large, 2003).

TRPC channels in midbrain dopaminergic neurons

All TRPC subtypes except TRPC2 are expressed in the substantia nigra (Chung *et al.*, 2007; Zeng *et al.*, 2016). Interestingly, there appear to be mismatches between the levels of TRPC mRNAs

and proteins in the SN: the levels of TRPC3 and TRPC6 mRNAs were the highest, whereas immunoreactivities for TRPC3, TRPC4, and TRPC7 were the most intense (Sylvester *et al.*, 2001; Chung *et al.*, 2007). The caveat was that these early studies did not distinguish SNc from SNr, nor did they identify the cell types involved. The first definite and detailed reports of TRPC protein expression in adult rat SNc DA neurons were done by Fusco and coworkers. Their immunohistochemical studies showed that TRPC1, TRPC5, and TRPC6 are expressed in SNc DA neurons (De March *et al.*, 2006; Martorana *et al.*, 2006; Giampa *et al.*, 2007). Importantly, TRPC1 and TRPC6 showed intense staining in the somatodendritic compartments and co-localization with mGluR1 (Martorana *et al.*, 2006; Giampa *et al.*, 2007). TRPC1 was preferentially localized in the distal dendrites and absent in the glia (Martorana *et al.*, 2006). In contrast, TRPC5 was found localized in the neuronal nuclei and did not co-localize with TRPC1 or mGluR1 (De March *et al.*, 2006). Finally, and intriguingly, TRPC3 showed preferential localization in oligodendrocytes in the SN, compared to the very light staining in a subset of DA neurons and little to no staining in astrocytes and microglia (Fusco *et al.*, 2004). Single-cell RT-PCR analysis performed by the Mercuri Lab found that the majority of SNc DA neurons express mRNAs for TRPC1 and TRPC5, a significant minority express TRPC4 and TRPC6, and very few cells express TRPC3 (Tozzi *et al.*, 2003). Their results were consistent with those of the Fusco Lab that TRPC1, TRPC5, and TRPC6 are the most abundant subtypes in SNc DA neurons, although TRPC7 was not examined by either lab group.

Activation of TRPC channels by mGluR1 in DA neurons was first demonstrated by Mercuri and coworkers. In their two studies using acute rat SNc slices, they found that mGluR1 agonism elicited an approximately linear, non-selective cationic current with a reversal potential around 0 mV (Tozzi *et al.*, 2003; Cucchiaroni *et al.*, 2010). The current correlated with membrane potential depolarization and an increase in spontaneous firing frequency (Cucchiaroni *et al.*, 2010). Pharmacological characterization showed that this mGluR1-induced

current was sensitive to non-selective TRP channel blockers such as SKF96365, 2-APB, and flufenamic acid but insensitive to manipulations of intracellular Ca^{2+} release such as thapsigargin, CPA, dantrolene, and BAPTA (Tozzi *et al.*, 2003). Those characteristics suggested that mGluR1s are coupled to TRPC channels via the ROCE pathway and are independent of SOCE. While there are currently no equivalent studies on VTA DA neurons, mGluR1- and M5 receptor-induced inward current and Ca^{2+} release have been reported in this brain region (Foster *et al.*, 2014), suggesting Gq-TRPC signaling likely also occurs in VTA DA neurons.

The participation of TRPC channels in SOCE has been documented in mouse SNc DA neurons by the lab group of Singh (Selvaraj *et al.*, 2012; Sun *et al.*, 2017). The pacemaking activity of SNc DA neurons is critically dependent on L-type calcium channels. It has been proposed that the increased Ca^{2+} load underlies the vulnerability of SNc DA neurons to degeneration compared to VTA DA neurons (Dragicevic *et al.*, 2015). The Singh Lab showed that, as opposed to generating an excitatory response, TRPC1 activation actually decreases excitability in SNc DA neurons via inhibition of L-type calcium current (Sun *et al.*, 2017), as previously reported in other systems. Thapsigargin-induced Ca^{2+} store depletion elicited a linear current with a reversal potential around 0 mV; this current was absent in TRPC1 KO mice (Selvaraj *et al.*, 2012; Sun *et al.*, 2017). Thapsigargin also increased the physical interaction between Cav1.3 and the TRPC1-STIM1 complex, decreased the maximal conductance of Cav1.3, and reduced the spontaneous firing frequency of SNc DA neurons (Sun *et al.*, 2017). Consistent with the animal studies, postmortem brain tissues from Parkinson's disease patients showed downregulation of TRPC1 and upregulation of Cav1.3 (Sun *et al.*, 2017). Overall, studies by the Singh Lab suggest that the antagonistic relationship between TRPC1 and Cav1.3 may underlie the selective vulnerability of SNc DA neurons.

So far, the physiological significance of TRPC channels in VTA DA neurons is largely unclear.

Nonetheless, one study implicated TRPC4 in the regulation of VTA DA neuron firing, sociability, and drug reward. TRPC4 mRNA and protein were found expressed in SN and a uniformly-distributed subset (~37%) of VTA DA neurons (Klipec *et al.*, 2016). This suggests that TRPC4 modulation may be circuit-specific and targets a subpopulation of DA neurons. In acute brain slices prepared from the TRPC4 KO rats, VTA DA neurons had significantly lower spontaneous firing rates (Klipec *et al.*, 2016). Behaviorally, the TRPC4 KO rats were less socially exploratory compared to WT counterparts, perhaps due to increased anxiety as proposed in previous studies. Importantly, the TRPC4 KO rats showed reduced cocaine self-administration, but did not differ in multiple learning tasks and sucrose self-administration compared to WT (Klipec *et al.*, 2016). Since this study utilized global TRPC4 KO, it was not known whether intrinsic processes in DA neurons or synaptic inputs were responsible for the phenotypes. Nevertheless, the findings that TRPC4 selectively modulates sociability and drug reward suggest that TRPC4 modulators may provide treatments for a variety of DA-related disorders.

SPECIFIC AIMS

Midbrain dopamine (DA) neurons in the ventral tegmental area (VTA) plays a crucial role in reward and motivational behaviors including addiction. Upon rewarding or conditioned stimuli, DA neurons are directly excited by cholinergic inputs from the pedunculopontine tegmental (PPT) and laterodorsal tegmental (LDT) nuclei. Activation of the Gq-coupled M5 muscarinic receptor (mAChR), the predominant subtype expressed in midbrain DA neurons, increases firing frequency and striatal DA release. Blockage of mAChRs in the VTA has shown promising results in preclinical models of drug addiction to attenuate acute reward and drug-conditioned behaviors.

Our working hypothesis is: "mAChRs activate a non-selective cationic conductance and/or inhibits a K^+ conductance resulting in an increase in electrical excitability of VTA DA neurons."

Aim 1: Investigating the modulation of action potential (AP) frequency, regularity, and kinetics by muscarinic agonism in VTA DA neuron.

1.1: Determining whether mAChR activation alters firing pattern. Inhibition of SK channels increases AP irregularity and facilitates burst firing in VTA DA neurons. To determine whether mAChRs modulate AP timing, acute brain slices will be prepared from WT C57BL/6 mice. Cell-attached and whole-cell voltage- and current-clamp will be used to record spontaneous firing of VTA DA neurons. The frequency and regularity of APs will be compared upon muscarinic activation by bath application of the agonist carbachol and inhibition by the antagonist atropine.

1.2: Determining whether mAChR activation alters the kinetics of AP shape. Changes in ion channel activities that regulate AP shape may underlie increases in firing frequency. However,

AP shape also varies with membrane potential and the availability of voltage-gated channels. To determine whether mAChRs modulate the kinetics of AP shape irrespective of membrane potential, the AP shape recorded during carbachol treatment in Sub-Aim 1.1 will be analyzed when the membrane potential changes are compensated by the clamping circuit.

Aim 2: Investigating the contribution of intrinsic membrane properties and extrinsic inputs in muscarinic excitation of VTA DA neurons.

2.1: Determining the modulation of intrinsic membrane properties by muscarinic agonism. To determine whether mAChRs modulate HCN and K^+ conductances in VTA DA neurons, intrinsic firing properties including sag ratio, spike frequency adaptation, and frequency-current relationship will be assessed using a current step protocol during carbachol bath treatment. In addition, the carbachol-induced changes in membrane potential and input resistance will be quantified using whole-cell current-clamp when spontaneous firing is inhibited by tetrodotoxin (TTX).

2.2: Determining whether mAChR activation alters sIPSCs in VTA DA neurons. VTA DA neurons are tonically inhibited by GABAergic neurons in the local circuit. To determine whether muscarinic inputs modulate VTA DA neuron activity via activation of mAChRs located on the GABAergic interneurons, sIPSCs will be recorded in VTA DA neurons with bath application of carbachol.

Aim 3: Characterizing the pharmacological sensitivity of mAChR-induced currents in VTA DA neurons.

3.1: Determining whether the mAChR-induced current is sensitive to non-selective ion channel blockers. To determine the ionic composition of mAChR-induced currents in VTA DA neurons, whole-cell voltage-clamp experiments will be performed with bath application of carbachol co-treated with the non-selective K^+ and Ca^{2+} channel blockers TEA, Cs^+, and Cd^{2+}.

3.2: Determining whether the mAChR-induced current is sensitive to a TRPC channel blocker.

In central neurons, TRPC are non-selective cationic channels commonly modulated by Gq signaling. To determine whether activation of TRPC channels participates in mAChR-induced currents in VTA DA neurons, carbachol-induced whole-cell currents will be recorded with bath application of the TRPC-selective blocker BTP2.

METHODS

Acute slice preparation and identification of cells

C57BL/6 mice of either sex, postnatal day 13-31 (median age = 18) were anesthetized with isoflurane and quickly decapitated. Horizontal 200-μm midbrain slices were prepared in ice-cold ACSF solution containing (in mM): 125 NaCl, 25 NaHCO$_3$, 3 KCl, 1.2 CaCl$_2$, 1.2 MgSO$_4$, 1.25 NaH$_2$PO$_4$, 10 glucose, 0.4 ascorbic acid, saturated with 95% O$_2$ and 5% CO$_2$. Slice were incubated at 32 °C in the same ACSF solution for at least 30 min. before patch-clamp recordings. For all patch-clamp recordings, slices were transferred to a chamber with continuous perfusion of ACSF at 34 °C. Borosilicate glass patch electrodes with a tip resistance of 3-6 MΩ were filled with intracellular solutions (see detailed methods of each experiment). Recordings were made using an A-M Systems 2400 amplifier and Strathclyde Electrophysiology Software (WinWCP & WinEDR, University of Strathclyde). On the horizontal brain slice, VTA was identified by anatomical location using substantia nigra pars compacta (SNc) and medial terminal nucleus of the accessory optic tract (MT) as the landmarks, as VTA is rostral to the MT and medial to both SNc and MT (Masi *et al.*, 2015; Krashia *et al.*, 2017). VTA dopaminergic (DA) neurons were identified by cell morphology with a large, fusiform or multipolar soma (Grace & Onn, 1989). Whenever possible, the identity was further confirmed by electrophysiological characteristics measured using a current step protocol (see Experiment 2). The majority of neurons recorded in this study were located in the lateral VTA. These neurons exhibit "conventional" electrophysiological characteristic including broad action potential width, slow spontaneous firing rates (<10 Hz), a prominent HCN sag, delayed evoked firing, and in addition, a hyperpolarizing response to dopamine (60 μM) that was applied by the end of the trials (Grace & Onn, 1989; Lammel *et al.*, 2008; Roeper, 2013; Masi *et al.*, 2015; Krashia *et al.*, 2017).

Recording solutions and measurements of liquid junction potential

The intracellular solution for patch-clamp experiments contained (in mM): 122 K-gluconate, 7 NaCl, 0.58 $MgCl_2$, 0.03 $CaCl_2$, 0.1 EGTA-K, 10 HEPES, 14 phosphocreatine, 4 ATP-Mg, 0.3 GTP-Na, pH 7.3 adjusted with KOH, 290 mOsm/L; this solution was used for all experiments except measurements of sIPSCs (Experiment 3). The online program Maxchelator was used to calculate the amounts of Ca^{2+}, EGTA, and Mg^{2+} added, resulting in final concentrations of 100 nM free Ca^{2+} and 1 mM free Mg^{2+}. The Ca^{2+} and EGTA concentrations were calculated based on the assumption that distilled water naturally contains ~5-7 μM free Ca^{2+}. The liquid junction potential (LJP) was measured empirically by constructing a 1 M KCl-infused agar bridge connected to the headstage. Switching from symmetrical intracellular solution to extracellular ACSF yielded a LJP of −8.7 mV, which was used to correct the action potential threshold potential and membrane potential data from Experiment 1 and 4. No LJP correction was applied to the voltage reset of the current step protocol in Experiment 2 and the holding voltage of voltage-clamp recordings in Experiment 3 and 5.

Drug application

All pharmacological reagents were perfused in bath. To stimulate or inhibit the mAChRs, the non-selective cholinergic agonist carbachol (10 μM) and the muscarinic antagonist atropine (5 μM) were used, respectively. For most experiments, one set of cells was first treated with carbachol followed by atropine to reverse the carbachol-induced effects, while a second set of cells was pretreated with atropine followed by simultaneous perfusion of atropine and carbachol to block the muscarinic components of carbachol-induced effects. Each drug was perfused for at least 4 min. to elicit the maximum response before measurements were taken. Drugs were prepared and aliquoted as either water or DMSO stock depending on the solubility. The final DMSO concentration in the ACSF was 0.05% (v/v).

Experiment 1: mAChR modulation of tonic pacemaking activity, AP shape, and AP kinetics

Spontaneous APs of VTA DA neurons were recorded in either gap-free cell-attached or whole-cell current-clamp configuration. Only cells that maintained stable firing were included. In the cell-attached experiments, smaller pipette tips (5-9 MΩ) were used to prevent rupture of the plasma membrane. After a tight seal (>1 GΩ) was formed, the cells were held at 0 mV in the voltage-clamp mode to record AP currents. After each trial, the cell identity was confirmed by a current step protocol and response to dopamine in the whole-cell configuration. In the current-clamp experiments, larger pipette tips (3-6 MΩ) were used. After forming a tight seal, the membrane was ruptured by gently applying negative pressure to achieve the whole-cell configuration. The cell identity was confirmed by application of a current step protocol in the beginning and response to dopamine after each trial. Spontaneous firing activity was recorded with a sampling interval of 0.02 ms and low-pass filtered at 5 kHz. The AP events were detected and analyzed using Mini Analysis, except the detection of afterhyperpolarization (AHP) amplitude and duration was done by running scripts in OriginPro. Firing frequency was calculated in Hz from the number of APs in a 1-min interval, while firing regularity was measured as the mean coefficient of variation (CoV) of interspike intervals (ISI). AP shape data were derived from the average AP threshold, amplitude, and half-width in the 1-min interval when there was no current injection. AP threshold was defined as the inflection point voltage at the onset of the sodium spike, amplitude the potential difference between the threshold and the peak of the AP, and half-width the AP duration at the voltage halfway between the threshold and the peak. To determine whether mAChR activation affects AP kinetics, the average Vm after drug treatments was restituted to the baseline value by current injection. The firing pattern and AP shape parameters were re-analyzed in this condition after the Vm changes were compensated. In addition, an average AP waveform was generated from APs in a 1-min interval for analysis of afterhyperpolarization (AHP) kinetics. AHP amplitude was

calculated by subtracting the threshold potential from the AHP peak potential, while AHP duration was the time between the AP threshold potential and the AHP peak. Only cells that maintained stable access resistance (either <20% change or within ± 2 MΩ if the initial access resistance was <10 MΩ) by the end of the trial were included in the data pool. In addition, cells with outlier result values were excluded using Peirce's criterion. Data were analyzed using one-way repeated measures (RM) ANOVA with post-hoc Tukey's test or the non-parametric Friedman test with post-hoc Dunn's test, depending on whether the distribution was normal. All results are shown as mean ± SEM.

Experiment 2: mAChR modulation of intrinsic firing properties

A current step protocol was performed in the whole-cell configuration. The protocol consisted of a series of 600-ms steps ranging from −200 pA to +200 pA, with a 25 pA increment between each step. Before applying the step protocol, the DA neurons were clamped at −60 mV. Intrinsic firing properties including HCN sag, frequency-current (f-I) relationship, and spike frequency adaptation were compared before and after bath perfusion of mAChR drugs. The HCN sag ratio was calculated by dividing the amplitude of steady-state potential by the amplitude of the most negative hyperpolarizing potential during the −200 pA step (steady-state potential/lowest potential; each value is calculated from differences from −60 mV). Spike frequency adaption ratio (FAR) was measured as the instantaneous firing frequency of the last AP to that of the first AP during the +200 pA step (last AP/first AP). The instantaneous firing frequency was defined as the reciprocal of the interval between two consecutive APs. Finally, the f-I relationship was determined as the mean firing frequency during the +200 pA step, since an f-I relationship plot across the entire range of current steps could not be constructed due to the low firing frequency of DA neurons. OriginPro scripts were used to analyze the intrinsic membrane properties. Data were analyzed using one-way RM ANOVA with post-hoc Tukey's test. All results are shown as mean ± SEM.

Experiment 3: the effects of mAChR activation on sIPSCs in DA neurons

Spontaneous inhibitory post-synaptic currents (sIPSCs) were recorded using whole-cell voltage-clamp from the DA neurons with the following intracellular solution (in mM): 120 Cs-methanesulfonate, 8 NaCl, 10 HEPES, 10 Cs-BAPTA, 10 QX-314 chloride, 2 ATP-Mg, 0.1 GTP-Na, pH 7.3 adjusted with CsOH. Since this intracellular solution prevented firing, HCN-mediated voltage sag, and activation of D2 autoreceptor response, VTA DA neurons were identified by anatomical location and cell morphology. No synaptic blockers were added to the bath solution to minimize disruption of tonic synaptic activity. sIPSCs were recorded as outward currents by holding the Vm at +15 mV, the reversal potential of ionotropic glutamate receptors, in order to eliminate excitatory post-synaptic currents. Carbachol and atropine were bath perfused for 5 min. before the measurements were taken. The average frequency and amplitude of sIPSCs in a 3-min. interval during each treatment were analyzed using Mini Analysis. Data were analyzed using one-way RM ANOVA with post-hoc Tukey's test. All results are shown as mean ± SEM.

Experiment 4: the effects of mAChR activation on membrane potential and input resistance without spontaneous firing activity

TTX (500 nM) was added to the bath solution to eliminate spontaneous firing. Vm was recorded in the gap-free whole-cell current-clamp mode before and after drug treatment. The average value of Vm was obtained by plotting the Vm at 20-sec intervals as a histogram of 0.1 mV width and fitting to Gaussian distribution function in ClampFit. Every 22 sec, a small current pulse, −15 to −40 pA in amplitude and 500 ms in duration, was injected to monitor the input resistance. The amount of current injected varied for each cell to evoke a hyperpolarization between 5 to 10 mV. Input resistance was calculated using Ohm's Law by dividing the peak hyperpolarization potential evoked during the step by the amount of current

injected. Trials with >20% change in access resistance or more than ± 2 MΩ change if the initial

access resistance was <10 MΩ were discarded from input resistance analysis and only used

for report of membrane potential. Data were analyzed using one-way RM ANOVA with post-

hoc Tukey's test or the non-parametric Friedman test with post-hoc Dunn's test, depending

on whether the distribution was normal. All results are shown as mean ± SEM.

Experiment 5: characterization of the mAChR-induced inward current

In the whole-cell voltage-clamp configuration, carbachol was used as the agonist to induce an

inward current. Atropine was used as a negative control applied at the end of the trial; if the

current failed to return to baseline level with atropine, the cell is discarded. Cells that had

>20% change in the access resistance were also discarded. TTX (500 nM, stock in water) was

added throughout all recordings to prevent synaptic activities. TEA was applied by substituting

20 mM TEA (from TEA-Cl powder) for equimolar NaCl in the ACSF solution. The other blockers

Cs^+ (10 mM, from CsCl powder), Cd^{2+} (200 μM, $CdCl_2$ stock in water), and BTP2 (5 μM, stock

in DMSO) were added directly to fully oxygenated ACSF. After bath perfusion of carbachol or

the blockers, the peak response was observed before switching to the next treatment, which

usually took 200-300 sec. except for BTP2 which was perfused for 10 min before

measurements were taken. The voltage-clamp recordings were acquired at a sampling interval

of 0.1 ms with 2 kHz low-pass filter and were further digitally filtered using ClampFit at 1 kHz

before data analysis. The peak current amplitude and the standard deviation (SD) of current

fluctuations were calculated by plotting the current traces in a 10-sec interval as a frequency

histogram and fitting the histogram to Gaussian distribution in ClampFit. The peak carbachol

current amplitude and changes in carbachol-induced current fluctuations in the presence of

different blockers were compared using the Kruskal-Wallis test with post-hoc Dunn's test,

except for the amplitudes of carbachol current before and after BTP2 treatment were

compared using paired t-test. The SD of current fluctuations from the same set of cells was

analyzed using one-way RM ANOVA with post-hoc Tukey's test or the non-parametric Friedman test with post-hoc Dunn's test, depending on whether the distribution was normal. The current amplitude data are shown as mean ± SEM, whereas the current fluctuation data are displayed as box and whisker plots.

Softwares used for graphing and statistical analysis

OriginPro was used to plot representative traces. The numerical data were graphed and performed statistical analysis in GraphPad Prism.

RESULTS

Activation of muscarinic receptors increases the firing rates of VTA dopamine neurons without affecting firing pattern

Cell-attached patch-clamp experiments were performed on VTA DA neurons in acutely prepared brain slices to determine the effects of muscarinic acetylcholine receptor (mAChR) agonism on endogenous firing pattern (**Figure 1A**). DA neurons of the lateral VTA were identified by relative location to the MT and SNc, large soma size, and electrophysiological characteristics including slow spontaneous firing, broad AP width, large HCN-mediated voltage sag evoked by a current step protocol, and hyperpolarizing response to DA (Grace & Onn, 1989; Lammel *et al.*, 2008; Roeper, 2013; Masi *et al.*, 2015; Krashia *et al.*, 2017). In the cell-attached experiments, the cell identity was confirmed *post-hoc* by breaking in the cell membrane and running the current step protocol in the whole-cell configuration. Consistent with previous reports (Vandecasteele *et al.*, 2011), VTA DA neurons are spontaneously active with a baseline firing rate of 4.53 ± 0.34 Hz (n = 17). The pacemaking is highly regular, quantified as a mean coefficient of variation of the interspike interval (CoV of ISI) of 0.064 ± 0.010. Bath application of carbachol (10 μM), a non-selective cholinergic agonist, significantly accelerated the firing frequency to 6.05 ± 0.37 Hz, corresponding to an average increase of 1.52 ± 0.18 Hz. After the carbachol treatment, carbachol was replaced by bath perfusion of the mAChR antagonist atropine (5 μM). Atropine reversed the firing frequency to 4.82 ± 0.34 Hz, which was not significantly different from the baseline value (**Figure 1B**; $F_{2.0,32} = 41.47$, p < 0.0001****, n = 17, one-way RM ANOVA with post-hoc Tukey's test, Base vs. Carb: p < 0.0001****, Base vs. Atro: p = 0.2794, Carb vs. Atro: p < 0.0001****). In contrast, firing regularity was not affected by carbachol or atropine; the CoV of ISI did not show significant changes (**Figure 1C**; Base = 0.064 ± 0.010, Carb = 0.053 ± 0.004, Atro = 0.057 ± 0.008; Fr =

0.3529, p = 0.8382, n = 17, Friedman test).
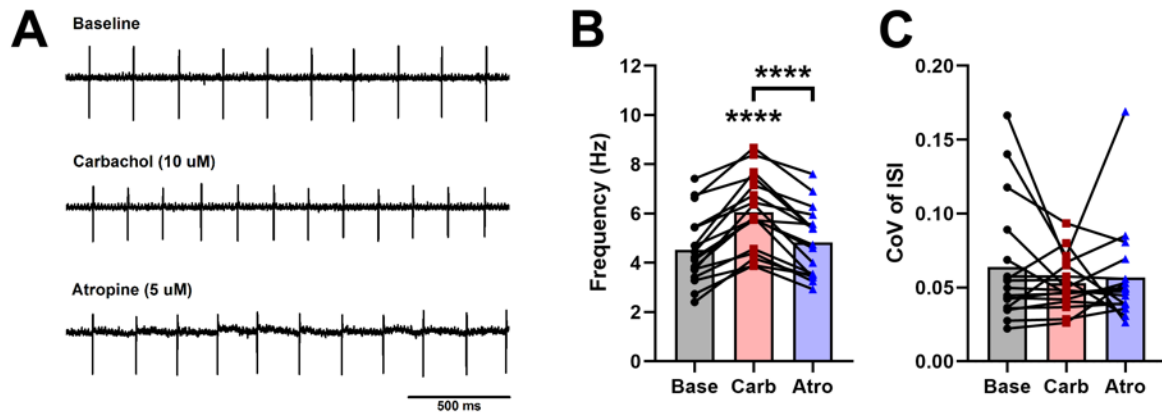
Figure 1. Activation of muscarinic receptors increases spontaneous firing frequency without affecting firing regularity in cell-attached patch-clamp recordings. (A) Representative cell-attached recording of VTA DA neuron activity in baseline, after muscarinic activation by bath perfusion of the agonist carbachol (10 μM), and muscarinic blockage by the antagonist atropine (5 μM). **(B)** Carbachol increased spontaneous firing frequency, an effect that was reversed by atropine. **(C)** Carbachol and atropine had no effects on firing regularity, measured as the coefficient of variation of the interspike interval (CoV of ISI). (**** $p < 0.0001$)

The same experiment was performed using the whole-cell current-clamp technique to gain access to measurements of action potential shape and membrane potential (**Figure 2A**). In this configuration, bath application of carbachol increased the pacemaking frequency by 1.79 ± 0.29 Hz, from the baseline value of 3.64 ± 0.23 to 5.43 ± 0.42 Hz. When atropine was subsequently applied, the pacemaking frequency decreased to 4.25 ± 0.43 Hz, again not significantly different from the baseline value (**Figure 2B**; $F_{1.5,21}$ = 24.34, p < 0.0001****, n = 15, one-way RM ANOVA with post-hoc Tukey's test, Base vs. Carb: p < 0.0001****, Base vs. Atro: p = 0.1450, Carb vs. Atro: p < 0.0001****). There was a slight decrease in firing regularity with carbachol treatment, as shown by the small increase in the CoV of ISI (**Figure 2C**; Base = 0.056 ± 0.005, Carb = 0.071 ± 0.004). However, this decrease in firing regularity was not reversed by atropine; the value of CoV of ISI further increased by the time atropine was perfused (**Figure 2C**; Atro = 0.081 ± 0.006; $F_{1.8,25}$ = 9.867, p = 0.0010***, n = 15, one-way RM ANOVA with post-hoc Tukey's test, Base vs. Carb: p = 0.0230*, Base vs. Atro: p = 0.0050**, Carb vs. Atro: p = 0.1933). This progressive increase in firing irregularity suggests a time-dependent effect not specific to mAChR activation, probably resulting from a loss of intracellular components during the long recordings in the whole-cell configuration.

To determine whether carbachol speeds up pacemaking via membrane potential depolarization, we injected hyperpolarizing current to bring the average Vm to baseline levels after carbachol and atropine treatments, shown in the set of cells in **Figure 2B & C**. When the carbachol-induced changes in Vm were compensated, the pacemaking frequency was restored to baseline value and no longer differed between any treatment (compare **Figure 2B vs. Figure 2D**; Base = 3.64 ± 0.23 Hz, Carb = 3.63 ± 0.29 Hz, Atro = 3.48 ± 0.26 Hz; $F_{1.8,25}$ = 0.7884, p = 0.4531, n = 15, one-way RM ANOVA). In contrast, during carbachol treatment there was a slight decrease in AP regularity (compare **Figure 2C vs. Figure 2E**; Base = 0.056 ± 0.005, Carb = 0.092 ± 0.007), which was not reversed by atropine, similar to the results when changes

in Vm were not compensated (Atro = 0.079 ± 0.005; $F_{1.7,24}$ = 11.93, p = 0.0004***, n = 15, one-way RM ANOVA with post-hoc Tukey's test, Base vs. Carb: p = 0.0029**, Base vs. Atro: p = 0.0073**, Carb vs. Atro: p = 0.1995). This suggests that mAChR activation increases pacemaking frequency mainly by depolarizing Vm and do not disrupt the ion channel mechanisms essential for spike generation.

To confirm that the reversal of the firing frequency increase was due to mAChR antagonism, a separate set of VTA DA neurons were pretreated with atropine for 5 min. before the co-treatment of atropine and carbachol. In this protocol, atropine completely prevented the effect of carbachol on firing frequency (**Figure 2F**; Base = 4.86 ± 0.33 Hz, Atro = 5.21 ± 0.31 Hz, Atro + Carb = 5.24 ± 0.33 Hz; $F_{1.3,19}$ = 3.394, p = 0.0718, n = 16, one-way RM ANOVA). Atropine and the following co-treatment with carbachol also had no effects on firing regularity (**Figure 2G**; CoV of ISI: Base = 0.059 ± 0.005, Atro = 0.066 ± 0.007, Atro + Carb = 0.078 ± 0.008; Fr = 6.125, p = 0.0468*, n = 16, Friedman test with post-hoc Dunn's test, which reveals no significant differences between treatments). Overall, the cell-attached and whole-cell experiments produced the same results. Both techniques show that mAChR activation increases pacemaking frequency without affecting firing regularity in VTA DA neurons in our experimental conditions.
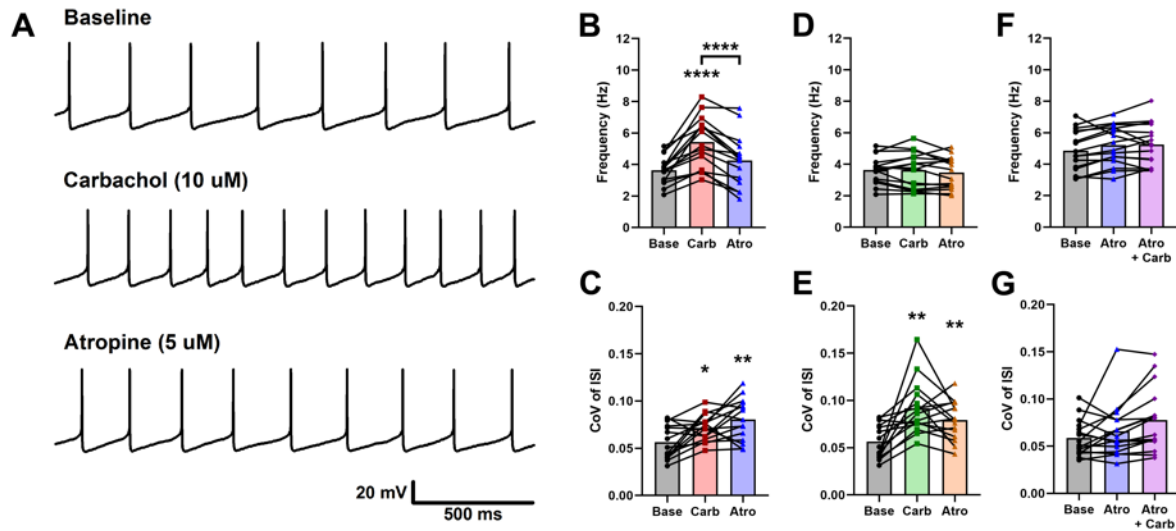
Figure 2. Activation of muscarinic receptors increases spontaneous firing frequency without affecting firing regularity in whole-cell current-clamp recordings. (A) Representative whole-cell current-clamp recording of VTA DA neuron activity in baseline and after carbachol and atropine application. **(B)** Carbachol increased spontaneous firing frequency, an effect that was reversed by atropine. **(C)** Carbachol caused a small decrease in firing regularity that was not reversed by atropine. **(D)** The effect of carbachol on firing frequency was eliminated when membrane potential was compensated to baseline level via current injection. **(E)** In contrast, alterations in firing regularity were not suppressed by resetting membrane potential. **(F, G)** Atropine pretreatment blocked the effects of carbachol. Atropine alone did not affect firing frequency and firing regularity. (* $p < 0.05$; ** $p < 0.01$; **** $p < 0.0001$)

Activation of muscarinic receptors alters action potential shape

The carbachol-induced increase in firing frequency was accompanied by changes in action potential (AP) shape (**Figure 3A, left panel**). To investigate the ionic conductances involved in carbachol-induced excitation during spontaneous firing, we analyzed changes in the average AP waveform. At baseline, VTA DA neurons have an AP threshold of -36.28 ± 0.62 mV, an AP amplitude of 61.60 ± 1.06 mV, and an AP half-width of 1.28 ± 0.07 ms (n = 15). Bath perfusion of carbachol significantly raised AP threshold to -33.39 ± 0.81 mV (**Figure 3B**), reduced AP amplitude to 52.69 ± 1.47 mV, (**Figure 3C**), and broadened AP half-width to 1.45 ± 0.10 ms (**Figure 3D**). The subsequent atropine treatment restored AP half-width to baseline value (**Figure 3D**; Atro = 1.31 ± 0.08 ms; $F_{1.7,24} = 24.05$, $p < 0.0001$****, n = 15, one-way RM ANOVA with post-hoc Tukey's test, Base vs. Carb: $p = 0.0001$***, Base vs. Atro: $p = 0.3780$, Carb vs. Atro: $p = 0.0005$***), but only partially reversed the carbachol-induced increase in in AP threshold (**Figure 3B**; Atro = -34.65 ± 0.84 mV; $F_{1.8,25} = 32.85$, $p < 0.0001$****, n = 15, one-way RM ANOVA with post-hoc Tukey's test, Base vs. Carb: $p < 0.0001$****, Base vs. Atro: $p = 0.0041$**, Carb vs. Atro: $p = 0.0035$**) and reduction in AP amplitude (**Figure 3C**; Atro = 56.89 ± 1.94 mV; $F_{1.8,26} = 36.82$, $p < 0.0001$****, n = 15, one-way RM ANOVA with post-hoc Tukey's test, Base vs. Carb: $p < 0.0001$****, Base vs. Atro: $p = 0.0034$**, Carb vs. Atro: $p = 0.0012$**).

In comparison, the set of cells pre-treated with atropine (**Figure 3A, right panel**) showed that there were progressive increases in AP threshold (**Figure 3J**; Base = -37.58 ± 0.44 mV, Atro = -37.01 ± 0.55 mV, Atro + Carb = -36.37 ± 0.69 mV; $F_{1.2,19} = 7.346$, $p = 0.0103$*, n = 16, one-way RM ANOVA with post-hoc Tukey's test, Base vs. Atro: $p = 0.0230$*, Base vs. Atro + Carb: $p = 0.0266$*, Atro vs. Atro + Carb: $p = 0.1212$) and reduction in AP amplitude (**Figure 3K**; Base = 56.44 ± 1.21 mV, Atro = 54.44 ± 1.19 mV, Atro + Carb = 52.06 ± 1.17 mV; $F_{1.4,20} = 23.46$, $p < 0.0001$****, n = 16, one-way RM ANOVA with post-hoc Tukey's test, Base vs. Atro: $p = $

0.0003***, Base vs. Atro + Carb: p = 0.0002***, Atro vs. Atro + Carb: p = 0.0070**) during atropine and the following atropine and carbachol co-treatment. Atropine alone did not affect AP half-width (Base = 1.09 ± 0.04 ms, Atro = 1.10 ± 0.04 ms). However, there was a small but significant increase in AP half-width during the subsequent atropine and carbachol co-treatment (**Figure 3L**; Base = 1.09 ± 0.04 ms, Atro = 1.10 ± 0.04 ms, Atro + Carb = 1.15 ± 0.04 ms; $F_{1.5,22}$ = 17.24, p = 0.0001***, n = 16, one-way RM ANOVA with post-hoc Tukey's test, Base vs. Atro: p = 0.2012, Base vs. Atro + Carb: p = 0.0012**, Atro vs. Atro + Carb: p = 0.0008***).

Though statistically significant, the changes in AP shape parameters in cells where carbachol was applied first were much smaller compared to those cells where atropine was applied first (compare **Figure 3B, 3C, and 3D** vs. **Figure 3J, 3K, and 3L**): carbachol treatment was accompanied by 8.0% increase in threshold, 14.5% reduction in amplitude, and 13.3% increase in half-width, while atropine was accompanied by 1.5%, 3.5%, and 0.9%, respectively. When carbachol was added after atropine pretreatment, the changes in AP shape were also smaller compared to those induced by carbachol alone, with 3.2% increase in threshold, 7.8% reduction in amplitude, and 5.5% increase in half-width. Since the two sets of cells had the same timeline of agonist and antagonist treatments but in reverse order, these results suggest that carbachol-induced excitation was accompanied by significant changes in AP shape. In contrast, atropine had minimal to no effects on AP shape and was able to block most of the carbachol-induced effects. The small but persistent effects observed in **Figure 3J, 3K and 3L** most likely correspond to the drift in the cellular condition and ion channel run-down during the long recordings in the whole-cell mode.

Activation of muscarinic receptors does not alter action potential kinetics

Next, we analyzed the effects of mAChR activation on AP kinetics. The carbachol-induced

changes in AP shape could involve at least two processes: inactivation of voltage-gated sodium channels due to Vm depolarization and GPCR-mediated modifications of ion channel functions via intracellular signaling (e.g., release of second messengers and protein phosphorylation). Theoretically, sodium channel inactivation should be recovered by injection of hyperpolarizing current, whereas signaling modifications of ion channels would be less dependent on the baseline voltage reset, especially for proteins not modulated by voltage such as in the case of the SK channel. To determine the contribution from these two processes, we used the clamping circuit to restitute the original Vm during bath perfusion of carbachol and the following atropine treatment of the set of cells shown in **Figure 3B, C, D**.

When the Vm was restituted to the baseline level, the average AP waveform during carbachol application almost completely aligned with that prior to the agonist treatment (**Figure 3A, center panel**). The carbachol-induced increases in AP threshold (**Figure 3E**; Carb = −35.43 ± 0.84 mV;) and AP half-width (**Figure 3G**; Carb = 1.26 ± 0.09 ms) were completely reversed by restituting the baseline potential. The AP threshold value also did not differ from the baseline during atropine treatment when Vm changes were compensated (**Figure 3E**; Atro = −35.88 ± 0.80 mV; $F_{1.4,20}$ = 4.162, p = 0.0420*, n = 15, one-way RM ANOVA with post-hoc Tukey's test, which reveals no significant differences between treatments), although there was a slight decrease in AP half-width with atropine compared to the baseline (**Figure 3G**; Atro = 1.24 ± 0.08 ms; $F_{1.7,24}$ = 4.099, p = 0.0339*, n = 15, one-way RM ANOVA with post-hoc Tukey's test, Base vs. Carb: p = 0.4671, Base vs. Atro: p = 0.0482*, Carb vs. Atro: p = 0.1611). The only AP shape parameter not completely reversed by Vm restitution was AP amplitude, which still showed a slight reduction during carbachol treatment but not atropine treatment (**Figure 3F**; Carb = 59.55 ± 1.31 mV, Atro = 60.58 ± 1.39 mV; $F_{1.7,23}$ = 7.163, p = 0.0055**, n = 15, one-way RM ANOVA with post-hoc Tukey's test, Base vs. Carb: p = 0.0091**, Base vs. Atro: p = 0.2516, Carb vs. Atro: p = 0.0577). This reduction in the AP amplitude was however much smaller

(3.3% decrease) compared to that when Vm changes were uncompensated (14.5% decrease).

The kinetics of afterhyperpolarization (AHP) were also analyzed. In DA neurons, AHP kinetics are regulated by SK and HCN channels and can influence firing patterns. Consistent with previous reports (Richards *et al.*, 1997), DA neurons exhibit prominent AHP with an average peak amplitude of −25.54 ± 0.83 mV and an average duration of 16.56 ± 1.23 ms. During carbachol application, the AHP amplitude and duration were apparently reduced (**Figure 3A, left panel**). However, when the Vm changes were offset via current injection, both AHP amplitude (**Figure 3H**; Carb = −25.61 ± 0.87 mV) and duration (**Figure 3I**; Carb = 16.12 ± 0.99 ms;) were restored to the baseline values. The kinetics of AHP only exhibited significant changes during atropine application, when there was a small but significant reduction in AHP amplitude (**Figure 3H**; Atro = −24.14 ± 0.82 mV; $F_{1.9,27}$ = 23.27, $p < 0.0001$****, n = 15, one-way RM ANOVA with post-hoc Tukey's test, Base vs. Carb: $p = 0.9438$, Base vs. Atro: $p = 0.0002$***, Carb vs. Atro: $p = 0.0001$***) and a large increase in the variability of AHP duration that resulted in a longer mean duration (**Figure 3I**; Atro = 24.52 ± 3.11 ms; $F_{1.0,15}$ = 8.694, $p = 0.0096$**, n = 15, one-way RM ANOVA with post-hoc Tukey's test, Base vs. Carb: $p = 0.6687$, Base vs. Atro: $p = 0.0242$*, Carb vs. Atro: $p = 0.0271$*). Taken together, these results showed that the effects of carbachol on firing frequency and AP shape were secondary to Vm depolarization. Although post-translational modifications and Gq/Ca^{2+}-induced modulation of ion channels may influence the carbachol effects on AP shape, the fact that these effects were fully reversed by current injection strongly suggests that changes in a voltage-insensitive conductance would be responsible for the carbachol-induced excitation.
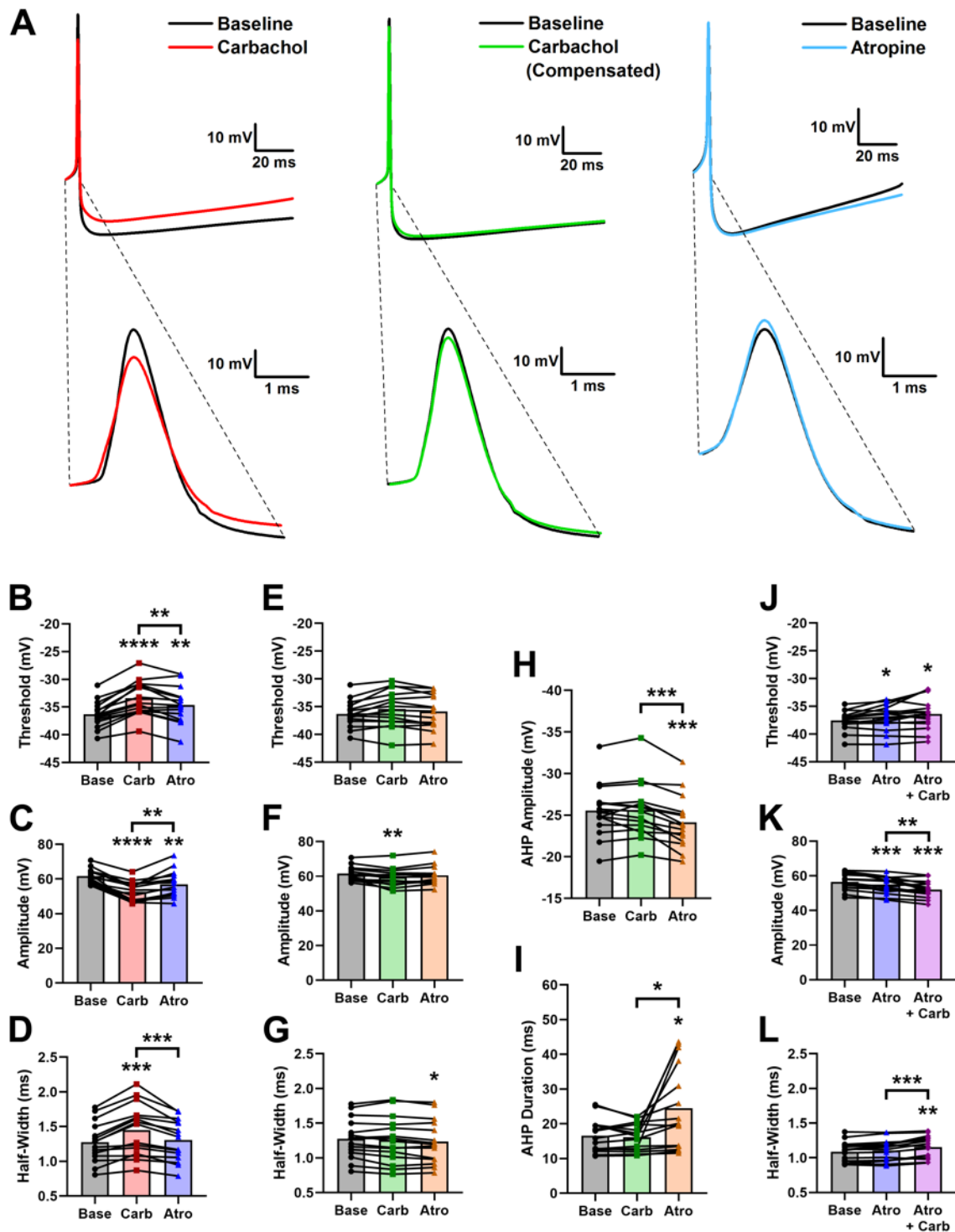
Figure 3. The muscarinic excitation was accompanied by alterations in action potential (AP) shape, effects that were reversed when membrane potential changes were compensated.
(A) Average AP waveforms in 1-min intervals of VTA DA neuron spontaneous firing in baseline (black) and after treatment with carbachol (red), membrane potential compensated by current injection in the presence of carbachol (green), and a different cell in baseline and after

application of atropine (blue). **(B)** Carbachol application raised AP threshold, **(C)** reduced AP amplitude, and **(D)** increased AP half-width. Atropine reversed most of the carbachol-induced effects on AP shape, which were also different from the baseline except AP half-width. **(E, F, G)** Most effects of carbachol on AP shape were eliminated when the membrane potential was restituted to baseline levels using the clamping circuit. Carbachol-induced positive shift in AP threshold and broadening of AP half-width were fully reversed by current injection. The AP amplitude reduction was partially reversed. **(H, I)** Carbachol had no effects on the amplitude and duration of afterhyperpolarization (AHP) when membrane potential changes were compensated. However, there were significant changes in the AHP amplitude and duration during atropine treatment. **(J, K, L)** Atropine pretreatment had minimal effects on AP shape and blocked most of the effects of carbachol, although there were progressive positive shift in the AP threshold, reduction in the AP amplitude, and broadening of AP half-width. ($*$ $p <$ 0.05; $**$ $p < 0.01$; $***$ $p < 0.001$; $****$ $p < 0.0001$)

Activation of muscarinic receptors does not alter most intrinsic membrane properties

Previous work suggested that inhibition of voltage-gated potassium channels or calcium-activated potassium channels may underlie muscarinic excitation of DA neurons (Lacey *et al.*, 1990; Kitai *et al.*, 1999). Furthermore, Gq signaling has been shown to activate HCN channels in DA neurons (Goertz *et al.*, 2015). To determine whether these ion channel mechanisms are involved in carbachol-induced excitation, we performed current step experiments to assess changes in intrinsic membrane properties (**Figure 4A, B**). First, we examined whether mAChR activation alters the sag ratio, a conventional method for measuring HCN channel activity by injection of a hyperpolarizing current step. Bath perfusion of carbachol and atropine had no effect on the sag ratio evoked by the −200 pA step (**Figure 4C**; Base = 0.495 ± 0.025, Carb = 0.523 ± 0.028, Atro = 0.533 ± 0.030; $F_{1.4,11}$ = 2.981, p = 0.1037, n = 9, one-way RM ANOVA).

Spike frequency adaptation ratio (FAR) and frequency-current (f-I) relationship were also examined using the current step protocol. Those properties are affected by changes in potassium conductances, including currents through SK channels and voltage-gated K^+ channels, and correlate with spontaneous firing frequency and firing pattern in DA neurons (Vandecasteele *et al.*, 2011; Kimm *et al.*, 2015). Carbachol and the subsequent atropine treatment did not affect the FAR (**Figure 4D**; Base = 0.717 ± 0.051, Carb = 0.652 ± 0.052, Atro = 0.636 ± 0.084; $F_{1.2,8.2}$ = 1.401, p = 0.2779, n = 8, one-way RM ANOVA) or the average stimulated firing frequency during the +200 pA step, which represents the highest point on a f-I relationship plot (**Figure 4E**; Base = 7.76 ± 0.85 Hz, Carb = 8.29 ± 0.95 Hz, Atro = 8.11 ± 0.76 Hz; $F_{1.3,11}$ = 1.010, p = 0.3629, n = 9, one-way RM ANOVA). Hence, the current step experiments suggest that the participation of HCN and potassium channels in carbachol-induced excitation is unlikely.
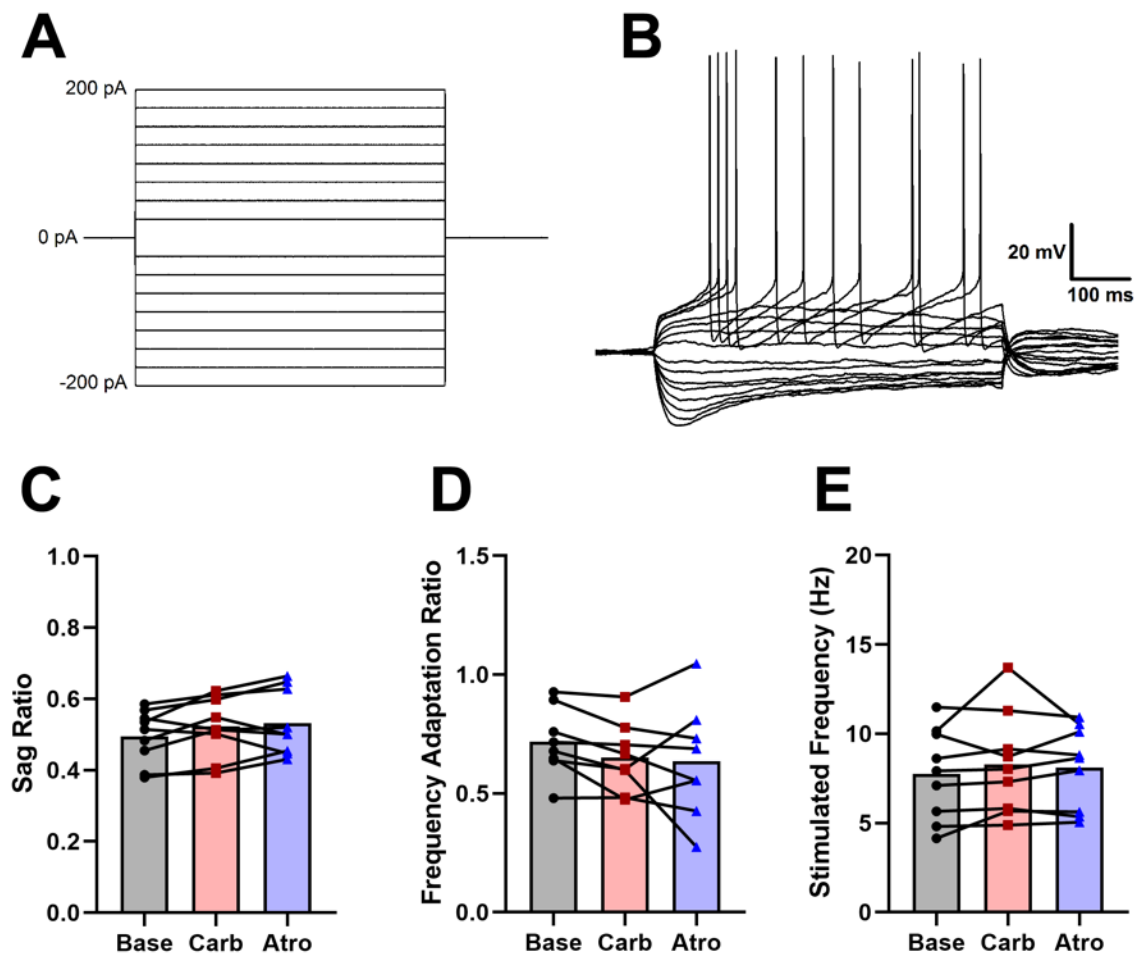
Figure 4. Activation of muscarinic receptors had no effects on sag ratio, frequency adaptation ratio (FAR), and frequency-current (f-I) relationship. (A) The current step protocol (600-ms, from −200 pA to +200 pA, 25 pA each step). **(B)** Representative voltage response of a VTA DA neuron evoked by the current step protocol. **(C)** Carbachol had no effects on sag ratio evoked by the −200 pA step. **(D)** Carbachol had no effects on spike frequency adaptation ratio. **(E)** Carbachol had no effects on the stimulated firing frequency during the +200 pA step.

Muscarinic stimulation does not affect inhibitory synaptic inputs in VTA DA neurons

VTA DA neurons are tonically inhibited by GABAergic afferents (Westerink *et al.*, 1996; Theile *et al.*, 2011), a major source being the local GABAergic interneurons (Polter *et al.*, 2018). Interestingly, previous work reported that VTA GABAergic neurons express the M3 mAChR and are excited by muscarinic stimulation (Michel *et al.*, 2004; Michel *et al.*, 2005). Conversely, there was a report that optogenetic stimulation of cholinergic terminals in the VTA inhibits GABAergic neuron activity (Coimbra *et al.*, 2021). Since the results here show that activation of mAChRs had minimal effects on the intrinsic membrane properties or AP kinetics in DA neurons, we speculated that carbachol may modulate DA neuron excitability via stimulating the mAChRs on GABAergic neurons and altering inhibitory synaptic inputs to the DA neurons. To test this possibility, a whole-cell voltage-clamp experiment was performed to record spontaneous inhibitory post-synaptic currents (sIPSCs) in VTA DA neurons during bath perfusion of muscarinic agents (**Figure 5A**). A Cs-based low-chloride intracellular solution with the strong Ca^{2+} chelator BAPTA and the membrane-impermeant voltage-gated Na^+ channel blocker QX-314 was used to block most ion channels in the DA neurons (see methods). No synaptic blockers were added to the bath solution to minimize disruption of tonic synaptic activity. In order to minimize excitatory post-synaptic currents, sIPSCs were recorded by clamping the cells at +15 mV, the reversal potential of ionotropic glutamate receptor currents. Surprisingly, carbachol and the subsequent atropine treatment affected neither the average frequency (**Figure 5B**; Base = 10.85 ± 1.73 Hz, Carb = 12.12 ± 2.05 Hz, Atro = 12.96 ± 2.32 Hz; $F_{1.4,21}$ = 4.358, p = 0.0369*, n = 16, one-way RM ANOVA with post-hoc Tukey's test, which reveals no significant differences, Base vs. Carb: p = 0.1886, Base vs. Atro: p = 0.0829, Carb vs. Atro: p = 0.2528) nor the average amplitude of sIPSC events (**Figure 5C**; Base = 27.01 ± 1.28 pA, Carb = 27.89 ± 1.43 pA, Atro = 26.27 ± 1.40 pA; $F_{1.7,26}$ = 5.072, p = 0.0171*, n = 16, one-

way RM ANOVA with post-hoc Tukey's test, which reveals a difference only between Carb and Atro, Base vs. Carb: p = 0.2604, Base vs. Atro: p = 0.4217, Carb vs. Atro: p = 0.0029**). These results showed that mAChR stimulation does not affect the fast inhibitory synaptic inputs to DA neurons, consistent with a direct effect of carbachol on the DA neurons.
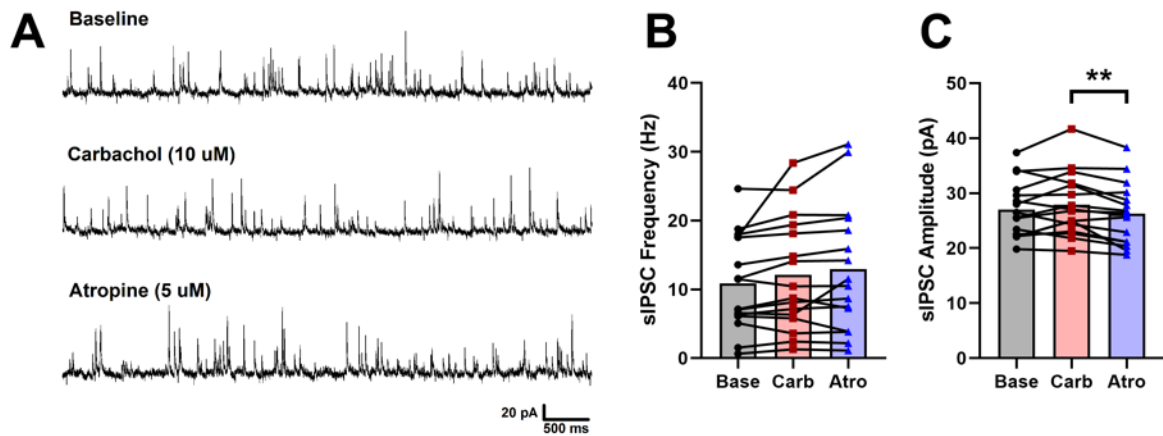
Figure 5. Muscarinic receptor stimulation had no effects on spontaneous inhibitory postsynaptic currents (sIPSCs) in VTA DA neurons. (A) Representative trace of sIPSCs in a VTA DA neuron in baseline and after carbachol and atropine application. sIPSCs were recorded as outward currents by holding the membrane potential at +15 mV. **(B)** Carbachol did not affect the average frequency and **(C)** amplitude of sIPSCs in 3-minute intervals. (** $p < 0.01$)

Muscarinic receptors depolarize VTA DA neurons via a TTX-insensitive cationic conductance

Our results suggest that membrane potential depolarization accounts for most of the mAChR-induced effects at firing frequency and AP shape in VTA DA neurons. Therefore, we sought to quantify the Vm depolarization and changes in input resistance (Ri) in the absence of spontaneous firing activity. TTX (500 nM) was perfused in bath to silence spiking and revealed low-amplitude calcium-dependent oscillations around a mean resting Vm of -44.43 ± 0.52 mV (n = 65). Under this condition, bath perfusion of carbachol caused an average depolarization of 2.68 ± 0.38 mV from the baseline potential -45.22 ± 0.80 mV to -42.53 ± 0.65 mV. This depolarization was fully revered by atropine to -44.98 ± 0.70 mV (**Figure 6A, C**; Fr = 42.25, p < 0.0001****, n = 32, Friedman test with post-hoc Dunn's test: Base vs. Carb: p < 0.0001, Base vs. Atro: p > 0.9999, Carb vs. Atro: p < 0.0001****). In agreement with the observations from the whole-cell current-clamp experiments depicted in **Figure 2 & 3**, the carbachol-induced depolarization was persistent and did not appear to desensitize. In a separate set of cells pre-treated with atropine, atropine alone had no effects on Vm. This atropine pretreatment blocked most of the carbachol-induced depolarization. (**Figure 6B, E**; Base = -43.66 ± 0.66 mV, Atro = -44.08 ± 0.75 mV, Atro + Carb = -43.53 ± 0.67 mV; $F_{1.8,59}$ = 3.359, p = 0.0453*, n = 33, one-way RM ANOVA with post-hoc Tukey's test, which reveals a difference only between Atro and Atro + Carb, Base vs. Atro: p = 0.0927, Base vs. Atro + Carb: p = 0.8535, Atro vs. Atro + Carb: p = 0.0453*). All of the cells tested appeared to be DAergic neurons expressing the inhibitory D2 autoreceptor, since they showed strong hyperpolarization (~-20 mV) when exposed to DA (60 μM).

A small hyperpolarizing current step was injected every 22 s to assess the input resistance throughout the experiment. Accompanying the Vm depolarization, carbachol induced a

significant decrease in Ri by 106.5 ± 20.31 MΩ, which showed partial reversal by atropine

(**Figure 6D**; Base = 320.2 ± 28.49 MΩ, Carb = 213.6 ± 15.78 MΩ, Atro = 250.8 ± 19.00 MΩ;

$F_{1.3,20}$ = 23.32, p < 0.0001****, n = 16, one-way RM ANOVA with post-hoc Tukey's test, Base

vs. Carb: p = 0.0003***, Base vs. Atro: p = 0.0011**, Carb vs. Atro: p = 0.0065**). In contrast,

atropine alone had no significant effects on Ri, although there was a small reduction of Ri

during the following co-treatment of atropine and carbachol (**Figure 6F**; Base = 278.6 ± 34.87

MΩ, Atro = 263.9 ± 32.08 MΩ, Atro + Carb = 238.0 ± 27.32 MΩ; Fr = 14.00, p = 0.0009***, n =

16, Friedman test with post-hoc Dunn's test, Base vs. Atro: p > 0.9999, Base vs. Atro + Carb: p

= 0.0012**, Atro vs. Atro + Carb: p = 0.0140*). The decrease in Ri induced by carbachol

suggests opening of ion channels, which is inconsistent with excitation mediated by inhibition

of potassium conductances. In our experimental settings, the intracellular and extracellular

ionic concentrations correspond to a theoretical potassium reversal potential at −103.56 mV,

a chloride reversal potential at −73.16 mV, a sodium reversal potential at 80.23 mV, and a

calcium reversal potential at 124.30 mV. Since the DA neurons have a resting Vm around −44

mV, the opening of K^+ or Cl^- channels would result in hyperpolarization, whereas the opening

of Na^+ or Ca^{2+} channels would result in depolarization. Therefore, the results here suggest that

activation of a TTX-insensitive cation current, rather than inhibition of potassium current or

activation of chloride current, produces the main ionic conductance underling muscarinic

excitation of VTA DA neurons.
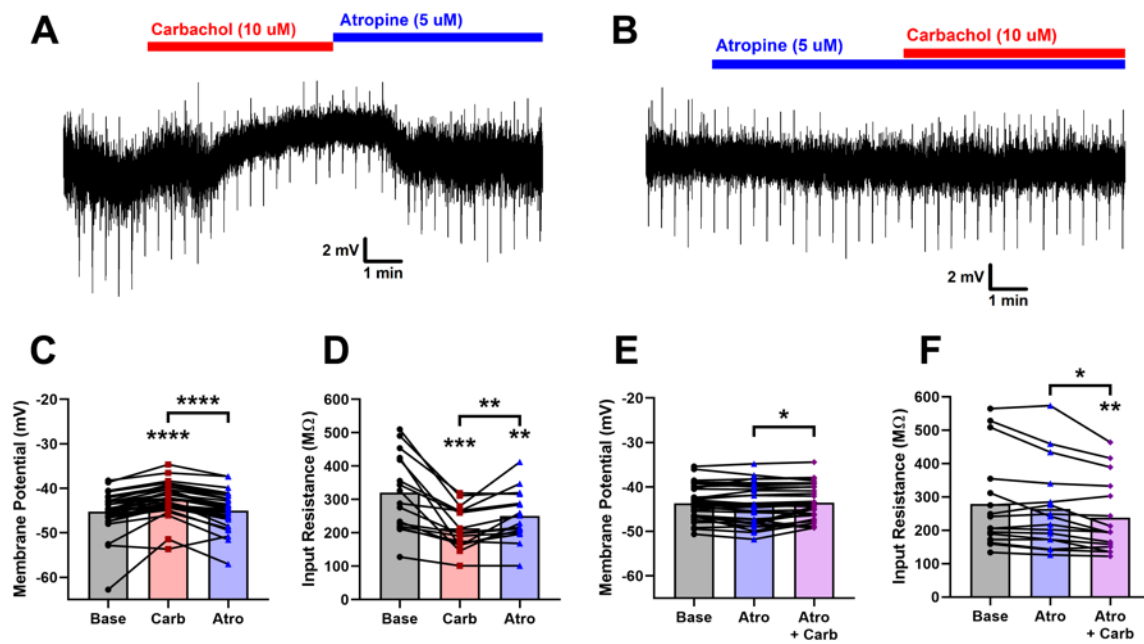
Figure 6. Activation of muscarinic receptors depolarized membrane potential and decreased input resistance in the presence of tetrodotoxin (TTX). (A, B) Representative whole-cell current-clamp recordings of VTA DA neurons with continuous bath application of the voltage-gated sodium channel blocker TTX, treated with carbachol or atropine in the labeled respective order. A small current step was injected every 22 seconds to assess the input resistance. **(C)** Carbachol depolarized membrane potential and **(D)** decreased input resistance. **(E)** Atropine pretreatment prevented the effects of carbachol on membrane potential and **(F)** input resistance. (* $p < 0.05$; ** $p < 0.01$; *** $p < 0.001$; **** $p < 0.0001$)

Muscarinic receptors activate TRPC-like currents in VTA DA neurons

To further determine the ionic composition of the carbachol-activated conductance in VTA DA neurons, we tested the sensitivity of carbachol-induced current to non-selective blockers of Na^+, Ca^{2+}, and K^+ channels using the whole-cell voltage-clamp technique. When held at a constant Vm of −60 mV, all the DA neurons recorded exhibited a negative holding current with an average amplitude of −119.4 ± 8.1 pA (n = 42). TTX (500 nM) was perfused throughout all recordings to inhibit synaptic activities. TTX alone had no effects on the holding current, which only changed by 4.0 ± 1.2 pA (n = 11) after the toxin was added. Under this condition, bath perfusion of carbachol induced an inward current of −46.96 ± 5.51 pA, which was completely blocked by atropine (**Figure 7A**; n = 11). When a separate set of DA neurons was treated with the K^+ channel blocker tetraethylammonium (TEA, 20 mM), there was a visible change in the holding current (by 32.9 ± 7.7 pA, n = 7). Since the blocker alone caused a difference in the baseline current, DA neurons were pretreated with TEA before the co-treatment of TEA and carbachol to assess the degree of blockage more accurately (changes in the holding current induced by different blockers are summarized in **Figure 7E**). Co-treatment with TEA completely eliminated the carbachol-induced inward current (compare **Figure 7B** vs. **Figure 7A**; I_{Carb} in TEA = 0.44 ± 1.25 pA, n = 7). Pretreating DA neurons with Cs^+ (10 mM), another blocker of K^+ channels, caused a drastic change in the holding current (by 60.6 ± 15.8 pA, n = 9). This inhibition of the inward holding current is likely due to blockage of HCN channels. Bath perfusion of carbachol in the presence of Cs^+ induced an inward current (**Figure 7C**; I_{Carb} in Cs^+ = −76.67 ± 13.64 pA, n = 9) that was not significantly different from the control current. Finally, a set of cells was pretreated with Cd^{2+} (200 μM), a blocker of voltage-gated Ca^{2+} channels, which also produced a change in the holding current (by 23.5 ± 3.8 pA, n = 8). In the presence of Cd^{2+}, the carbachol-induced current (**Figure 7D**; I_{Carb} in Cd^{2+} = −18.34 ± 6.62 pA, n = 8) was significantly different from that in Cs^+, but not different from that in TEA and the control

condition, indicating a partial blockage. The average amplitudes of I_{Carb} in different blockers and the *post-hoc* comparisons are summarized in **Figure 7F** ($H_3 = 24.86$, $p < 0.0001****$, $n_{Carb} = 11$, $n_{TEA} = 7$, $n_{Cs+} = 9$, $n_{Cd2+} = 8$, Kruskal-Wallis test with post-hoc Dunn's test, Carb vs. TEA + Carb: $p = 0.0009***$, Carb vs. Cs^+ + Carb: $p > 0.9999$, Carb vs. Cd^{2+} + Carb: $p = 0.2624$, TEA + Carb vs. Cs^+ + Carb: $p < 0.0001****$, TEA + Carb vs. Cd^{2+} + Carb: $p = 0.5119$, Cs^+ + Carb vs. Cd^{2+} + Carb: $p = 0.0242*$)
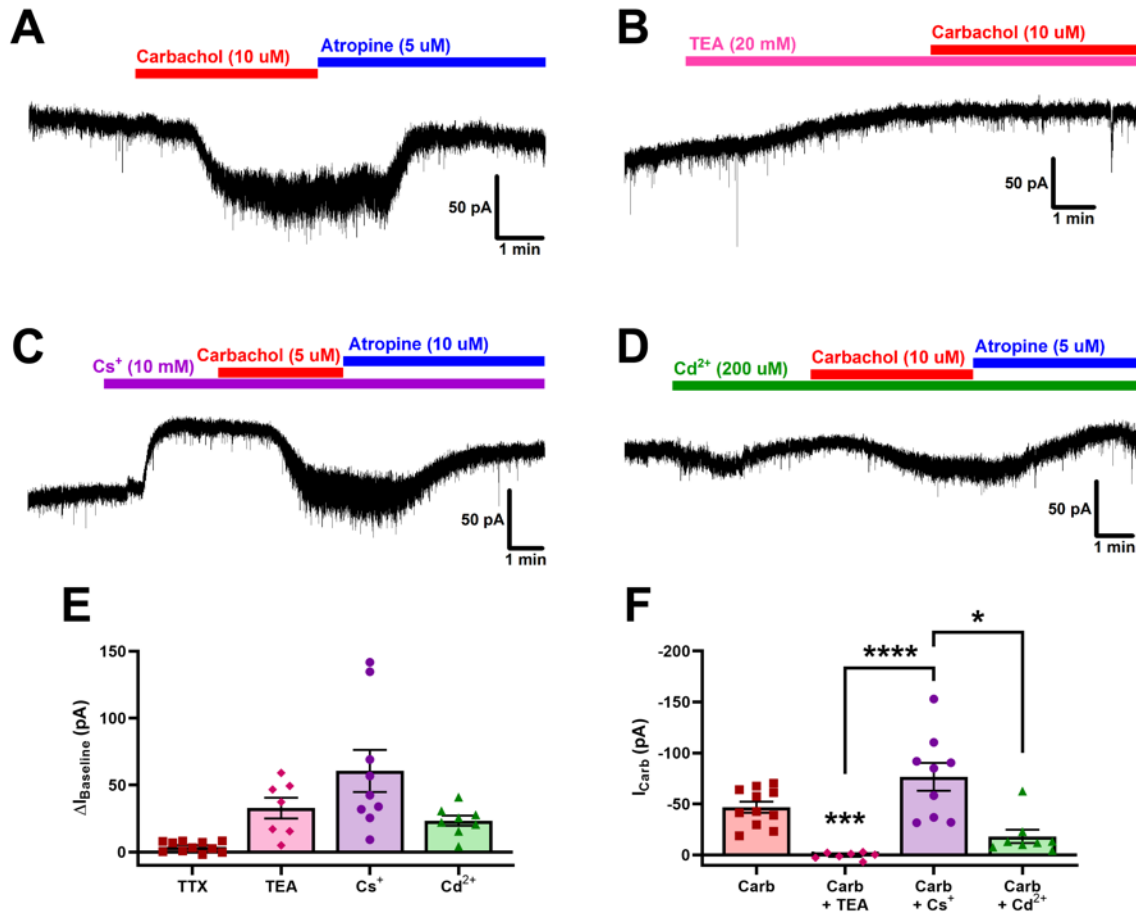
Figure 7. Inhibition of carbachol-induced inward current by non-selective ion channel blockers. (A) Representative whole-cell voltage-clamp recording showing carbachol application induced a TTX-insensitive inward current that was blocked by atropine. **(B)** Pretreatment with TEA (20 mM) completely blocked the carbachol current. **(C)** Pretreatment with Cs$^+$ (10 mM) had no effects on the carbachol current, which was not different from control but larger than in TEA. **(D)** Pretreatment with Cd^{2+} (200 μM) caused a partial blockage of the carbachol current that was not different from control and in TEA but smaller than in Cs$^+$. **(E)** Summary graph showing changes in the amplitudes of holding current by the ion channel blockers alone. **(F)** Summary graph showing the amplitudes of carbachol-induced current in the presence of the ion channel blockers. The asterisks denote statistical differences from control (Carb with no blockers), unless indicated by brackets (* $p < 0.05$; *** $p < 0.001$; **** $p < 0.0001$).

The induction of carbachol current correlated with an increase of noise in the current traces. Whole-cell current is the summed activities of all single channels. The openings and closings are rapid flickering and stochastic events that produce fluctuations in the macroscopic currents (Alvarez *et al.*, 2002). Therefore, the amplitude of noise is a fair estimation of channel activities. To quantify the noise, current traces from 10-sec intervals were plotted as frequency histograms and fitted to Gaussian distribution (**Figure 8A**). In the control condition, carbachol produced a robust increase in the standard deviation (SD) of current fluctuations, which was reversed by atropine to the baseline value (**Figure 8B**; Base = 3.25 ± 0.16 pA, TTX = 3.26 ± 0.14 pA, Carb = 7.19 ± 0.79 pA, Atro = 3.60 ± 0.17 pA; $F_{1.0,10}$ = 30.94, p < 0.0002***, n = 11, one-way RM ANOVA with post-hoc Tukey's test, Base vs. TTX: p = 0.9988, Base vs. Carb: p = 0.0010**, Base vs. Atro: p = 0.0009***, TTX vs. Carb: p = 0.0009***, TTX vs. Atro: p = 0.0008***, Carb vs. Atro: p = 0.0015**).

Along with complete inhibition of the carbachol-induced current, TEA eliminated the carbachol-induced current noise (**Figure 8C**; Base = 3.65 ± 0.24 pA, TEA = 3.35 ± 0.22 pA, TEA + Carb = 3.19 ± 0.17 pA; Fr = 12.29, p = 0.0003***, n = 7, Friedman test with post-hoc Dunn's test, Base vs. TEA: p = 0.0975, Base vs. TEA + Carb: p = 0.0015**, TEA vs. TEA + Carb: p = 0.5443). In fact, there was a small but significant reduction in noise with continuous TEA perfusion relative to baseline even after carbachol was added, suggesting slow inhibition of ion channels. In contrast, the levels of noise induced by carbachol were unaffected by the presence of Cs^+ but was subsequently blocked by atropine (**Figure 8D**; Base = 3.23 ± 0.21 pA, Cs^+ = 3.21 ± 0.29 pA, Cs^+ + Carb = 8.37 ± 1.66 pA, Cs^+ + Atro = 3.55 ± 0.41 pA; Fr = 12.77, p = 0.0052**, n = 7, Friedman test with post-hoc Dunn's test, Base vs. Cs^+: p > 0.9999, Base vs. Cs^+ + Carb: p = 0.0225*, Base vs. Cs^+ + Atro: p > 0.9999, Cs^+ vs. Cs^+ + Carb: p = 0.0114*, Cs^+ vs. Cs^+ + Atro: p > 0.9999, Cs^+ + Carb vs. Cs^+ + Atro: p = 0.0427*). In the presence of Cd^{2+}, carbachol was still able to increase noise significantly, although the subsequent atropine-induced

inhibition did not reach statistical significance (**Figure 8E**; Base = 3.64 ± 0.24 pA, Cd^{2+} = 3.51 ± 0.30 pA, Cd^{2+} + Carb = 5.62 ± 0.38 pA, Cd^{2+} + Atro = 3.95 ± 0.24 pA; Fr = 17.55, p = 0.0005***, n = 8, Friedman test with post-hoc Dunn's test, Base vs. Cd^{2+}: p > 0.9999, Base vs. Cd^{2+} + Carb: p = 0.0060**, Base vs. Cd^{2+} + Atro: p > 0.9999, Cd^{2+} vs. Cd^{2+} + Carb: p < 0.0006***, Cd^{2+} vs. Cd^{2+} + Atro: p = 0.4882, Cd^{2+} + Carb vs. Cd^{2+} + Atro: p = 0.1990), suggesting the carbachol-induced noise is smaller in Cd^{2+} compared to control. In our experimental conditions, none of the ion channel blockers changed the baseline noise level after 5 min of treatment, even though they produced changes in the holding current.

When the changes in carbachol-induced noise in the presence of different blockers were compared against one another, the noise increase in TEA was significantly smaller than both control and Cs^+ conditions. Noise increase in Cs^+ was not significantly different from control, while in Cd^{2+} was not significantly different from any other treatment, suggesting no blockage by Cs^+ and partial blockage by Cd^{2+}. The data and the *post-hoc* comparisons are summarized in **Figure 8F** (Carb = 3.93 ± 0.69 pA, TEA + Carb = -0.47 ± 0.12 pA, Cs^+ + Carb = 5.15 ± 1.57 pA, Cd^{2+} + Carb = 1.99 ± 0.32 pA; H_3 = 19.34, p = 0.0002***, n_{Carb} = 11, n_{TEA} = 7, n_{Cs+} = 7, n_{Cd2+} = 8, Kruskal-Wallis test with post-hoc Dunn's test, Carb vs. TEA + Carb: p = 0.0005***, Carb vs. Cs^+ + Carb: p > 0.9999, Carb vs. Cd^{2+} + Carb: p = 0.6909, TEA + Carb vs. Cs^+ + Carb: p = 0.0011**, TEA + Carb vs. Cd^{2+} + Carb: p = 0.1382, Cs^+ + Carb vs. Cd^{2+} + Carb: p = 0.6836). In summary, the degrees of inhibition of the current noise by the blockers are consistent with inhibition of the current amplitude. The increase in current fluctuations with carbachol application suggests increased channel activities. Since the macroscopic current (I) is the product of the single-channel current (i), the number of channels (N), and the open probability of the channel (P_o), or I = iNP_o (Alvarez *et al.*, 2002), the effects of carbachol could be mediated by increased probability of channels opening, plasma membrane insertion of channels, increase in the unitary conductance of the channels, or a combination of these mechanisms.
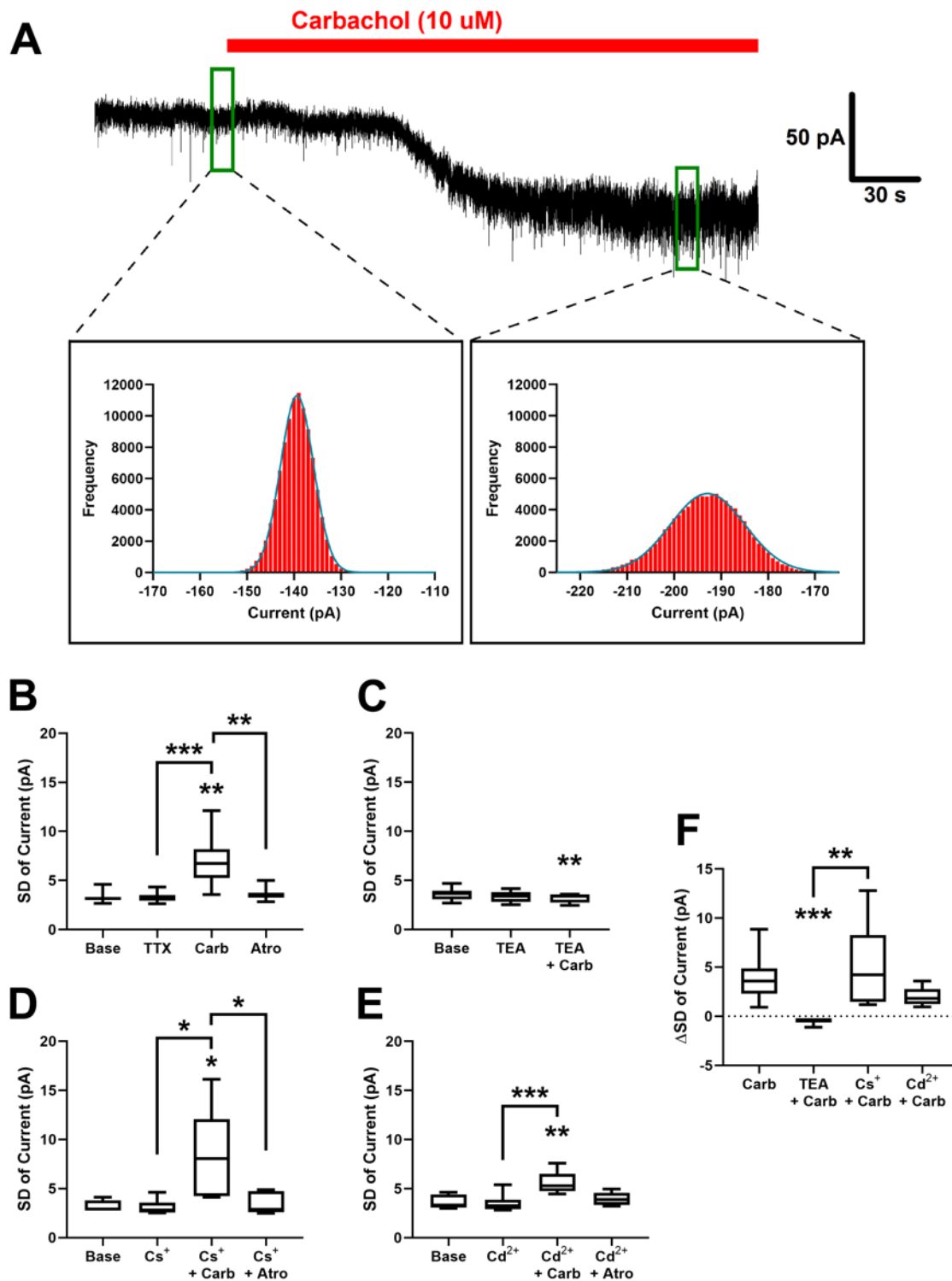
Figure 8. Inhibition of carbachol-induced noise in the whole-cell current by non-selective ion channel blockers. (A) Representative whole-cell voltage-clamp trace showing the carbachol-induced inward current was accompanied by an increase of noise in the recordings. The amplitudes of noise were quantified by plotting the current fluctuations in 10-s intervals

as frequency histograms and fitting the histograms to Gaussian distribution. **(B)** Carbachol induced an increase in the standard deviation (SD) of current fluctuations that was blocked by atropine. **(C)** Pretreatment with TEA (20 mM) completely inhibited the carbachol-induced noise. **(D)** Pretreatment with Cs^+ (10 mM) did not inhibit the carbachol-induced noise. **(E)** Pretreatment with Cd^{2+} (200 μM) also did not inhibit the carbachol-induced noise. **(F)** Summary graph showing changes in the current noise (noise in the blockers alone subtracted from noise in carbachol) in the presence of different blockers. The data are consistent with complete blockage of the noise by TEA, no blockage by Cs^+, and partial blockage by Cd^{2+}. The asterisks denote statistical differences from baseline (Base) or control (Carb with no blockers), unless indicated by brackets (* $p < 0.05$; ** $p < 0.01$; *** $p < 0.001$).

This pharmacological profile shows that HCN channels, which are expected to be blocked by Cs^+, and voltage-gated Ca^{2+} channels, which should be completely blocked by Cd^{2+} but unaffected by TEA, are unlikely to underlie the carbachol-induced current, suggesting that another, as yet unidentified channel is required. Interestingly, previous work showed that Cd^{2+} inhibited TRPC6 channels with an IC_{50} of ~210 μM (Inoue *et al.*, 2001), comparable to the concentration used here. In addition, TEA was found to block TRPC and TRPV channels (Larsson *et al.*, 2005; Rivera-Acevedo *et al.*, 2012), while Cs^+ permeates TRP channels and does not cause blockage (McKemy *et al.*, 2002; Feng, 2017). Therefore, members of the TRP channel family are potential candidates mediating the carbachol-induced current. To test this possibility, a set of DA neurons were treated with carbachol to induce a robust inward current and current noise, followed by the co-treatment of carbachol with BTP2 (5 μM), a blocker of TRPC channels (**Figure 9A**). The inhibition kinetics of BTP2 was slow and required 10 min. of incubation to reach maximum effect, as previously observed (He *et al.*, 2005). After ~10 min of bath perfusion, BTP2 significantly reduced the amplitude of carbachol current from −116.2 ± 29.88 to −32.33 ± 11.70 pA (**Figure 9B**; t_6 = 3.02, p = 0.0117*, n = 7, paired t-test), corresponding to 67.0 ± 8.6% inhibition. The carbachol activation caused a significant increase in the standard deviation of current noise from 3.56 ± 0.19 to 14.78 ± 2.74 pA. Co-treatment with BTP2 reduced the noise amplitude to 6.55 ± 1.24 pA, which was not significantly different from either the baseline or carbachol alone, consistent with partial blockage (**Figure 9C**; Fr = 14.00, p < 0.0001****, n = 7, Friedman test with post-hoc Dunn's test, Base vs. Carb: p = 0.0005***, Base vs. Carb + BTP2: p = 0.1841, Carb vs. Carb + BTP2: p = 0.1841). These results showed that a major component of the carbachol-induced current and increase in channel activities is sensitive to BTP2, a relatively selective blocker of the TRPC subfamily. Taken together, evidence from the present study suggests that activation of a cationic conductance involving TRPC channels is a main mechanism underlying muscarinic excitation of VTA DA neurons.
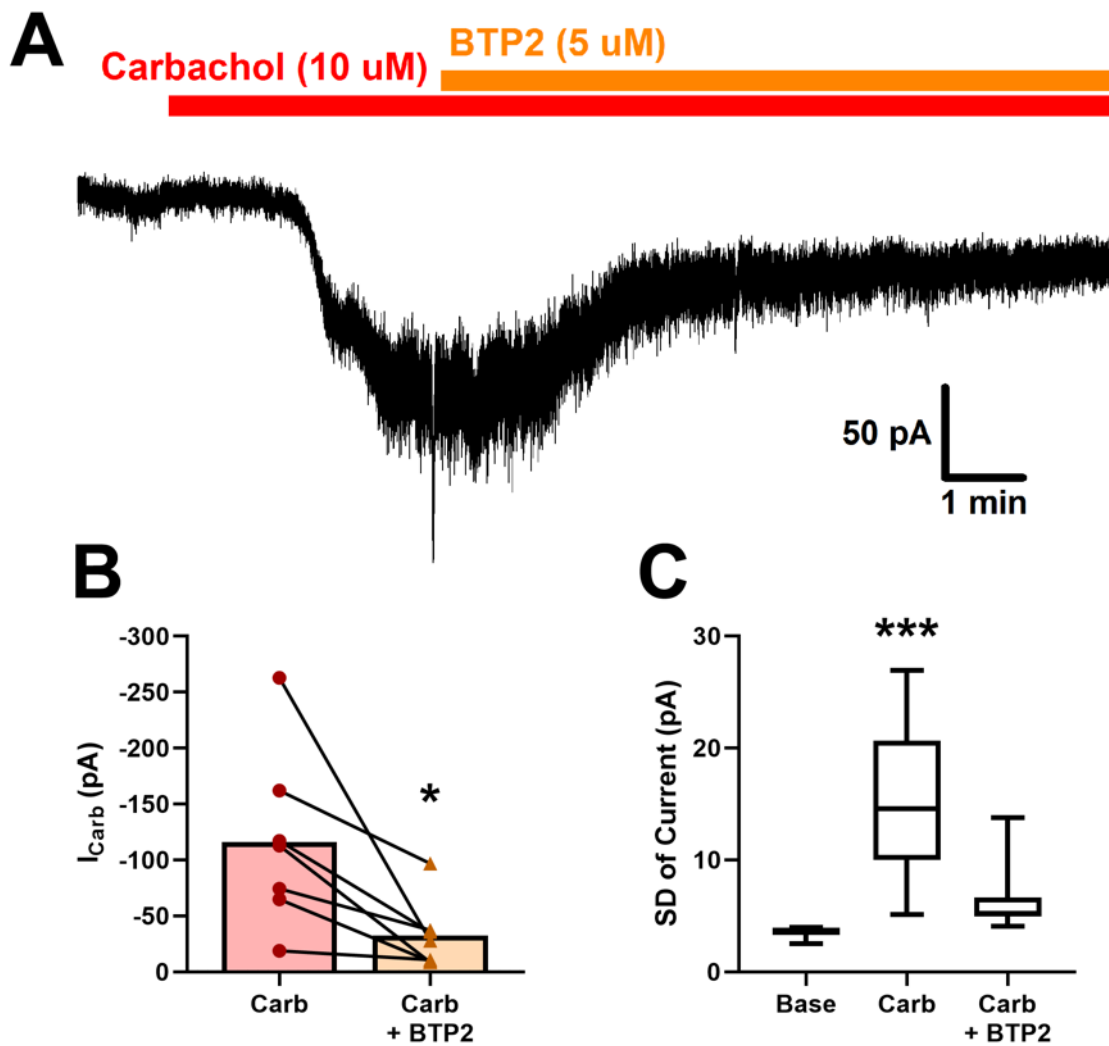
Figure 9. Inhibition of carbachol-induced whole-cell current and current noise by a TRPC channel blocker. (A) Representative whole-cell voltage-clamp recording showing inhibition of carbachol-induced inward current by BTP2 (5 μM), a blocker of TRPC channels. **(B)** BTP2 inhibited a major component (67.0 ± 8.6%) of the carbachol-induced inward current. **(C)** BTP2 caused a partial reduction in the carbachol-induced noise in the macroscopic currents. (* p < 0.05; *** p < 0.001)

DISCUSSION

Cholinergic afferents originated in the PPT and LDT provide a major source of excitatory drive to midbrain DA neurons. Activation of mAChRs on VTA DA neurons increases excitability and is heavily implicated in reward and addiction-related behaviors. Here, we provide the first evidence that a cationic conductance consistent with TRPC channel activation participates in muscarinic excitation of VTA DA neurons. Our data show that the main effect of mAChR agonism in VTA DA neurons is a persistent membrane potential depolarization concomitant with a decrease in input resistance, whereas the shape of action potentials is changed because of the membrane depolarization. The mAChR-induced depolarization is correlated with activation of an inward current that exhibits a pharmacological profile suggestive of TRPC channels. In addition, our data support a direct effect of muscarinic inputs on the DA neurons as inhibitory synaptic currents are not altered by muscarinic stimulation. The consequence of this muscarinic depolarization is an increase of pacemaking frequency without changes in the firing pattern. While the involvement of other ion channel mechanisms is not completely excluded, the results here suggest that HCN channels, SK channels, voltage-gated K^+ channels, voltage-gated Ca^{2+} channels, and NALCN are unlikely to be mediators of this excitation. Thus, we identified TRPC channels as a likely downstream effector of muscarinic signaling that provide a non-selective cationic current to increase the excitability of VTA DA neurons.

DA neurons of the lateral VTA and physiological implications

DA neurons of the VTA comprise subpopulations with heterogenous biochemical properties, electrophysiological characteristics, and projection targets. While there is no distinct boundary between the SNc and VTA, the mesostriatal DA system is arranged in a dorsolateral-

ventromedial topography (Wise, 2009; Burton *et al.*, 2015). Located laterally relative to the VTA, the SNc receive cholinergic inputs from the PPT and send DAergic projections to the dorsal striatum, both of which are laterally located. VTA predominantly receive cholinergic inputs from the more medially located LDT and project to the NAc (Baik, 2020). Within the VTA, DA neurons of the medial VTA are more heterogenous in their firing properties and project to the medial NAc and the prefrontal cortex, whereas DA neurons of the lateral VTA selectively project to the lateral NAc and possess intermediate properties between the VTA and SNc (Roeper, 2013; Baik, 2020). Here, the majority of DA neurons studied are located in the lateral VTA, in close proximity to the SNc. These DA neurons exhibit "conventional" SN-like electrophysiological characteristics including slow pacemaking, broad AP width, prominent voltage sag, delayed evoked firing, and sensitivity to DA (Lammel *et al.*, 2008; Roeper, 2013) that were used as selection criteria. Those properties indicate expression of HCN channels, A-type K^+ channels, and D2 autoreceptors. The M5 mAChR is the primary muscarinic receptor subtype expressed on midbrain DA neurons (Vilaro *et al.*, 1990; Weiner *et al.*, 1990; Reever *et al.*, 1997; Garzon & Pickel, 2013). Previous studies have shown that there is a lateral-medial gradient of M5 mAChR expression, which is more concentrated in the SNc and lateral VTA compared to the medial VTA (Gould *et al.*, 2019). In the cell bodies of midbrain DA neurons, the M5 mAChR is highly co-expressed with the D2 receptor (Vilaro *et al.*, 1990; Weiner *et al.*, 1990). This suggests that the expression of M5 mAChR is correlated with "conventional" electrophysiological characteristics in midbrain DA neurons. Indeed, when the aforementioned selection criteria are applied, almost all VTA DA neurons recorded in this study responded to carbachol with increased excitation, suggesting the expression of M5 mAChR. There is recent evidence that DA neurons of the lateral VTA are selectively activated by cholinergic inputs from the LDT. Optogenetic activation of cholinergic terminals in the VTA is sufficient to induce conditioned place preference as well as increased motivation for a fixed reward (Coimbra *et al.*, 2021). These lateral VTA DA neurons signal to D1-expressing MSNs in

the NAc core and shell (Coimbra *et al.*, 2021), which are highly implicated in reward and the development of drug addictions (Volkow *et al.*, 2017). This suggests that the DA neurons recorded in this study are the same population targeted by pontine cholinergic afferents involved in reward and motivation signaling.

The electrophysiological similarity between SNc and lateral VTA DA neurons suggests that these two populations of DA neurons likely share the same cholinergic signaling mechanisms, which would affect motor and reward behaviors. In fact, we are the first to characterize mAChR-induced current in VTA DA neurons in the voltage-clamp configuration. In previous reports, *in vitro* application of muscarinic agonists to SNc DA neurons induced an inward current with amplitude and kinetics that were not distinct from the current observed in our study (Foster *et al.*, 2014; Martini *et al.*, 2019). This muscarinic current was associated with an apparent increase in current noise (not quantified by previous work) and correlated with a modest increase in pacemaking frequency and a broadening of AP half-width, effects that are also consistent with our data. The physiological consequence of muscarinic activation is promotion of DA release and DA-driven behaviors mediated by both nigrostriatal and mesolimbic circuitry (Lester *et al.*, 2010b), although modulation of motor and reward behaviors are dissociable when cholinergic terminals in the SNc and in the VTA are selectively targeted (Xiao *et al.*, 2016). In support of the signaling similarities between SNc and VTA DA neurons, M5 mAChR KO mice showed reduced locomotor and reward responses induced by cocaine and morphine (Basile *et al.*, 2002; Fink-Jensen *et al.*, 2003; Thomsen *et al.*, 2005; Steidl & Yeomans, 2009). However, the *in vivo* studies also suggested motor function and food-maintained behaviors are less sensitive to disruption of M5 mAChR signaling compared to the reinforcing effects of addictive drugs. Although their psychomotor responses to cocaine and morphine were attenuated, M5 mAChR KO mice did not differ in their operant responding to liquid food, sensorimotor outputs, and motor skills (Fink-Jensen *et al.*, 2003; Thomsen *et al.*,

2005). Systemic administration of ML375, a M5-selective negative allosteric modulator, attenuated self-administration of addictive drugs at a lower dose than that would cause motor impairments (Berizzi *et al.*, 2018; Gunter *et al.*, 2018). Thus, despite SNc and VTA DA neurons display similar electrophysiological response to muscarinic stimulation, the *in vivo* studies suggest that pharmacological modulation of the M5 mAChR may be more effective at treating addiction disorders than movement disorders. On the flip side, adverse motor effects may be dose-limiting and restrict the usefulness of M5 mAChR-targeting strategies for treating other DA-related disorders such as addictions, major depression, ADHD, and schizophrenia. Future studies should investigate whether there exist circuitry or signaling differences in muscarinic regulation of the mesolimbic and nigrostriatal DA pathways.

Muscarinic activation of TRPC channels in VTA DA neurons

Activation of TRPC channels by Gq signaling is a widely documented process in excitable and non-excitable cells. TRPC channels comprise a subfamily of 7 members in the larger TRP superfamily and are divided into the TRPC1, TRPC2, TRPC4/5, and TRPC3/6/7 subgroups based on sequence homology and physiological functions (Clapham *et al.*, 2001; Chen *et al.*, 2020). Except TRPC2, all TRPC subtypes are expressed throughout the brain (Clapham *et al.*, 2001; Nilius & Owsianik, 2011) and conduct non-selective cationic currents that modulate cellular excitability, synaptic plasticity, and other critical neuronal functions (Bollimuntha *et al.*, 2011). In neurons, TRPC channels have been shown to underlie the excitatory response mediated by a variety of Gq-coupled GPCRs, including mAChRs (Yan *et al.*, 2009; Tai *et al.*, 2011; Zhang *et al.*, 2011; Ratte *et al.*, 2018), mGluRs (Hartmann *et al.*, 2008; Riccio *et al.*, 2009; Riccio *et al.*, 2014; Gualdani & Gailly, 2020), histamine H1 receptors (Sato *et al.*, 2020), 5-HT2 receptors (Munsch *et al.*, 2003), and neuropeptide receptors (Riccio *et al.*, 2009; Bollimuntha *et al.*, 2011; Riccio *et al.*, 2014). Although the precise mechanisms of activation are not entirely understood,

all TRPC subtypes are activated by PLC and multiple components of the Gq-mediated Ca^{2+} signaling pathway (Clapham *et al.*, 2001; Chen *et al.*, 2020; Wang *et al.*, 2020). In general, these comprise of two intricately related but dissociable pathways: store-operated calcium entry (SOCE) and receptor-operated calcium entry (ROCE). SOCE can occur without receptor stimulation and is triggered by ER Ca^{2+} store depletion, which leads to assembly of the STIM-Orai complex and activation of TRPC channels (Cheng *et al.*, 2011; Ambudkar *et al.*, 2017). ROCE is dependent on GPCR activation and is mainly mediated by generation of DAG, which is a direct agonist of TRPC channels (Albert & Large, 2003; Itsuki *et al.*, 2014; Storch *et al.*, 2017). PLC-mediated PIP_2 depletion (Otsuguro *et al.*, 2008; Trebak *et al.*, 2009; Itsuki *et al.*, 2014) and direct binding of IP_3 receptors to TRPC channels (Kiselyov *et al.*, 1998; Tang *et al.*, 2001; Zhang *et al.*, 2001) also contribute to ROCE. Thus, activation of TRPC channels appears to be a core feature of Gq signaling, especially in the excitatory synapse of the central nervous system.

Here, we show that TRPC channels are a likely component of mAChR-induced current in VTA DA neurons by using pharmacological manipulations (**Table 1**). Our results show that the carbachol-induced current and the concurrent increase in current noise is insensitive to TTX (500 nM) and Cs^+ (10 mM) but sensitive to TEA (20 mM) and Cd^{2+} (200 μM). TRP channels conduct non-selective cationic currents and permeate Na^+, K^+, Cs^+, and Ca^{2+} with very little selectivity (Inoue *et al.*, 2001; McKemy *et al.*, 2002; Feng, 2017). In fact, TTX and Cs^+ added to extracellular solutions, and/or intracellular solutions in which Cs^+ is the major cation, are typically used to isolate TRP channel currents (Zhang *et al.*, 2011). The insensitivity of mAChR-induced excitation to TTX and Cs^+ is also in agreement with previous work recorded from SNc and VTA DA neurons (Lacey *et al.*, 1990; Foster *et al.*, 2014). Though information about the interactions between TRP channels and other non-selective ion channel blockers is limited, it appears that TRP channels are sensitive to blockage by quaternary ammonium compounds.

TEA potently inhibited capsaicin-induced TRPV1 currents in *Xenopus* oocytes with an IC_{50} of 41 nM (Rivera-Acevedo *et al.*, 2012). The inhibition mechanism likely involves TEA binding to negatively charged residues in the selectivity filter and is voltage-dependent, being more effective at hyperpolarized (Vm = −60 mV) than at depolarized potentials (Rivera-Acevedo *et al.*, 2012). In HEK cells, the endogenous TRPC currents activated by the orexin 1 receptor was completely inhibited by 70 mM TEA (Larsson *et al.*, 2005). Although an IC_{50} was not determined in the previous study with TRPC, it is possible that TEA is a potent blocker of TRPC channels and would inhibit TRPC currents at a lower concentration, similar to its action on the TRPV1 channel. Finally, TRPC channels show sensitivity to inhibition by Cd^{2+}. Cd^{2+} inhibited carbachol-induced TRPC6 currents in HEK cells and α1-adrenoceptor-activated TRPC6 currents in cultured vascular myocytes with IC_{50} values of 253 and 213 μM, respectively (Inoue *et al.*, 2001). Our results show approximately half reduction in the amplitude of the carbachol-induced current by 200 μM Cd^{2+}, consistent with the previously reported IC_{50} value for TRPC6. Interestingly, TRPC5 expressed in HEK cells was only inhibited by Cd^{2+} (100 μM) after being treated with the reducing agent DTT, which breaks an extracellular disulfide bridge that uniquely confers redox sensitivity to TRPC1/4/5 channels (Xu *et al.*, 2008). In our experimental setting, the extracellular solution is constantly being oxygenated and likely creates an oxidizing, rather than reducing, environment. Therefore, it is possible that the carbachol-induced current in DA neurons is mainly mediated by the TRPC3/6/7 rather than the TRPC1/4/5 subgroup. In summary, the pharmacological profiling of carbachol-induced currents in DA neurons using charged ion channel blockers points to a TRP-like non-selective cationic conductance.

Since ionic or small molecule blockers such as Cs^+, TEA, and Cd^{2+} have poor selectivity and inhibit wide ranges of ion channels, the key result that suggests the involvement of TRPC channels is sensitivity of the carbachol current to BTP2 (also known as Pyr2 or YM-58483).

Our data show that co-treatment with BTP2 (5 μM) inhibited a major component of the carbachol-induced current (67%) and current noise. BTP2 is a small molecule pyrazole derivative that inhibits both SOCE and ROCE with relatively high selectivity. In lymphocyte cell and HEK cell lines, BTP2 inhibited thapsigargin-induced SOCE-mediated Ca^{2+} entry with an IC_{50} of 0.1-0.3 μM (Ishikawa *et al.*, 2003; He *et al.*, 2005). It has been reported that BTP2 is slow-acting, requiring an incubation of at least 10 min to reach the maximum effect (Zitt *et al.*, 1996; He *et al.*, 2005). In our experiments, BTP2 also exhibited slower inhibition kinetics compared to the aforementioned non-selective ion channel blockers. The kinetics were somewhat variable between cells, although no further blockage was observed after 10 min of bath perfusion, which matches the time course reported by He et al. (2005). When SOCE was activated by a more physiological agent, the muscarinic agonist carbachol in HEK cells, BTP2 did not alter the initial store-mediated Ca^{2+} release but inhibited the subsequent extracellular Ca^{2+} entry at 1 μM (He *et al.*, 2005). This suggests that BTP2 does not significantly affect components of the signal transduction pathway that leads to SOCE, such as the mAChR, G protein, PLC, and IP_3 receptors. Importantly, at 3 μM, BTP2 greatly reduced the open probability of TRPC3 channels in single-channel recordings across the voltage range of -80 to 80 mV and completely inhibited OAG-induced TRPC3 currents in whole-cell recordings (He *et al.*, 2005). BTP2 still inhibited TRPC3 when TRPC3-mediated depolarization was prevented by replacement of extracellular Na^+ with the impermeant NMDG (He *et al.*, 2005). Because the inhibitory action was not a secondary effect of membrane potential changes, BTP2 likely antagonizes TRPC channels directly. The direct binding to BTP2 and related compounds to TRPC channels is supported by photoaffinity labeling experiment showing pull-down of a Pyr derivative with TRPC3 (Kiyonaka *et al.*, 2009). Therefore, though the exact binding site of BTP2 on TRPC channels has not been identified, it is highly likely that BTP2 acts as a direct inhibitor of TRPC.

While BTP2 antagonizes SOCE and ROCE non-selectively, this compound appears to be selective for the TRPC subfamily relative to other ion channels. When the selectivity of BTP2 was examined using the same carbachol-induced Ca^{2+} or Sr^{2+} entry protocol, BTP2 suppressed TRPC5 and TRPC6 activity with similar potency to that of TRPC3, whereas TRPV6-mediated Ca^{2+} entry was unaffected by 10 μM BTP2 (He *et al.*, 2005). Instead of inhibition, it has been suggested that BTP2 may activate TRPM4 in lymphocytes (Takezawa *et al.*, 2006). Furthermore, the TRPC3-selective BTP2 analogue Pyr3 failed to inhibit carbachol- and OAG-induced TRPM2, TRMP4, and TRPM7 currents (Kiyonaka *et al.*, 2009). These results suggest that the inhibitory action of BTP2 is mainly mediated by antagonizing TRPC-type TRP channels. The selectivity of BTP2 versus other cellular targets was further demonstrated by the lack of activity against non-TRP components of the Ca^{2+} signaling pathway. In the catecholaminergic PC12 cell line, BTP2 inhibited depolarization-induced Ca^{2+} influx through voltage-gated Ca^{2+} channels with an IC_{50} of 4.7 μM, which is 30-fold less than that for SOCE (Ishikawa *et al.*, 2003). Even at 10 μM, BTP2 did not significantly inhibit K^+ channels endogenously expressed in Jurkat T cells, such as Kv1.3, SK, and inward rectifiers (Zitt *et al.*, 1996; Takezawa *et al.*, 2006). Furthermore, BTP2 was still effective when mitochondrial Ca^{2+} uptake and SERCA were inhibited and did not affect Ca^{2+} extrusion rate, suggesting ER and mitochondrial Ca^{2+} signaling, as well as plasma membrane Ca^{2+} pumps, were not altered by BTP2 (Zitt *et al.*, 1996). Hence, while midbrain DA neurons express a diverse repertoire of voltage-gated channels and functional TRPV1, TRPM2, TRPM4, and TRPM7 channels (Mezey *et al.*, 2000; Mrejeru *et al.*, 2011; Sun *et al.*, 2018; Sun *et al.*, 2020), the available data suggest that the inhibitory effects of BTP2 on the carbachol-induced current is likely mediated by combined blockage of TRPC channels and the STIM-Orai complex, but not blockage of other TRP subfamilies, voltage-gated Ca^{2+} channels, or K^+ channels.

	TTX	TEA	Cs$^+$	Cd^{2+}	BTP2
Carbachol	−	+	−	+	+
K$_V$	− [1, 2]	+ [3, 4]			− [5]
K$_{Ca}$ (SK and BK)	− [2, 6]	+ [7, 8]	− [9]		− [5]
Kir (e.g., GIRK)	− [10]		+ [10]		− [5]
Na$_V$	+ [11]	− [4]			
Ca$_V$	− [12]	− [12]	− [13]	+ [14]	− [15]
HCN	− [16, 17]	− [16, 17]	+ [16]	− [17]	
NALCN	− [18, 19]	− [19]	− [18]		
TRPC	− [20]	+ [21]	− [20]	+ [22]	+ [23]

Table 1: Summary of the pharmacological profile of the carbachol-induced current in VTA DA neurons compared to that of a list of candidate channels. TRPCs are the only candidate channels that exhibit a similar pharmacological profile as the carbachol-induced current in the present study. Plus sign with green background indicates sensitivity to the ion channel blocker whereas minus sign with orange background indicates insensitivity. (Note: only selective members for each channel family are represented in this table both for the purpose of simplification and the limitation of available data.)

References:

[1] (Hansen *et al.*, 2006), **[2]** (Kimm *et al.*, 2015), **[3]** (Koyama & Appel, 2006), **[4]** (Khodakhah *et al.*, 1997), **[5]** (Takezawa *et al.*, 2006), **[6]** (Fiorillo & Williams, 1998), **[7]** (Monaghan *et al.*, 2004), **[8]** (Su *et al.*, 2010), **[9]** (Yuhas & Fuchs, 1999), **[10]** (Davila *et al.*, 2003), **[11]** (Tucker *et al.*, 2012), **[12]** (Philippart *et al.*, 2016), **[13]** (Evans *et al.*, 2017), **[14]** (Lansman *et al.*, 1986), **[15]** (Ishikawa *et al.*, 2003), **[16]** (Liu *et al.*, 2003), **[17]** (Gambardella *et al.*, 2012), **[18]** (Philippart & Khaliq, 2018), **[19]** (Kschonsak *et al.*, 2020), **[20]** (Zhang *et al.*, 2011), **[21]** (Larsson *et al.*, 2005), **[22]** (Inoue *et al.*, 2001), **[23]** (He *et al.*, 2005).

Midbrain DA neurons express multiple subtypes of TRPC. All TRPC subtypes except TRPC2 are expressed in the substantia nigra (Tozzi *et al.*, 2003; Chung *et al.*, 2007; Zeng *et al.*, 2016). Immunohistochemical studies by the Fusco Lab showed intense staining of TRPC1, TRPC5, and TRPC6 in SNc DA neurons: TRPC1 and TRPC6 are expressed in the somatodendritic compartments (Martorana *et al.*, 2006; Giampa *et al.*, 2007), TRPC5 was found localized in the neuronal nuclei and did not co-localize with TRPC1 or mGluR1 (De March *et al.*, 2006), while TRPC3 showed preferential localization in oligodendrocytes and appeared to be absent in most DA neurons of the SN (Fusco *et al.*, 2004). However, a recent study showed that virtually all TH$^+$ SNc DA neurons (92% of cells) express TRPC3, which provide a cationic leak current that maintains the pacemaking activity (Um *et al.*, 2021). Inhibition of TRPC3 current by the selective blocker Pyr3 hyperpolarized membrane potential and stopped the pacemaking of SNc DA neurons without altering the kinetics of AP shape (Um *et al.*, 2021). This result contradicts the findings of the previous immunohistochemical studies and demonstrates an essential role of TRPC3 in the physiological of SNc DA neurons. Compared to the SN, studies of the expression and functions of TRPC in the VTA are scarce. One study showed expression of TRPC4 in the SN and a subset (~37%) of VTA DA neurons that are uniformly-distributed throughout this brain region (Klipec *et al.*, 2016). In TRPC4 KO rats, ~1/3 of VTA DA neurons showed lower spontaneous firing rates; the proportion of affected cells matched that express the TRPC4 subunit (Klipec *et al.*, 2016). Those TRPC4 KO rats were less socially exploratory and showed reduced cocaine self-administration, suggesting TRPC4 may modulate selective subpopulations of VTA DA neurons and circuit-specific DA-driven behaviors (Klipec *et al.*, 2016). In the TRPC channel literature, there is abundant evidence that one cell type commonly expresses multiple TRPC subtypes, which may form homomeric or heterometic channels. When forming heteromeric channels, TRPC subunits appear to preferentially assemble with members of the same subgroup (e.g. TRPC1/4/5 co-assemble and TRPC3/6/7 co-assemble) (Goel *et al.*, 2002; Hofmann *et al.*, 2002), but inter-subgroup heteromeric channels have also

been reported (Strubing *et al.*, 2003; Poteser *et al.*, 2006; Yuan *et al.*, 2007; Storch *et al.*, 2012). In our results, the majority of DA neurons of the lateral VTA responded to carbachol with increased excitation and the induction of a BTP2-sensitive inward current. This is a larger proportion than those expressing the TRPC4 subunit. Since BTP2 is non-selective for all TRPC subtypes, the current data suggest that mAChRs in VTA DA neurons activate multiple subtypes of TRPC, which possibly exist as heteromeric channels. In recent years, several high-affinity small molecule inhibitors selective for TRPC subgroups have been developed [See reviews (Chen *et al.*, 2020; Wang *et al.*, 2020; Gao *et al.*, 2021)]. Future studies should utilize these blockers or dominant-negative TRPC subunits to determine the specific subtypes underlying the muscarinic response in midbrain DA neurons. In addition, in the context of developing TRPC-targeting therapeutics for DA-related disorders, it would be important to map the expression patterns of specific TRPC subtypes in the VTA and whether they co-localize with the M5 mAChR.

In SNc DA neurons, TRPC1 has been shown to mediate SOCE and SOCE-related signaling. In this brain region, thapsigargin-induced store depletion elicited an inward current around −100 pA in amplitude that was absent in TRPC1 KO mice (Selvaraj *et al.*, 2012; Sun *et al.*, 2017). However, instead of generating an excitatory response, TRPC1 activation actually decreased the pacemaking frequency in SNc DA neurons via inhibition of L-type Ca^{2+} current (Sun *et al.*, 2017). This effect appeared to be mediated by physical interaction between Cav1.3 and the TRPC1-STIM1 complex and a decrease in the maximal conductance of Cav1.3 channels (Sun *et al.*, 2017). The antagonistic relationship between SOCE and L-type Ca^{2+} channels, termed "store-inhibited channels", has been discovered in various excitable cell types including cortical neurons and vascular smooth muscle cells (Moreno & Vaca, 2011). Nonetheless, while these studies show that DA neurons are equipped with the SOCE machinery comprising of STIM-Orai and TRPC channels, the coupling of this signaling complex to GPCRs has not been

demonstrated. One proposed mechanism underlying muscarinic excitation of VTA DA neurons is an increase in L-type Ca^{2+} current (Zhang *et al.*, 2005; Liu & Chen, 2008), which appear to contradict the effects of "store-inhibited channels". Our results also show that mAChR activation increased VTA DA neurons pacemaking frequency, an opposite effect of store-operated TRPC1 activation reported in the previous study. Therefore, while TRPC1-mediated SOCE likely occurs upon muscarinic stimulation of DA neurons, it may not be the major activation mechanism of TRPC channels downstream of this GPCR. Moreover, even though BTP2 inhibits TRPC and Orai channels non-selectively, the SOCE current conducted by Orai channels is very small (Ambudkar *et al.*, 2017) and the divalent ion entry (i.e., Ca^{2+}) is insensitive to TEA blockage (Schindl *et al.*, 2009). Thus, pure Orai-mediated current is unlikely to be a major component of the carbachol-activated conductance measured by patch-clamp recordings. In future studies, calcium imaging will be a more appropriate technique to investigate SOCE downstream of muscarinic signaling in DA neurons.

In SNc DA neurons, mGluR1-mediated activation of a TRP-like currents via ROCE-related mechanism is well-documented. TRPC1 and TRPC6 have been shown to express in the somatodendritic compartments of SNc DA neurons and co-localize with mGluR1 (Martorana *et al.*, 2006; Giampa *et al.*, 2007), making them the potential TRPC subtypes involved in the excitatory mGluR1 response. In acute brain slice preparation, the mGluR1 agonist DHPG elicited a non-selective cation current that correlated with membrane potential depolarization and an increase in spontaneous firing frequency (Tozzi *et al.*, 2003; Cucchiaroni *et al.*, 2010). Pharmacological characterization showed that this mGluR1-induced current was sensitive to Na^+ substitution and extracellular application of non-selective TRP channel blockers such as SKF96365, 2-APB, ruthenium red, and flufenamic acid. Further experiments revealed that the mGluR1-induced current was not altered by treatments that disrupt the intracellular Ca^{2+} pathways: store depletion by thapsigargin and CPA, intracellular inclusion of

the strong Ca^{2+} chelator BAPTA, or intracellular application of reagents that affect the IP_3 receptors and ryanodine receptors including ryanodine, dantrolene, ruthenium red, and 2-APB, even when they reduced the concurrent Gq-mediated Ca^{2+} transients (Tozzi *et al.*, 2003). This result is significant because it shows that the mGluR1-mediated response is not dependent on Ca^{2+} store release, suggesting ROCE via the generation of DAG and/or rapid membrane insertion of channels [see: (Cheng *et al.*, 2011; Tai *et al.*, 2011)] are the most likely mechanisms of activation. Since cholinergic and glutamatergic inputs work in conjunction to modulate the firing activity of DA neurons, it is possible that the molecular components downstream of mGluR and mAChR signaling are in close proximity in the dendritic microdomains. It would be interesting to determine the relative contribution of ROCE and SOCE in muscarinic activation of TRPC currents using the experimental manipulations discussed above, and whether mGluRs and mAChRs signal to the same or separate pools of TRPC channels.

Despite the likelihood that activation of TRPC channels underlie both mGluR1- and mAChR-induced excitation in midbrain DA neurons, there are apparent differences in the magnitude and kinetics of mGluR1- and mAChR-induced inward currents. The mGluR1 agonist DHPG elicited a larger inward current with a peak amplitude around −350 pA (Tozzi *et al.*, 2003; Martini *et al.*, 2019). It was reported that the mGluR1-induced current and Ca^{2+} transients quickly desensitized with bath application or repeated application of the agonist (Guatteo *et al.*, 1999; Tozzi *et al.*, 2003). Even in the same cell, the DHPG-induced current consistently had larger amplitude and faster kinetics compared to the muscarine-induced current, which was slow and had an average amplitude around −90 pA (Martini *et al.*, 2019). Bath application of muscarine did not reduce the DHPH-induced current (Martini *et al.*, 2019), suggesting cross-desensitization does not occur. Our results show that bath perfusion of an mAChR agonist induced a slow inward current that peaked at around −50 pA and membrane potential

depolarization that were non-desensitizing. Together, those results suggest that there are signaling differences between mGluR- and mAChR-mediated responses, although the mechanisms responsible for these differences are unknown. Compared to the large-amplitude, rapidly-desensitizing response of mGluR1, the mAChR response in DA neurons resembles the mAChR-evoked TRPC-mediated plateau potential in the cortex and the hippocampus. In cortical and hippocampal excitatory neurons, carbachol induced a slow, sustained depolarization that leads to persistent AP spiking (Yan *et al.*, 2009; Tai *et al.*, 2011; Zhang *et al.*, 2011; Ratte *et al.*, 2018). This depolarizing response does not desensitize and can last up to 1 hour if the cholinergic stimulation is sustained (Zhang *et al.*, 2011). The persistent nature of the plateau potential is maintained by positive feedback interactions between TRPC channel-induced depolarization and Ca^{2+} entry through voltage-gated Ca^{2+} channels (Ratte *et al.*, 2018). It is possible that such positive feedback mechanism also exists in midbrain DA neurons to exert powerful excitatory control on pacemaking activity upon muscarinic stimulation. PKC has been found to mediate the rapid desensitization of TRPC4/5 after activation of Gq-coupled GPCRs. In HEK cells expressing TRPC5, the desensitization of carbachol-induced TRPC5 current depended on extracellular and intracellular Ca^{2+}, intracellular ATP, and PKC phosphorylation of T972 on the C-terminal domain of TRPC5 (Zhu *et al.*, 2005). The T972 residue binds to PDZ domain-containing scaffold proteins such as NHERF, which is a critical regulator of the activation kinetics and DAG sensitivity of receptor-activated TRPC4/5 currents (Obukhov & Nowycky, 2004; Storch *et al.*, 2017). In the light of these results, mAChR signaling in midbrain DA neurons may not be coupled to the PKC pathway, or alternatively, activates other TRPC subtypes than TRPC4/5.

NALCN is another non-selective cation channel that plays an important role in the physiology of midbrain DA neurons. NALCN provides a persistent sodium current that drives pacemaking in VTA DA neurons (Khaliq & Bean, 2010). Recently, NALCN is found to play a similar role in

SNc neurons. Using selective pharmacological inhibitors and KO mice, it was shown that NALCN and TRPC3 contribute equally to sustained low depolarization that maintain pacemaking activity of SNc neurons (Um *et al.*, 2021). Despite being a leak channel, NALCN is regulated by GPCRs. In VTA DA neurons, the neuropeptides neurotensin and substance P activate a slow NALCN-mediated cation current (Lu *et al.*, 2009). In pancreatic cells and HEK cells, this leak channel is activated by the M3 mAChR (Lu & Feng, 2012). However, it should be noted that although neurotensin receptor and M3 mAChR are preferentially coupled to the Gq pathway, activation of NALCN is mediated through a G protein-independent but SFK-dependent mechanism (Lu *et al.*, 2009; Lu & Feng, 2012). This is in contrast with the proposed G protein-dependent activation of TRPC channels. Being a TTX- and Cs^+-insensitive leak cation channel modulated by acetylcholine, NALCN it is another likely candidate underlying muscarinic depolarization in VTA DA neurons. Although we demonstrated BTP2 sensitivity of the carbachol-induced current in DA neurons, BTP2 has never been tested against NALCN. In addition, BTP2 (5 μM) did not fully block the carbachol-induced current. However, NALCN heterologously expressed in HEK cells was not blocked by TEA (10 mM) (Chua *et al.*, 2020; Kschonsak *et al.*, 2020) whereas the carbachol current was completely eliminated by 20 mM TEA (**Figure 7B, F**), suggesting that NALCN is not a participant in this response. To determine whether NALCN activity is regulated by mAChRs in DA neurons, future studies should test the effects of L-703,606, a novel selective blocker of NALCN used by Um et al. (2021), and NALCN KO on muscarinic actions in midbrain DA neurons.

Other ion channel mechanisms involved in cholinergic excitation of VTA DA neurons

It is common for GPCRs to affect cell excitability via modulating the functions of multiple ion channels. In addition to a "leak-like" cationic conductance, activation of voltage-gated Ca^{2+}

channels, inhibition of SK channels, and inhibition of voltage-gated K^+ channels have also been proposed to mediate the excitatory effects of muscarinic activation in midbrain DA neurons. Here, one key finding that prompted us to examine activation of cationic channels was a reduction in input resistance induced by carbachol. However, while a decrease in input resistance and an increase in current noise indicate that the dominant ion carrier is cationic, inhibition of K^+ channels still could not be completely excluded. Upon muscarinic excitation, Lacey et al. (1990) detected a decrease in membrane conductance between −50 and −65 mV but an increase in conductance between −40 and −50 mV in midbrain DA neurons (Lacey *et al.*, 1990). Thus, it is possible that mAChR activation modulates multiple ion channels that are activated at different membrane potentials. In addition, the TRPC channel blocker BTP2 did not inhibit a minor component of the carbachol-induced current, suggesting activation of other channels. This section will discuss the likelihood that other candidate channels are involved in cholinergic excitation of VTA DA neurons.

Cholinergic neurotransmission is mediated by nAChRs and mAChRs. nAChRs are non-selective cation channels that induce an inward current and excitation of DA neurons. Structurally, carbachol is highly similar to acetylcholine and binds all cholinergic receptors non-selectively. Therefore, activation of nAChRs may contribute to the excitatory effects of carbachol. The study by the Chen Lab showed that carbachol depolarized membrane potential and induced burst firing of VTA DA neurons in acute slice preparation via combined activation of nAChRs and mAChRs (Zhang *et al.*, 2005). However, while the excitatory role of nAChRs in DA neurons is well-known, midbrain DA neurons predominantly express the $\alpha 4\beta 2$ subtype of nAChRs that are sensitive to agonist-induced desensitization. The excitatory nicotinic response disappeared within a few minutes even upon treatment of sub-micromolar concentrations (80-500 nM) of nicotine (Pidoplichko *et al.*, 1997; Wooltorton *et al.*, 2003; Pidoplichko *et al.*, 2004). In agreement, the Chen Lab showed that nicotinic activation by carbachol induced a

transient depolarization and increase in firing that lasted ~1 min, while the muscarinic response was slower (Zhang *et al.*, 2005). In our study, we perfused the brain slices with carbachol for at least 3-4 min before the measurements were taken, when most of the nicotinic responses were expected to desensitize. We also showed that atropine could reversed the carbachol-induced increase in firing frequency and carbachol-induced inward current to baseline levels. Atropine is a prototypical mAChR antagonist that does not inhibit $\alpha4\beta2$ nAChR currents activated by micromolar concentration of agonists (Zwart & Vijverberg, 1997). Nonetheless, there is a few carbachol-induced effects that were not completely blocked by atropine. While atropine alone did not significantly affect Vm in the presence of TTX, the subsequent atropine and carbachol co-treatment produced a very mild depolarization. In spontaneously firing cells, carbachol induced a small decrease in on firing regularity that was not reversed by atropine, which could be due to the burst-inducing effect of nicotinic activation. These results suggest that while activation of nAChRs may account for some of the carbachol-induced effects, it is not the major contributor of the slow depolarization observed in this study.

SK channels are a master regulator of firing pattern in midbrain DA neurons. Coincidentally, cholinergic inputs have been proposed to underlie the switch from tonic to burst firing. Excitatory inputs from the PPT and LDT enable NMDA-induced bursting and cause an irregular firing pattern (Lodge & Grace, 2006), effects that were consistent with SK channel inhibition. Furthermore, SK channels are inhibited by the Gq-coupled $\alpha1$-adrenoceptor in midbrain DA neurons (Goertz *et al.*, 2015). Thus, as elaborated by Kitai and colleagues, inhibition of SK channels is a plausible mechanism underlying muscarinic excitation of DA neurons (Kitai *et al.*, 1999). Here, we provide evidence against the involvement of SK channels in the muscarinic actions in VTA DA neurons. First, while DA neurons in acute slice preparation exhibit regular pacemaking activity and do not burst, selective blockage of SK channels by apamin

significantly decreased firing regularity, increasing the mean CoV of ISI from 0.05 to 0.30 (Deignan *et al.*, 2012). In our experiments, the pacemaking of DA neurons remained highly regular in all treatments. While there was a small increase of CoV of ISI from 0.056 to 0.092 during carbachol treatment in the whole-cell recordings, the difference is not present in the cell-attached configuration and is much smaller compared to the effects of apamin. Second, SK channels mediate the most hyperpolarizing phase of AHP (Shepard & Bunney, 1991; Ping & Shepard, 1996). Modifications of SK channel function would affect the kinetics of AHP, an effect that we did not observe. Finally, by regulating AHP kinetics, SK channel activities influence spike frequency adaptation and f-I relationship (Shepard & Bunney, 1991; Vandecasteele *et al.*, 2011). In our current step protocol, carbachol did not affect the frequency adaptation ratio and stimulated firing frequency. Instead of inhibiting SK channels, it has been shown that mAChRs on DA neurons activate SK channels via stimulation of the Gq pathway and release of intracellular Ca^{2+} (Fiorillo & Williams, 2000). The hyperpolarizing response caused by SK channel activation is transient and, with prolonged receptor stimulation, is replaced by a depolarization mediated by an unidentified conductance (Fiorillo & Williams, 2000). In our bath perfusion protocol, we only observed depolarizing response with carbachol. The lack of changes in firing regularity and spike frequency adaptation also suggests that SK channel activity is not significantly affected after sustained muscarinic stimulation. Together, our results do not place SK channel inhibition as a major mechanism of the slow depolarization and increased firing rate resulting from muscarinic agonism in VTA DA neurons.

The possibility that other potassium conductances are modulated by muscarinic inputs was also examined. Midbrain DA neurons express a rich repertoire of potassium channels including voltage-gated K^+ channels, calcium-activated K^+ channels, and GIRK channels. The voltage-gated Kv7 channels are inhibited by the depletion of PIP^2 mediated by Gq signaling and

constitute the "M-current", which depolarizes membrane potential and increases firing frequency (Delmas & Brown, 2005). In heterologous expression systems, the Gq-coupled M1, M3, and M5 mAChRs inhibit Kv7 current with equal efficacy (Guo & Schofield, 2003), making the Kv7 channel a likely candidate. Kv7 channels mediate the slow component of AHP while having minimal effects on other parameters of AP shape (Stocker, 2004; Koyama & Appel, 2006; Mateos-Aparicio *et al.*, 2014; Greene & Hoshi, 2017), though the effects of Kv7 blockage in midbrain DA neurons were somewhat conflicting across studies (Hansen *et al.*, 2006; Koyama & Appel, 2006; Sotty *et al.*, 2009; Drion *et al.*, 2010). Here, we failed to detect changes in AHP kinetics and f-I relationship, properties that are affected by inhibition of Kv7 channels (Hansen *et al.*, 2006; Koyama & Appel, 2006). These data are consistent with the report of Lacey et al. (1990), who showed that the slow activating inward current elicited by a hyperpolarization step – a conventional method for measuring Kv7 activity – was unaffected by muscarine treatment (Lacey *et al.*, 1990). Therefore, although midbrain DA neurons exhibit robust Kv7 current, Kv7 channels are not modulated by mAChRs in this native system. The unchanged f-I relationship suggests that other prominent voltage-gated potassium conductances, such as Kv4, the "A-type current", and Kv2, are also not modulated by muscarinic signaling even though inhibition of A-type currents was suggested to be a widespread effect of Gq-mediated endocannabinoid mobilization (Gantz & Bean, 2017). The lack of changes in AHP kinetics does not support the involvement of BK channels, which is potentially activated by the Gq-mediated Ca^{2+} release and regulates the repolarization and hyperpolarization phases of APs in DA neurons (Kimm *et al.*, 2015). Lastly, GIRK channels have been shown to be inhibited by Gq signaling in DA neurons (Kramer & Williams, 2016), but these inward rectifiers are sensitive to Cs^+ and would be blocked in our voltage-clamp experiments. Thus, in addition to a decrease in input resistance, our examination of various firing and pharmacological properties provides ample evidence that potassium conductances are not main contributors in the mAChR-mediated excitation of DA neurons in our

experimental conditions.

The voltage-gated cation channels include the HCN, voltage-gated Ca^{2+}, and voltage-gated Na^+ channels, which are all important regulators of firing pattern in midbrain DA neurons. HCN channels conduct non-selective cation currents and contribute to membrane potential depolarization during the pacemaking activity of DA neurons (Gambardella *et al.*, 2012). In addition, HCN channels regulate the shape of AHP by reducing the amplitude and duration of AHP upon hyperpolarization (Neuhoff *et al.*, 2002; Okamoto *et al.*, 2006; Wanat *et al.*, 2008). Along with inhibition of SK channels, activation of HCN channels was shown to underlie the excitatory actions of α1-adrenoceptor, a Gq-coupled GPCR, in midbrain DA neurons (Goertz *et al.*, 2015). Here, our data show that muscarinic activation did not affect the HCN-mediated sag ratio and the kinetics of AHP. HCN channels are sensitive to blockage by extracellular Cs^+ (3-5 mM) (Liu *et al.*, 2003; Khaliq & Bean, 2010), and their action would be completely eliminated in our voltage-clamp experiments using 10 mM Cs^+. Moreover, HCN channels are insensitive to TEA and Cd^{2+} (Liu *et al.*, 2003; Okamoto *et al.*, 2006; Gambardella *et al.*, 2012). This is drastically different from the pharmacological profile of the carbachol-induced current, which is TEA- and Cd^{2+}-sensitive but Cs^+-insensitive. Therefore, our results provide strong evidence that HCN activity is not altered by activation of mAChRs in DA neurons.

Work by Chen and colleagues have implicated activation of L-type Ca^{2+} channels in the depolarizing and burst-inducing effects of muscarinic activation in VTA DA neurons (Zhang *et al.*, 2005; Liu & Chen, 2008). In their acute brain slice preparation, VTA DA neurons in the presence of TTX exhibit very little to no membrane potential oscillations at baseline. Bath application of carbachol induced robust Ca^{2+}-mediated oscillations, which correlated with induction of burst firing in 20% of cells. In contrast to their results, carbachol-induced burst firing is a rare occasion in our preparation. Out of the 38 spontaneously firing VTA DA neurons

recorded using cell-attached and whole-cell techniques, only 2 cells (5.3%) converted to burst-like firing pattern upon carbachol treatment. One cell was bursting with carbachol alone, while the other cell only exhibited the unusual firing pattern with combined carbachol and hyperpolarizing current injection. Due to the low number of samples, these cells were not included in the data set and we did not pursue further. We speculate that the differences in the techniques could account for our respective observations. While the previous studies used perforated patch-clamp, we did not observe burst firing in the cell-attached experiments; both techniques would preserve the intracellular content intact and make this a less likely factor. The other major difference is the thickness of the brain slices prepared. Their 400-μm slices were twice as thick as ours and could preserve more dendritic processes where the Ca^{2+} channels are located. Interestingly, while the Chen Lab demonstrated that the burst-inducing effect of carbachol could be prevented by L-type Ca^{2+} channel blockers, there was a component of carbachol-induced depolarization that was slow and insensitive to Cd^{2+} (100 μM) and nifedipine. In our voltage-clamp experiments, the carbachol-induced current shows high sensitivity to TEA (20 mM) but only partial sensitivity to Cd^{2+} (200 μM), a pharmacological profile inconsistent with Ca^{2+} channel currents. This suggests that, at least when Vm was held constantly at -60 mV, voltage-gated Ca^{2+} channels are not major contributors to the mAChR-induced current. Therefore, while we appear to have reached different conclusions at the first glance, our data in fact complement the previous findings. Together, our results suggest that the ionic conductances modulated by mAChRs in midbrain DA neurons are complex. Our data point to TRPC channels as additional effectors downstream of mAChR signaling that mediate a non-selective cationic current and slow depolarization.

As previously discussed, α1-adrenoceptor excites midbrain DA neurons via activation of HCN channels and inhibition of SK channels (Goertz *et al.*, 2015), effects that are not observed for mAChRs in the present study. This indicates that while both α1-adrenoceptor and M5 mAChR

are preferentially coupled to the Gq protein, they signal to different downstream pathways in DA neurons. The previous work on adrenergic effects in DA neurons did not pursue further the signal transduction pathways, but we could speculate that PKC may underly these differences. In midbrain DA neurons, regulation of HCN channels by PKC is complex, perhaps due to different PKC isoforms and sites of phosphorylation. Serotonin has been reported to inhibit HCN currents in DA neurons via Gq-mediated PKC activation (Liu *et al.*, 2003; Gambardella *et al.*, 2012), while CRF enhanced HCN currents via activation of the PLC/PKC pathway (Wanat *et al.*, 2008). Therefore, it is possible that α1-adrenoceptor is coupled to PKC activation in midbrain DA neurons, whereas mAChR lacks this mechanism. The differences in PKC signaling may also account for the lack of M5 mAChR-mediated modulation of SK channels, which have been shown to be inhibited by M1-mediated PKC activation in hippocampal neurons (Buchanan *et al.*, 2010). In addition, due to the role of PKC in the desensitization of some TRPC channels (Zhu *et al.*, 2005), the lack of PKC signaling may contribute to the persistent, non-desensitizing nature of mAChR-evoked currents in DA neurons. However, muscarinic activation of L-type Ca^{2+} channels and the accompanying excitation in VTA DA neurons is attenuated by the PKC inhibitors chelerythrine and GF 109203X (Liu & Chen, 2008). This implies that the mAChRs are capable of activating the PKC pathway. It remains to be tested whether the differences between adrenergic and muscarinic signaling in midbrain DA neurons lie in the PKC isoforms or other molecular mechanisms.

Muscarinic modulation of inhibitory synaptic inputs in VTA DA neurons

VTA DA neurons are tonically inhibited by the local GABAergic interneurons (Westerink *et al.*, 1996; Theile *et al.*, 2011; Polter *et al.*, 2018), which comprise of ~one-third of the total VTA neuronal population (Nair-Roberts *et al.*, 2008). Inhibition of VTA GABAergic interneuron activity, which causes disinhibition of DA neurons, is implicated in the addictive properties of

opioids, benzodiazepines, and alcohol (Nestler, 2005; Tan *et al.*, 2011). Tracing studies showed that cholinergic afferents from the PPT and LDT form synapses on VTA GABA neurons (Maskos, 2008). Nicotinic activation of VTA GABA neurons is important for GABA-dependent burst firing of VTA DA neurons and the reinforcing effects of nicotine (Tolu *et al.*, 2013), but it is unknown whether the same GABA neurons express mAChRs and if they are modulated by muscarinic activation. In studies using primary midbrain neuron cultures, GABA neurons showed immunoreactivity for M3 mAChR (Michel *et al.*, 2004). Agonists of mAChRs depolarize the membrane potential, induce Ca^{2+} transients, and increase the firing frequency of the GABA neurons (Michel *et al.*, 2004; Michel *et al.*, 2005). This increased excitation leads to an increase in the frequency of sIPSCs recorded from neighboring neurons which the GABAergic neurons synapse on (Michel *et al.*, 2004). The mAChR-induced Ca^{2+} transient and increase in sIPSCs were reduced by antagonists selective for the M3 mAChR (Michel *et al.*, 2004; Michel *et al.*, 2005). Although it could not be certain that these primary GABAergic neurons are VTA GABA interneurons, these results raise the possibility that muscarinic stimulation would excite GABAergic neurons and increase the inhibition of VTA DA neurons. On the other hand, a recent study showed that *in vivo* optogenetic activation of LDT cholinergic terminals in the VTA increased the activity of most putative DA neurons and decreased the activity of most putative GABA neurons. This suggests that cholinergic inputs inhibit VTA GABAergic interneurons, though this effect could be mediated by nAChRs in the circuitry rather than mAChRs. Here, we show that activation of mAChR by carbachol had no effects on the frequency or the amplitude of sIPSCs recorded in VTA DA neurons. This result is surprising because it suggests that VTA GABAergic interneurons are neither excited nor inhibited by muscarinic inputs, which was not predicted by previous findings. While we failed to detect a significant difference between the sIPSC amplitudes at baseline and during carbachol treatment, there was a very small but significant decrease in the sIPSC amplitude during atropine treatment compared to carbachol. If this difference is physiologically significant, it

would suggest that VTA GABAergic neurons express excitatory subtypes of mAChRs, such as M3 or M5. In the VTA, immunohistochemical staining for M2 and M5 mAChRs has found both M2 and M5 localized on dendrites that do not express the dopamine transporter (DAT), suggesting non-DAergic neurons (Garzon & Pickel, 2006, 2013). In line with these results, while the majority of M5-expressing cells in the midbrain are TH^+, a minority (~10%) are TH^- but co-express VGAT, indicating GABAergic identity (Gould *et al.*, 2019). It is possible that only specific sub-populations of VTA GABA neurons are excited by muscarinic activation and fail to reach statistical significance in our sampling. Another limitation of our study is that we relied solely on anatomical location and cell morphology to identify VTA DA neurons in this experiment. The intracellular solution used to record sIPSCs contains the Na^+ channel blocker QX-314, the HCN and K^+ channel blocker Cs^+, and the Ca^{2+} chelator BAPTA. Blockage of major ion channels in DA neurons prevented firing, activation of voltage sag, and D2 autoreceptor response; thus, identification of cell type by electrophysiology was not possible. In future studies, cell identities could be better determined by using transgenic animals expressing fluorescent proteins under the promoters of DAergic and GABAergic markers.

Conclusions

The present work suggests that mAChRs directly excite VTA DA neurons via activation of TRPC channels. This finding is supported by electrophysiological data showing that activation of mAChRs induces an increase in pacemaking frequency due to membrane potential depolarization. This increase in excitation was accompanied by a decrease in input resistance, alterations of AP shape that were secondary to membrane depolarization, and no changes in the firing pattern, suggesting HCN and K^+ conductances are not involved. At hyperpolarized potentials, activation of mAChRs induced a cationic inward current sensitive to a TRPC channel blocker. Thus, our data suggest that TRPC channels are likely downstream effectors of mAChRs

that bridge the mesopontine cholinergic inputs and the increase in midbrain DA neuron excitability (**Figure 10**). Additional studies are needed to determine the specific signal transduction pathways and TRPC subtypes mediating this excitation. Furthermore, this research identifies novel molecular candidates for the treatment of neurological and psychiatric disorders characterized by aberrant DAergic neurotransmission.
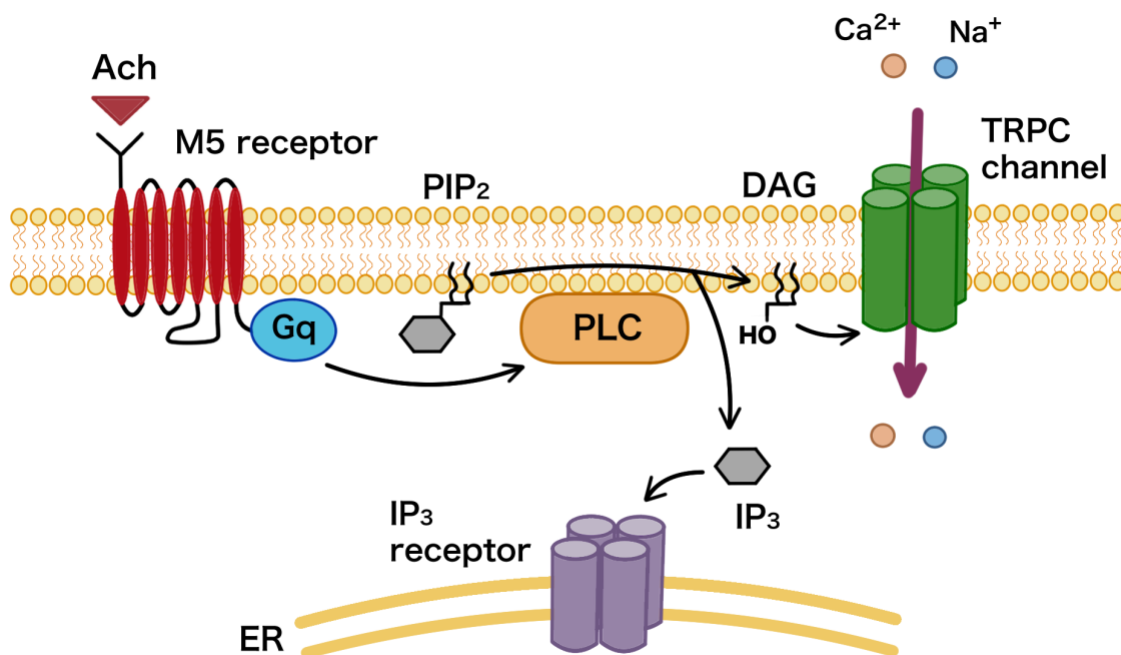
Figure 10. Proposed mechanism of M5 mAChR-mediated activation of TRPC channels in midbrain DA neurons. We predict that the M5 muscarinic acetylcholine receptor (mAChR) on midbrain dopamine (DA) neurons activates transient receptor potential canonical (TRPC) channels via a receptor-operated mechanism. The binding of acetylcholine (Ach) to the M5 mAChR activates $G\alpha q$ and phospholipase C (PLC), leading to PLC-mediated hydrolysis of phosphatidylinositol 4,5-bisphosphate (PIP_2) and production of diacylglycerol (DAG) and inositol 1,4,5-triphosphate (IP_3). DAG acts as a direct activator of TRPC channels. PIP_2 depletion and the IP_3-activated IP_3 receptor also contribute to receptor-operated TRPC channel activation. TRPC channels open and conduct a non-selective cation current, which depolarizes and excites DA neurons.

REFERENCES

Albert AP & Large WA. (2003). Synergism between inositol phosphates and diacylglycerol on native TRPC6-like channels in rabbit portal vein myocytes. *J Physiol* **552,** 789-795.

Alvarez O, Gonzalez C & Latorre R. (2002). Counting channels: a tutorial guide on ion channel fluctuation analysis. *Adv Physiol Educ* **26,** 327-341.

Ambudkar IS, de Souza LB & Ong HL. (2017). TRPC1, Orai1, and STIM1 in SOCE: Friends in tight spaces. *Cell Calcium* **63,** 33-39.

Baik JH. (2020). Stress and the dopaminergic reward system. *Exp Mol Med* **52,** 1879-1890.

Basile AS, Fedorova I, Zapata A, Liu X, Shippenberg T, Duttaroy A, Yamada M & Wess J. (2002). Deletion of the M5 muscarinic acetylcholine receptor attenuates morphine reinforcement and withdrawal but not morphine analgesia. *Proc Natl Acad Sci U S A* **99,** 11452-11457.

Beckstead MJ, Grandy DK, Wickman K & Williams JT. (2004). Vesicular dopamine release elicits an inhibitory postsynaptic current in midbrain dopamine neurons. *Neuron* **42,** 939-946.

Belkacemi T, Niermann A, Hofmann L, Wissenbach U, Birnbaumer L, Leidinger P, Backes C, Meese E, Keller A, Bai X, Scheller A, Kirchhoff F, Philipp SE, Weissgerber P, Flockerzi V & Beck A. (2017). TRPC1- and TRPC3-dependent Ca(2+) signaling in mouse cortical astrocytes affects injury-evoked astrogliosis in vivo. *Glia* **65,** 1535-1549.

Bello EP, Mateo Y, Gelman DM, Noain D, Shin JH, Low MJ, Alvarez VA, Lovinger DM & Rubinstein M. (2011). Cocaine supersensitivity and enhanced motivation for reward in mice lacking dopamine D2 autoreceptors. *Nat Neurosci* **14,** 1033-1038.

Berizzi AE, Perry CJ, Shackleford DM, Lindsley CW, Jones CK, Chen NA, Sexton PM, Christopoulos A, Langmead CJ & Lawrence AJ. (2018). Muscarinic M5 receptors modulate ethanol seeking in rats. *Neuropsychopharmacology* **43,** 1510-1517.

Bird GS, DeHaven WI, Smyth JT & Putney JW, Jr. (2008). Methods for studying store-operated calcium entry. *Methods* **46,** 204-212.

Blythe SN, Atherton JF & Bevan MD. (2007). Synaptic activation of dendritic AMPA and NMDA receptors generates transient high-frequency firing in substantia nigra dopamine neurons in vitro. *J Neurophysiol* **97,** 2837-2850.

Bokor G & Anderson PD. (2014). Obsessive-compulsive disorder. *J Pharm Pract* **27,** 116-130.

Bollimuntha S, Selvaraj S & Singh BB. (2011). Emerging roles of canonical TRP channels in neuronal function. *Adv Exp Med Biol* **704,** 573-593.

Brown DA. (2018). Regulation of neural ion channels by muscarinic receptors. *Neuropharmacology* **136,** 383-400.

Brunzell DH, McIntosh JM & Papke RL. (2014). Diverse strategies targeting alpha7

homomeric and alpha6beta2* heteromeric nicotinic acetylcholine receptors for smoking cessation. *Ann N Y Acad Sci* **1327,** 27-45.

Buchanan KA, Petrovic MM, Chamberlain SE, Marrion NV & Mellor JR. (2010). Facilitation of long-term potentiation by muscarinic M(1) receptors is mediated by inhibition of SK channels. *Neuron* **68,** 948-963.

Burton AC, Nakamura K & Roesch MR. (2015). From ventral-medial to dorsal-lateral striatum: neural correlates of reward-guided decision-making. *Neurobiol Learn Mem* **117,** 51-59.

Cao E. (2020). Structural mechanisms of transient receptor potential ion channels. *J Gen Physiol* **152**.

Chan CS, Guzman JN, Ilijic E, Mercer JN, Rick C, Tkatch T, Meredith GE & Surmeier DJ. (2007). 'Rejuvenation' protects neurons in mouse models of Parkinson's disease. *Nature* **447,** 1081-1086.

Chaudhuri KR & Schapira AH. (2009). Non-motor symptoms of Parkinson's disease: dopaminergic pathophysiology and treatment. *Lancet Neurol* **8,** 464-474.

Chaudhury D, Walsh JJ, Friedman AK, Juarez B, Ku SM, Koo JW, Ferguson D, Tsai HC, Pomeranz L, Christoffel DJ, Nectow AR, Ekstrand M, Domingos A, Mazei-Robison MS, Mouzon E, Lobo MK, Neve RL, Friedman JM, Russo SJ, Deisseroth K, Nestler EJ & Han MH. (2013). Rapid regulation of depression-related behaviours by control of midbrain dopamine neurons. *Nature* **493,** 532-536.

Chen X, Sooch G, Demaree IS, White FA & Obukhov AG. (2020). Transient Receptor Potential Canonical (TRPC) Channels: Then and Now. *Cells* **9**.

Cheng KT, Liu X, Ong HL, Swaim W & Ambudkar IS. (2011). Local Ca(2)+ entry via Orai1 regulates plasma membrane recruitment of TRPC1 and controls cytosolic Ca(2)+ signals required for specific cell functions. *PLoS Biol* **9,** e1001025.

Chergui K, Suaud-Chagny MF & Gonon F. (1994). Nonlinear relationship between impulse flow, dopamine release and dopamine elimination in the rat brain in vivo. *Neuroscience* **62,** 641-645.

Chieng B, Azriel Y, Mohammadi S & Christie MJ. (2011). Distinct cellular properties of identified dopaminergic and GABAergic neurons in the mouse ventral tegmental area. *J Physiol* **589,** 3775-3787.

Chu HY & Zhen X. (2010). Hyperpolarization-activated, cyclic nucleotide-gated (HCN) channels in the regulation of midbrain dopamine systems. *Acta Pharmacol Sin* **31,** 1036-1043.

Chua HC, Wulf M, Weidling C, Rasmussen LP & Pless SA. (2020). The NALCN channel complex is voltage sensitive and directly modulated by extracellular calcium. *Sci Adv* **6,** eaaz3154.

Chung YH, Kim D, Moon NJ, Oh CS, Lee E, Shin DH, Kim SS, Lee WB, Lee JY & Cha CI. (2007).

Immunohistochemical study on the distribution of canonical transient receptor potential channels in rat basal ganglia. *Neurosci Lett* **422,** 18-23.

Clapham DE, Runnels LW & Strubing C. (2001). The TRP ion channel family. *Nat Rev Neurosci* **2,** 387-396.

Coimbra B, Domingues AV, Soares-Cunha C, Correia R, Pinto L, Sousa N & Rodrigues AJ. (2021). Laterodorsal tegmentum-ventral tegmental area projections encode positive reinforcement signals. *J Neurosci Res*.

Cornwall J, Cooper JD & Phillipson OT. (1990). Afferent and efferent connections of the laterodorsal tegmental nucleus in the rat. *Brain Res Bull* **25,** 271-284.

Cruz HG, Ivanova T, Lunn ML, Stoffel M, Slesinger PA & Luscher C. (2004). Bi-directional effects of GABA(B) receptor agonists on the mesolimbic dopamine system. *Nat Neurosci* **7,** 153-159.

Cucchiaroni ML, Viscomi MT, Bernardi G, Molinari M, Guatteo E & Mercuri NB. (2010). Metabotropic glutamate receptor 1 mediates the electrophysiological and toxic actions of the cycad derivative beta-N-Methylamino-L-alanine on substantia nigra pars compacta DAergic neurons. *J Neurosci* **30,** 5176-5188.

Davila V, Yan Z, Craciun LC, Logothetis D & Sulzer D. (2003). D3 dopamine autoreceptors do not activate G-protein-gated inwardly rectifying potassium channel currents in substantia nigra dopamine neurons. *J Neurosci* **23,** 5693-5697.

De March Z, Giampa C, Patassini S, Bernardi G & Fusco FR. (2006). Cellular localization of TRPC5 in the substantia nigra of rat. *Neurosci Lett* **402,** 35-39.

de Vrind V, Scuvee-Moreau J, Drion G, Hmaied C, Philippart F, Engel D & Seutin V. (2016). Interactions between calcium channels and SK channels in midbrain dopamine neurons and their impact on pacemaker regularity: Contrasting roles of N- and L-type channels. *Eur J Pharmacol* **788,** 274-279.

Deignan J, Lujan R, Bond C, Riegel A, Watanabe M, Williams JT, Maylie J & Adelman JP. (2012). SK2 and SK3 expression differentially affect firing frequency and precision in dopamine neurons. *Neuroscience* **217,** 67-76.

Del Campo N, Chamberlain SR, Sahakian BJ & Robbins TW. (2011). The roles of dopamine and noradrenaline in the pathophysiology and treatment of attention-deficit/hyperactivity disorder. *Biol Psychiatry* **69,** e145-157.

Delmas P & Brown DA. (2005). Pathways modulating neural KCNQ/M (Kv7) potassium channels. *Nat Rev Neurosci* **6,** 850-862.

Dou Y, Xia J, Gao R, Gao X, Munoz FM, Wei D, Tian Y, Barrett JE, Ajit S, Meucci O, Putney JW, Jr., Dai Y & Hu H. (2018). Orai1 Plays a Crucial Role in Central Sensitization by Modulating Neuronal Excitability. *J Neurosci* **38,** 887-900.

Dragicevic E, Poetschke C, Duda J, Schlaudraff F, Lammel S, Schiemann J, Fauler M, Hetzel A, Watanabe M, Lujan R, Malenka RC, Striessnig J & Liss B. (2014). Cav1.3 channels

control D2-autoreceptor responses via NCS-1 in substantia nigra dopamine neurons. *Brain* **137,** 2287-2302.

Dragicevic E, Schiemann J & Liss B. (2015). Dopamine midbrain neurons in health and Parkinson's disease: emerging roles of voltage-gated calcium channels and ATP-sensitive potassium channels. *Neuroscience* **284,** 798-814.

Drion G, Bonjean M, Waroux O, Scuvee-Moreau J, Liegeois JF, Sejnowski TJ, Sepulchre R & Seutin V. (2010). M-type channels selectively control bursting in rat dopaminergic neurons. *Eur J Neurosci* **31,** 827-835.

Dufour MA, Woodhouse A & Goaillard JM. (2014). Somatodendritic ion channel expression in substantia nigra pars compacta dopaminergic neurons across postnatal development. *J Neurosci Res* **92,** 981-999.

Estacion M, Sinkins WG, Jones SW, Applegate MA & Schilling WP. (2006). Human TRPC6 expressed in HEK 293 cells forms non-selective cation channels with limited Ca2+ permeability. *J Physiol* **572,** 359-377.

Estep CM, Galtieri DJ, Zampese E, Goldberg JA, Brichta L, Greengard P & Surmeier DJ. (2016). Transient Activation of GABAB Receptors Suppresses SK Channel Currents in Substantia Nigra Pars Compacta Dopaminergic Neurons. *PLoS One* **11,** e0169044.

Evans RC, Zhu M & Khaliq ZM. (2017). Dopamine Inhibition Differentially Controls Excitability of Substantia Nigra Dopamine Neuron Subpopulations through T-Type Calcium Channels. *J Neurosci* **37,** 3704-3720.

Exley R, Clements MA, Hartung H, McIntosh JM & Cragg SJ. (2008). Alpha6-containing nicotinic acetylcholine receptors dominate the nicotine control of dopamine neurotransmission in nucleus accumbens. *Neuropsychopharmacology* **33,** 2158-2166.

Exley R, Maubourguet N, David V, Eddine R, Evrard A, Pons S, Marti F, Threlfell S, Cazala P, McIntosh JM, Changeux JP, Maskos U, Cragg SJ & Faure P. (2011). Distinct contributions of nicotinic acetylcholine receptor subunit alpha4 and subunit alpha6 to the reinforcing effects of nicotine. *Proc Natl Acad Sci U S A* **108,** 7577-7582.

Exley R, McIntosh JM, Marks MJ, Maskos U & Cragg SJ. (2012). Striatal alpha5 nicotinic receptor subunit regulates dopamine transmission in dorsal striatum. *J Neurosci* **32,** 2352-2356.

Faber ES & Sah P. (2007). Functions of SK channels in central neurons. *Clin Exp Pharmacol Physiol* **34,** 1077-1083.

Faure P, Tolu S, Valverde S & Naude J. (2014). Role of nicotinic acetylcholine receptors in regulating dopamine neuron activity. *Neuroscience* **282,** 86-100.

Feng S. (2017). TRPC Channel Structure and Properties. *Adv Exp Med Biol* **976,** 9-23.

Fink-Jensen A, Fedorova I, Wortwein G, Woldbye DP, Rasmussen T, Thomsen M, Bolwig TG, Knitowski KM, McKinzie DL, Yamada M, Wess J & Basile A. (2003). Role for M5

muscarinic acetylcholine receptors in cocaine addiction. *J Neurosci Res* **74,** 91-96.

Fiorillo CD & Williams JT. (1998). Glutamate mediates an inhibitory postsynaptic potential in dopamine neurons. *Nature* **394,** 78-82.

Fiorillo CD & Williams JT. (2000). Cholinergic inhibition of ventral midbrain dopamine neurons. *J Neurosci* **20,** 7855-7860.

Floresco SB, West AR, Ash B, Moore H & Grace AA. (2003). Afferent modulation of dopamine neuron firing differentially regulates tonic and phasic dopamine transmission. *Nat Neurosci* **6,** 968-973.

Ford CP. (2014). The role of D2-autoreceptors in regulating dopamine neuron activity and transmission. *Neuroscience* **282,** 13-22.

Forster GL & Blaha CD. (2000). Laterodorsal tegmental stimulation elicits dopamine efflux in the rat nucleus accumbens by activation of acetylcholine and glutamate receptors in the ventral tegmental area. *Eur J Neurosci* **12,** 3596-3604.

Forster GL, Yeomans JS, Takeuchi J & Blaha CD. (2002). M5 muscarinic receptors are required for prolonged accumbal dopamine release after electrical stimulation of the pons in mice. *J Neurosci* **22,** RC190.

Foster DJ, Gentry PR, Lizardi-Ortiz JE, Bridges TM, Wood MR, Niswender CM, Sulzer D, Lindsley CW, Xiang Z & Conn PJ. (2014). M5 receptor activation produces opposing physiological outcomes in dopamine neurons depending on the receptor's location. *J Neurosci* **34,** 3253-3262.

Franklin KB. (1978). Catecholamines and self-stimulation: reward and performances effects dissociated. *Pharmacol Biochem Behav* **9,** 813-820.

Franz O, Liss B, Neu A & Roeper J. (2000). Single-cell mRNA expression of HCN1 correlates with a fast gating phenotype of hyperpolarization-activated cyclic nucleotide-gated ion channels (Ih) in central neurons. *Eur J Neurosci* **12,** 2685-2693.

Freichel M, Tsvilovskyy V & Camacho-Londono JE. (2014). TRPC4- and TRPC4-containing channels. *Handb Exp Pharmacol* **222,** 85-128.

Fulton S, Thibault D, Mendez JA, Lahaie N, Tirotta E, Borrelli E, Bouvier M, Tempel BL & Trudeau LE. (2011). Contribution of Kv1.2 voltage-gated potassium channel to D2 autoreceptor regulation of axonal dopamine overflow. *J Biol Chem* **286,** 9360-9372.

Fusco FR, Martorana A, Giampa C, De March Z, Vacca F, Tozzi A, Longone P, Piccirilli S, Paolucci S, Sancesario G, Mercuri NB & Bernardi G. (2004). Cellular localization of TRPC3 channel in rat brain: preferential distribution to oligodendrocytes. *Neurosci Lett* **365,** 137-142.

Futami T, Takakusaki K & Kitai ST. (1995). Glutamatergic and cholinergic inputs from the pedunculopontine tegmental nucleus to dopamine neurons in the substantia nigra pars compacta. *Neurosci Res* **21,** 331-342.

Gambardella C, Pignatelli A & Belluzzi O. (2012). The h-current in the substantia Nigra pars

compacta neurons: a re-examination. *PLoS One* **7,** e52329.

Gantz SC & Bean BP. (2017). Cell-Autonomous Excitation of Midbrain Dopamine Neurons by Endocannabinoid-Dependent Lipid Signaling. *Neuron* **93,** 1375-1387 e1372.

Gao YY, Tian W, Zhang HN, Sun Y, Meng JR, Cao W & Li XQ. (2021). Canonical transient receptor potential channels and their modulators: biology, pharmacology and therapeutic potentials. *Arch Pharm Res* **44,** 354-377.

Garzon M & Pickel VM. (2006). Subcellular distribution of M2 muscarinic receptors in relation to dopaminergic neurons of the rat ventral tegmental area. *J Comp Neurol* **498,** 821-839.

Garzon M & Pickel VM. (2013). Somatodendritic targeting of M5 muscarinic receptor in the rat ventral tegmental area: implications for mesolimbic dopamine transmission. *J Comp Neurol* **521,** 2927-2946.

Giampa C, DeMarch Z, Patassini S, Bernardi G & Fusco FR. (2007). Immunohistochemical localization of TRPC6 in the rat substantia nigra. *Neurosci Lett* **424,** 170-174.

Giessel AJ & Sabatini BL. (2010). M1 muscarinic receptors boost synaptic potentials and calcium influx in dendritic spines by inhibiting postsynaptic SK channels. *Neuron* **68,** 936-947.

Goel M, Sinkins WG & Schilling WP. (2002). Selective association of TRPC channel subunits in rat brain synaptosomes. *J Biol Chem* **277,** 48303-48310.

Goertz RB, Wanat MJ, Gomez JA, Brown ZJ, Phillips PE & Paladini CA. (2015). Cocaine increases dopaminergic neuron and motor activity via midbrain alpha1 adrenergic signaling. *Neuropsychopharmacology* **40,** 1151-1162.

Gonon FG. (1988). Nonlinear relationship between impulse flow and dopamine released by rat midbrain dopaminergic neurons as studied by in vivo electrochemistry. *Neuroscience* **24,** 19-28.

Gonzalez-Cabrera C, Meza R, Ulloa L, Merino-Sepulveda P, Luco V, Sanhueza A, Onate-Ponce A, Bolam JP & Henny P. (2017). Characterization of the axon initial segment of mice substantia nigra dopaminergic neurons. *J Comp Neurol* **525,** 3529-3542.

Gould RW, Gunter BW, Bubser M, Matthews RT, Teal LB, Ragland MG, Bridges TM, Garrison AT, Winder DG, Lindsley CW & Jones CK. (2019). Acute Negative Allosteric Modulation of M5 Muscarinic Acetylcholine Receptors Inhibits Oxycodone Self-Administration and Cue-Induced Reactivity with No Effect on Antinociception. *ACS Chem Neurosci* **10,** 3740-3750.

Grace AA & Onn SP. (1989). Morphology and electrophysiological properties of immunocytochemically identified rat dopamine neurons recorded in vitro. *J Neurosci* **9,** 3463-3481.

Greene DL & Hoshi N. (2017). Modulation of Kv7 channels and excitability in the brain. *Cell Mol Life Sci* **74,** 495-508.

Gross SA, Guzman GA, Wissenbach U, Philipp SE, Zhu MX, Bruns D & Cavalie A. (2009). TRPC5 is a Ca2+-activated channel functionally coupled to Ca2+-selective ion channels. *J Biol Chem* **284,** 34423-34432.

Gualdani R & Gailly P. (2020). How TRPC Channels Modulate Hippocampal Function. *Int J Mol Sci* **21**.

Guatteo E, Mercuri NB, Bernardi G & Knopfel T. (1999). Group I metabotropic glutamate receptors mediate an inward current in rat substantia nigra dopamine neurons that is independent from calcium mobilization. *J Neurophysiol* **82,** 1974-1981.

Gunter BW, Gould RW, Bubser M, McGowan KM, Lindsley CW & Jones CK. (2018). Selective inhibition of M5 muscarinic acetylcholine receptors attenuates cocaine self-administration in rats. *Addict Biol* **23,** 1106-1116.

Guo J & Schofield GG. (2003). Activation of muscarinic m5 receptors inhibits recombinant KCNQ2/KCNQ3 K+ channels expressed in HEK293T cells. *Eur J Pharmacol* **462,** 25-32.

Hansen HH, Ebbesen C, Mathiesen C, Weikop P, Ronn LC, Waroux O, Scuvee-Moreau J, Seutin V & Mikkelsen JD. (2006). The KCNQ channel opener retigabine inhibits the activity of mesencephalic dopaminergic systems of the rat. *J Pharmacol Exp Ther* **318,** 1006-1019.

Hartmann J, Dragicevic E, Adelsberger H, Henning HA, Sumser M, Abramowitz J, Blum R, Dietrich A, Freichel M, Flockerzi V, Birnbaumer L & Konnerth A. (2008). TRPC3 channels are required for synaptic transmission and motor coordination. *Neuron* **59,** 392-398.

Hartmann J, Karl RM, Alexander RP, Adelsberger H, Brill MS, Ruhlmann C, Ansel A, Sakimura K, Baba Y, Kurosaki T, Misgeld T & Konnerth A. (2014). STIM1 controls neuronal Ca(2)(+) signaling, mGluR1-dependent synaptic transmission, and cerebellar motor behavior. *Neuron* **82,** 635-644.

He LP, Hewavitharana T, Soboloff J, Spassova MA & Gill DL. (2005). A functional link between store-operated and TRPC channels revealed by the 3,5-bis(trifluoromethyl)pyrazole derivative, BTP2. *J Biol Chem* **280,** 10997-11006.

Herrik KF, Christophersen P & Shepard PD. (2010). Pharmacological modulation of the gating properties of small conductance Ca2+-activated K+ channels alters the firing pattern of dopamine neurons in vivo. *J Neurophysiol* **104,** 1726-1735.

Hill JJ & Peralta EG. (2001). Inhibition of a Gi-activated potassium channel (GIRK1/4) by the Gq-coupled m1 muscarinic acetylcholine receptor. *J Biol Chem* **276,** 5505-5510.

Hofmann T, Schaefer M, Schultz G & Gudermann T. (2002). Subunit composition of mammalian transient receptor potential channels in living cells. *Proc Natl Acad Sci U S A* **99,** 7461-7466.

Howard CD, Li H, Geddes CE & Jin X. (2017). Dynamic Nigrostriatal Dopamine Biases Action Selection. *Neuron* **93,** 1436-1450 e1438.

Ikemoto S & Wise RA. (2002). Rewarding effects of the cholinergic agents carbachol and neostigmine in the posterior ventral tegmental area. *J Neurosci* **22,** 9895-9904.

Ilango A, Shumake J, Wetzel W, Scheich H & Ohl FW. (2012). The role of dopamine in the context of aversive stimuli with particular reference to acoustically signaled avoidance learning. *Front Neurosci* **6,** 132.

Inanobe A, Yoshimoto Y, Horio Y, Morishige KI, Hibino H, Matsumoto S, Tokunaga Y, Maeda T, Hata Y, Takai Y & Kurachi Y. (1999). Characterization of G-protein-gated K+ channels composed of Kir3.2 subunits in dopaminergic neurons of the substantia nigra. *J Neurosci* **19,** 1006-1017.

Inoue R, Okada T, Onoue H, Hara Y, Shimizu S, Naitoh S, Ito Y & Mori Y. (2001). The transient receptor potential protein homologue TRP6 is the essential component of vascular alpha(1)-adrenoceptor-activated Ca(2+)-permeable cation channel. *Circ Res* **88,** 325-332.

Ishikawa J, Ohga K, Yoshino T, Takezawa R, Ichikawa A, Kubota H & Yamada T. (2003). A pyrazole derivative, YM-58483, potently inhibits store-operated sustained Ca2+ influx and IL-2 production in T lymphocytes. *J Immunol* **170,** 4441-4449.

Itsuki K, Imai Y, Hase H, Okamura Y, Inoue R & Mori MX. (2014). PLC-mediated PI(4,5)P2 hydrolysis regulates activation and inactivation of TRPC6/7 channels. *J Gen Physiol* **143,** 183-201.

Jeon JP, Hong C, Park EJ, Jeon JH, Cho NH, Kim IG, Choe H, Muallem S, Kim HJ & So I. (2012). Selective Galphai subunits as novel direct activators of transient receptor potential canonical (TRPC)4 and TRPC5 channels. *J Biol Chem* **287,** 17029-17039.

Ji H, Tucker KR, Putzier I, Huertas MA, Horn JP, Canavier CC, Levitan ES & Shepard PD. (2012). Functional characterization of ether-a-go-go-related gene potassium channels in midbrain dopamine neurons - implications for a role in depolarization block. *Eur J Neurosci* **36,** 2906-2916.

Johnson SW & Wu YN. (2004). Multiple mechanisms underlie burst firing in rat midbrain dopamine neurons in vitro. *Brain Res* **1019,** 293-296.

Jones IW & Wonnacott S. (2004). Precise localization of alpha7 nicotinic acetylcholine receptors on glutamatergic axon terminals in the rat ventral tegmental area. *J Neurosci* **24,** 11244-11252.

Jung S, Muhle A, Schaefer M, Strotmann R, Schultz G & Plant TD. (2003). Lanthanides potentiate TRPC5 currents by an action at extracellular sites close to the pore mouth. *J Biol Chem* **278,** 3562-3571.

Kang Y & Kitai ST. (1993). Calcium spike underlying rhythmic firing in dopaminergic neurons of the rat substantia nigra. *Neurosci Res* **18,** 195-207.

Katona I & Freund TF. (2012). Multiple functions of endocannabinoid signaling in the brain. *Annu Rev Neurosci* **35,** 529-558.

Khaliq ZM & Bean BP. (2008). Dynamic, nonlinear feedback regulation of slow pacemaking by A-type potassium current in ventral tegmental area neurons. *J Neurosci* **28,** 10905-10917.

Khaliq ZM & Bean BP. (2010). Pacemaking in dopaminergic ventral tegmental area neurons: depolarizing drive from background and voltage-dependent sodium conductances. *J Neurosci* **30,** 7401-7413.

Khodakhah K, Melishchuk A & Armstrong CM. (1997). Killing K channels with TEA+. *Proc Natl Acad Sci U S A* **94,** 13335-13338.

Kim J, Kwak M, Jeon JP, Myeong J, Wie J, Hong C, Kim SY, Jeon JH, Kim HJ & So I. (2014). Isoform- and receptor-specific channel property of canonical transient receptor potential (TRPC)1/4 channels. *Pflugers Arch* **466,** 491-504.

Kimm T, Khaliq ZM & Bean BP. (2015). Differential Regulation of Action Potential Shape and Burst-Frequency Firing by BK and Kv2 Channels in Substantia Nigra Dopaminergic Neurons. *J Neurosci* **35,** 16404-16417.

Kiselyov K, Xu X, Mozhayeva G, Kuo T, Pessah I, Mignery G, Zhu X, Birnbaumer L & Muallem S. (1998). Functional interaction between InsP3 receptors and store-operated Htrp3 channels. *Nature* **396,** 478-482.

Kitai ST, Shepard PD, Callaway JC & Scroggs R. (1999). Afferent modulation of dopamine neuron firing patterns. *Curr Opin Neurobiol* **9,** 690-697.

Kiyonaka S, Kato K, Nishida M, Mio K, Numaga T, Sawaguchi Y, Yoshida T, Wakamori M, Mori E, Numata T, Ishii M, Takemoto H, Ojida A, Watanabe K, Uemura A, Kurose H, Morii T, Kobayashi T, Sato Y, Sato C, Hamachi I & Mori Y. (2009). Selective and direct inhibition of TRPC3 channels underlies biological activities of a pyrazole compound. *Proc Natl Acad Sci U S A* **106,** 5400-5405.

Klink R, de Kerchove d'Exaerde A, Zoli M & Changeux JP. (2001). Molecular and physiological diversity of nicotinic acetylcholine receptors in the midbrain dopaminergic nuclei. *J Neurosci* **21,** 1452-1463.

Klipec WD, Burrow KR, O'Neill C, Cao JL, Lawyer CR, Ostertag E, Fowler M, Bachtell RK, Illig KR & Cooper DC. (2016). Loss of the trpc4 gene is associated with a reduction in cocaine self-administration and reduced spontaneous ventral tegmental area dopamine neuronal activity, without deficits in learning for natural rewards. *Behav Brain Res* **306,** 117-127.

Koob GF & Volkow ND. (2010). Neurocircuitry of addiction. *Neuropsychopharmacology* **35,** 217-238.

Koyama S & Appel SB. (2006). Characterization of M-current in ventral tegmental area dopamine neurons. *J Neurophysiol* **96,** 535-543.

Kramer PF & Williams JT. (2016). Calcium Release from Stores Inhibits GIRK. *Cell Rep* **17,** 3246-3255.

Krashia P, Martini A, Nobili A, Aversa D, D'Amelio M, Berretta N, Guatteo E & Mercuri NB. (2017). On the properties of identified dopaminergic neurons in the mouse substantia nigra and ventral tegmental area. *Eur J Neurosci* **45,** 92-105.

Kravitz AV, Freeze BS, Parker PR, Kay K, Thwin MT, Deisseroth K & Kreitzer AC. (2010). Regulation of parkinsonian motor behaviours by optogenetic control of basal ganglia circuitry. *Nature* **466,** 622-626.

Kschonsak M, Chua HC, Noland CL, Weidling C, Clairfeuille T, Bahlke OO, Ameen AO, Li ZR, Arthur CP, Ciferri C, Pless SA & Payandeh J. (2020). Structure of the human sodium leak channel NALCN. *Nature* **587,** 313-318.

Lacey MG, Calabresi P & North RA. (1990). Muscarine depolarizes rat substantia nigra zona compacta and ventral tegmental neurons in vitro through M1-like receptors. *J Pharmacol Exp Ther* **253,** 395-400.

Lammel S, Hetzel A, Hackel O, Jones I, Liss B & Roeper J. (2008). Unique properties of mesoprefrontal neurons within a dual mesocorticolimbic dopamine system. *Neuron* **57,** 760-773.

Lansman JB, Hess P & Tsien RW. (1986). Blockade of current through single calcium channels by Cd2+, Mg2+, and Ca2+. Voltage and concentration dependence of calcium entry into the pore. *J Gen Physiol* **88,** 321-347.

Larsson KP, Peltonen HM, Bart G, Louhivuori LM, Penttonen A, Antikainen M, Kukkonen JP & Akerman KE. (2005). Orexin-A-induced Ca2+ entry: evidence for involvement of trpc channels and protein kinase C regulation. *J Biol Chem* **280,** 1771-1781.

Lei Q, Talley EM & Bayliss DA. (2001). Receptor-mediated inhibition of G protein-coupled inwardly rectifying potassium channels involves G(alpha)q family subunits, phospholipase C, and a readily diffusible messenger. *J Biol Chem* **276,** 16720-16730.

Lemonnier L, Trebak M & Putney JW, Jr. (2008). Complex regulation of the TRPC3, 6 and 7 channel subfamily by diacylglycerol and phosphatidylinositol-4,5-bisphosphate. *Cell Calcium* **43,** 506-514.

Lester DB, Miller AD & Blaha CD. (2010a). Muscarinic receptor blockade in the ventral tegmental area attenuates cocaine enhancement of laterodorsal tegmentum stimulation-evoked accumbens dopamine efflux in the mouse. *Synapse* **64,** 216-223.

Lester DB, Miller AD, Pate TD & Blaha CD. (2008). Midbrain acetylcholine and glutamate receptors modulate accumbal dopamine release. *Neuroreport* **19,** 991-995.

Lester DB, Rogers TD & Blaha CD. (2010b). Acetylcholine-dopamine interactions in the pathophysiology and treatment of CNS disorders. *CNS Neurosci Ther* **16,** 137-162.

Levey AI. (1993). Immunological localization of m1-m5 muscarinic acetylcholine receptors in peripheral tissues and brain. *Life Sci* **52,** 441-448.

Li L, Sun H, Ding J, Niu C, Su M, Zhang L, Li Y, Wang C, Gamper N, Du X & Zhang H. (2017). Selective targeting of M-type potassium Kv 7.4 channels demonstrates their key role

in the regulation of dopaminergic neuronal excitability and depression-like behaviour. *Br J Pharmacol* **174,** 4277-4294.

Lintschinger B, Balzer-Geldsetzer M, Baskaran T, Graier WF, Romanin C, Zhu MX & Groschner K. (2000). Coassembly of Trp1 and Trp3 proteins generates diacylglycerol- and Ca2+-sensitive cation channels. *J Biol Chem* **275,** 27799-27805.

Lipscombe D, Helton TD & Xu W. (2004). L-type calcium channels: the low down. *J Neurophysiol* **92,** 2633-2641.

Liss B, Franz O, Sewing S, Bruns R, Neuhoff H & Roeper J. (2001). Tuning pacemaker frequency of individual dopaminergic neurons by Kv4.3L and KChip3.1 transcription. *EMBO J* **20,** 5715-5724.

Liu X, Bandyopadhyay BC, Singh BB, Groschner K & Ambudkar IS. (2005). Molecular analysis of a store-operated and 2-acetyl-sn-glycerol-sensitive non-selective cation channel. Heteromeric assembly of TRPC1-TRPC3. *J Biol Chem* **280,** 21600-21606.

Liu Y & Chen X. (2008). Cholinergic excitation of dopaminergic cells depends on sequential activation of protein kinase C and the L-type calcium channel in ventral tegmental area slices. *Brain Res* **1245,** 41-51.

Liu Y, Harding M, Pittman A, Dore J, Striessnig J, Rajadhyaksha A & Chen X. (2014). Cav1.2 and Cav1.3 L-type calcium channels regulate dopaminergic firing activity in the mouse ventral tegmental area. *J Neurophysiol* **112,** 1119-1130.

Liu Z, Bunney EB, Appel SB & Brodie MS. (2003). Serotonin reduces the hyperpolarization-activated current (Ih) in ventral tegmental area dopamine neurons: involvement of 5-HT2 receptors and protein kinase C. *J Neurophysiol* **90,** 3201-3212.

Lodge DJ & Grace AA. (2006). The laterodorsal tegmentum is essential for burst firing of ventral tegmental area dopamine neurons. *Proc Natl Acad Sci U S A* **103,** 5167-5172.

Lu B, Su Y, Das S, Wang H, Wang Y, Liu J & Ren D. (2009). Peptide neurotransmitters activate a cation channel complex of NALCN and UNC-80. *Nature* **457,** 741-744.

Lu TZ & Feng ZP. (2012). NALCN: a regulator of pacemaker activity. *Mol Neurobiol* **45,** 415-423.

Luquin E, Huerta I, Aymerich MS & Mengual E. (2018). Stereological Estimates of Glutamatergic, GABAergic, and Cholinergic Neurons in the Pedunculopontine and Laterodorsal Tegmental Nuclei in the Rat. *Front Neuroanat* **12,** 34.

Luscher C & Slesinger PA. (2010). Emerging roles for G protein-gated inwardly rectifying potassium (GIRK) channels in health and disease. *Nat Rev Neurosci* **11,** 301-315.

Majewski L & Kuznicki J. (2015). SOCE in neurons: Signaling or just refilling? *Biochim Biophys Acta* **1853,** 1940-1952.

Mameli-Engvall M, Evrard A, Pons S, Maskos U, Svensson TH, Changeux JP & Faure P. (2006). Hierarchical control of dopamine neuron-firing patterns by nicotinic receptors. *Neuron* **50,** 911-921.

Mao J, Wang X, Chen F, Wang R, Rojas A, Shi Y, Piao H & Jiang C. (2004). Molecular basis for the inhibition of G protein-coupled inward rectifier K(+) channels by protein kinase C. *Proc Natl Acad Sci U S A* **101,** 1087-1092.

Martini A, Cordella A, Pisani A, Mercuri NB & Guatteo E. (2019). Neurotensin receptors inhibit mGluR I responses in nigral dopaminergic neurons via a process that undergoes functional desensitization by G-protein coupled receptor kinases. *Neuropharmacology* **155,** 76-88.

Martorana A, Giampa C, DeMarch Z, Viscomi MT, Patassini S, Sancesario G, Bernardi G & Fusco FR. (2006). Distribution of TRPC1 receptors in dendrites of rat substantia nigra: a confocal and electron microscopy study. *Eur J Neurosci* **24,** 732-738.

Masi A, Narducci R, Resta F, Carbone C, Kobayashi K & Mannaioni G. (2015). Differential contribution of Ih to the integration of excitatory synaptic inputs in substantia nigra pars compacta and ventral tegmental area dopaminergic neurons. *Eur J Neurosci* **42,** 2699-2706.

Maskos U. (2008). The cholinergic mesopontine tegmentum is a relatively neglected nicotinic master modulator of the dopaminergic system: relevance to drugs of abuse and pathology. *Br J Pharmacol* **153 Suppl 1,** S438-445.

Mateos-Aparicio P, Murphy R & Storm JF. (2014). Complementary functions of SK and Kv7/M potassium channels in excitability control and synaptic integration in rat hippocampal dentate granule cells. *J Physiol* **592,** 669-693.

Matsubayashi H, Amano T, Seki T, Sasa M & Sakai N. (2003). Electrophysiological characterization of nicotine-induced excitation of dopaminergic neurons in the rat substantia nigra. *J Pharmacol Sci* **93,** 143-148.

Maylie J, Bond CT, Herson PS, Lee WS & Adelman JP. (2004). Small conductance Ca2+-activated K+ channels and calmodulin. *J Physiol* **554,** 255-261.

McCutcheon RA, Abi-Dargham A & Howes OD. (2019). Schizophrenia, Dopamine and the Striatum: From Biology to Symptoms. *Trends Neurosci* **42,** 205-220.

McFarland K & Ettenberg A. (1995). Haloperidol differentially affects reinforcement and motivational processes in rats running an alley for intravenous heroin. *Psychopharmacology (Berl)* **122,** 346-350.

McKemy DD, Neuhausser WM & Julius D. (2002). Identification of a cold receptor reveals a general role for TRP channels in thermosensation. *Nature* **416,** 52-58.

Mezey E, Toth ZE, Cortright DN, Arzubi MK, Krause JE, Elde R, Guo A, Blumberg PM & Szallasi A. (2000). Distribution of mRNA for vanilloid receptor subtype 1 (VR1), and VR1-like immunoreactivity, in the central nervous system of the rat and human. *Proc Natl Acad Sci U S A* **97,** 3655-3660.

Michel FJ, Fortin GD, Martel P, Yeomans J & Trudeau LE. (2005). M3-like muscarinic receptors mediate Ca2+ influx in rat mesencephalic GABAergic neurones through a protein

kinase C-dependent mechanism. *Neuropharmacology* **48,** 796-809.

Michel FJ, Robillard JM & Trudeau LE. (2004). Regulation of rat mesencephalic GABAergic neurones through muscarinic receptors. *J Physiol* **556,** 429-445.

Minke B. (2010). The history of the Drosophila TRP channel: the birth of a new channel superfamily. *J Neurogenet* **24,** 216-233.

Mogenson GJ, Jones DL & Yim CY. (1980). From motivation to action: functional interface between the limbic system and the motor system. *Prog Neurobiol* **14,** 69-97.

Monaghan AS, Benton DC, Bahia PK, Hosseini R, Shah YA, Haylett DG & Moss GW. (2004). The SK3 subunit of small conductance Ca2+-activated K+ channels interacts with both SK1 and SK2 subunits in a heterologous expression system. *J Biol Chem* **279,** 1003-1009.

Morel C, Fattore L, Pons S, Hay YA, Marti F, Lambolez B, De Biasi M, Lathrop M, Fratta W, Maskos U & Faure P. (2014). Nicotine consumption is regulated by a human polymorphism in dopamine neurons. *Mol Psychiatry* **19,** 930-936.

Moreno C & Vaca L. (2011). SOC and now also SIC: store-operated and store-inhibited channels. *IUBMB Life* **63,** 856-863.

Mrejeru A, Wei A & Ramirez JM. (2011). Calcium-activated non-selective cation currents are involved in generation of tonic and bursting activity in dopamine neurons of the substantia nigra pars compacta. *J Physiol* **589,** 2497-2514.

Munsch T, Freichel M, Flockerzi V & Pape HC. (2003). Contribution of transient receptor potential channels to the control of GABA release from dendrites. *Proc Natl Acad Sci U S A* **100,** 16065-16070.

Nair-Roberts RG, Chatelain-Badie SD, Benson E, White-Cooper H, Bolam JP & Ungless MA. (2008). Stereological estimates of dopaminergic, GABAergic and glutamatergic neurons in the ventral tegmental area, substantia nigra and retrorubral field in the rat. *Neuroscience* **152,** 1024-1031.

Negus SS & Miller LL. (2014). Intracranial self-stimulation to evaluate abuse potential of drugs. *Pharmacol Rev* **66,** 869-917.

Nesin V & Tsiokas L. (2014). Trpc1. *Handb Exp Pharmacol* **222,** 15-51.

Nestler EJ. (2005). Is there a common molecular pathway for addiction? *Nat Neurosci* **8,** 1445-1449.

Neuhoff H, Neu A, Liss B & Roeper J. (2002). I(h) channels contribute to the different functional properties of identified dopaminergic subpopulations in the midbrain. *J Neurosci* **22,** 1290-1302.

Nilius B & Owsianik G. (2011). The transient receptor potential family of ion channels. *Genome Biol* **12,** 218.

Nunes EJ, Rupprecht LE, Foster DJ, Lindsley CW, Conn PJ & Addy NA. (2020). Examining the role of muscarinic M5 receptors in VTA cholinergic modulation of depressive-like and

anxiety-related behaviors in rats. *Neuropharmacology* **171,** 108089.

Oakman SA, Faris PL, Kerr PE, Cozzari C & Hartman BK. (1995). Distribution of pontomesencephalic cholinergic neurons projecting to substantia nigra differs significantly from those projecting to ventral tegmental area. *J Neurosci* **15,** 5859-5869.

Obukhov AG & Nowycky MC. (2004). TRPC5 activation kinetics are modulated by the scaffolding protein ezrin/radixin/moesin-binding phosphoprotein-50 (EBP50). *J Cell Physiol* **201,** 227-235.

Obukhov AG & Nowycky MC. (2005). A cytosolic residue mediates Mg2+ block and regulates inward current amplitude of a transient receptor potential channel. *J Neurosci* **25,** 1234-1239.

Okamoto T, Harnett MT & Morikawa H. (2006). Hyperpolarization-activated cation current (Ih) is an ethanol target in midbrain dopamine neurons of mice. *J Neurophysiol* **95,** 619-626.

Omelchenko N & Sesack SR. (2006). Cholinergic axons in the rat ventral tegmental area synapse preferentially onto mesoaccumbens dopamine neurons. *J Comp Neurol* **494,** 863-875.

Otsuguro K, Tang J, Tang Y, Xiao R, Freichel M, Tsvilovskyy V, Ito S, Flockerzi V, Zhu MX & Zholos AV. (2008). Isoform-specific inhibition of TRPC4 channel by phosphatidylinositol 4,5-bisphosphate. *J Biol Chem* **283,** 10026-10036.

Paladini CA & Roeper J. (2014). Generating bursts (and pauses) in the dopamine midbrain neurons. *Neuroscience* **282,** 109-121.

Palmiter RD. (2008). Dopamine signaling in the dorsal striatum is essential for motivated behaviors: lessons from dopamine-deficient mice. *Ann N Y Acad Sci* **1129,** 35-46.

Pascoli V, Terrier J, Hiver A & Luscher C. (2015). Sufficiency of Mesolimbic Dopamine Neuron Stimulation for the Progression to Addiction. *Neuron* **88,** 1054-1066.

Pecina S, Cagniard B, Berridge KC, Aldridge JW & Zhuang X. (2003). Hyperdopaminergic mutant mice have higher "wanting" but not "liking" for sweet rewards. *J Neurosci* **23,** 9395-9402.

Philippart F, Destreel G, Merino-Sepulveda P, Henny P, Engel D & Seutin V. (2016). Differential Somatic Ca2+ Channel Profile in Midbrain Dopaminergic Neurons. *J Neurosci* **36,** 7234-7245.

Philippart F & Khaliq ZM. (2018). Gi/o protein-coupled receptors in dopamine neurons inhibit the sodium leak channel NALCN. *Elife* **7**.

Picciotto MR, Higley MJ & Mineur YS. (2012). Acetylcholine as a neuromodulator: cholinergic signaling shapes nervous system function and behavior. *Neuron* **76,** 116-129.

Pidoplichko VI, DeBiasi M, Williams JT & Dani JA. (1997). Nicotine activates and desensitizes midbrain dopamine neurons. *Nature* **390,** 401-404.

Pidoplichko VI, Noguchi J, Areola OO, Liang Y, Peterson J, Zhang T & Dani JA. (2004). Nicotinic cholinergic synaptic mechanisms in the ventral tegmental area contribute to nicotine addiction. *Learn Mem* **11,** 60-69.

Ping HX & Shepard PD. (1996). Apamin-sensitive Ca(2+)-activated K+ channels regulate pacemaker activity in nigral dopamine neurons. *Neuroreport* **7,** 809-814.

Poetschke C, Dragicevic E, Duda J, Benkert J, Dougalis A, DeZio R, Snutch TP, Striessnig J & Liss B. (2015). Compensatory T-type Ca2+ channel activity alters D2-autoreceptor responses of Substantia nigra dopamine neurons from Cav1.3 L-type Ca2+ channel KO mice. *Sci Rep* **5,** 13688.

Polter AM, Barcomb K, Tsuda AC & Kauer JA. (2018). Synaptic function and plasticity in identified inhibitory inputs onto VTA dopamine neurons. *Eur J Neurosci* **47,** 1208-1218.

Poteser M, Graziani A, Rosker C, Eder P, Derler I, Kahr H, Zhu MX, Romanin C & Groschner K. (2006). TRPC3 and TRPC4 associate to form a redox-sensitive cation channel. Evidence for expression of native TRPC3-TRPC4 heteromeric channels in endothelial cells. *J Biol Chem* **281,** 13588-13595.

Puopolo M, Raviola E & Bean BP. (2007). Roles of subthreshold calcium current and sodium current in spontaneous firing of mouse midbrain dopamine neurons. *J Neurosci* **27,** 645-656.

Putney JW, Jr. (1986). A model for receptor-regulated calcium entry. *Cell Calcium* **7,** 1-12.

Putzier I, Kullmann PH, Horn JP & Levitan ES. (2009). Cav1.3 channel voltage dependence, not Ca2+ selectivity, drives pacemaker activity and amplifies bursts in nigral dopamine neurons. *J Neurosci* **29,** 15414-15419.

Rajadhyaksha A, Husson I, Satpute SS, Kuppenbender KD, Ren JQ, Guerriero RM, Standaert DG & Kosofsky BE. (2004). L-type Ca2+ channels mediate adaptation of extracellular signal-regulated kinase 1/2 phosphorylation in the ventral tegmental area after chronic amphetamine treatment. *J Neurosci* **24,** 7464-7476.

Ratte S, Karnup S & Prescott SA. (2018). Nonlinear Relationship Between Spike-Dependent Calcium Influx and TRPC Channel Activation Enables Robust Persistent Spiking in Neurons of the Anterior Cingulate Cortex. *J Neurosci* **38,** 1788-1801.

Raza C, Anjum R & Shakeel NUA. (2019). Parkinson's disease: Mechanisms, translational models and management strategies. *Life Sci* **226,** 77-90.

Reever CM, Ferrari-DiLeo G & Flynn DD. (1997). The M5 (m5) receptor subtype: fact or fiction? *Life Sci* **60,** 1105-1112.

Ren D. (2011). Sodium leak channels in neuronal excitability and rhythmic behaviors. *Neuron* **72,** 899-911.

Rezayof A, Nazari-Serenjeh F, Zarrindast MR, Sepehri H & Delphi L. (2007). Morphine-induced place preference: involvement of cholinergic receptors of the ventral

tegmental area. *Eur J Pharmacol* **562,** 92-102.

Riccio A, Li Y, Moon J, Kim KS, Smith KS, Rudolph U, Gapon S, Yao GL, Tsvetkov E, Rodig SJ, Van't Veer A, Meloni EG, Carlezon WA, Jr., Bolshakov VY & Clapham DE. (2009). Essential role for TRPC5 in amygdala function and fear-related behavior. *Cell* **137,** 761-772.

Riccio A, Li Y, Tsvetkov E, Gapon S, Yao GL, Smith KS, Engin E, Rudolph U, Bolshakov VY & Clapham DE. (2014). Decreased anxiety-like behavior and Galphaq/11-dependent responses in the amygdala of mice lacking TRPC4 channels. *J Neurosci* **34,** 3653-3667.

Rice ME & Patel JC. (2015). Somatodendritic dopamine release: recent mechanistic insights. *Philos Trans R Soc Lond B Biol Sci* **370**.

Richards CD, Shiroyama T & Kitai ST. (1997). Electrophysiological and immunocytochemical characterization of GABA and dopamine neurons in the substantia nigra of the rat. *Neuroscience* **80,** 545-557.

Rivera-Acevedo RE, Pless SA, Schwarz SK & Ahern CA. (2012). Extracellular quaternary ammonium blockade of transient receptor potential vanilloid subtype 1 channels expressed in Xenopus laevis oocytes. *Mol Pharmacol* **82,** 1129-1135.

Roberts DC, Corcoran ME & Fibiger HC. (1977). On the role of ascending catecholaminergic systems in intravenous self-administration of cocaine. *Pharmacol Biochem Behav* **6,** 615-620.

Robinson S, Sandstrom SM, Denenberg VH & Palmiter RD. (2005). Distinguishing whether dopamine regulates liking, wanting, and/or learning about rewards. *Behav Neurosci* **119,** 5-15.

Roeper J. (2013). Dissecting the diversity of midbrain dopamine neurons. *Trends Neurosci* **36,** 336-342.

Sato A, Arichi S, Kojima F, Hayashi T, Ohba T, Cheung DL, Eto K, Narushima M, Murakoshi H, Maruo Y, Kadoya Y, Nabekura J & Ishibashi H. (2020). Histamine depolarizes rat intracardiac ganglion neurons through the activation of TRPC non-selective cation channels. *Eur J Pharmacol* **886,** 173536.

Schaefer M, Plant TD, Obukhov AG, Hofmann T, Gudermann T & Schultz G. (2000). Receptor-mediated regulation of the nonselective cation channels TRPC4 and TRPC5. *J Biol Chem* **275,** 17517-17526.

Schindl R, Frischauf I, Bergsmann J, Muik M, Derler I, Lackner B, Groschner K & Romanin C. (2009). Plasticity in Ca2+ selectivity of Orai1/Orai3 heteromeric channel. *Proc Natl Acad Sci U S A* **106,** 19623-19628.

Schultz W. (1998). Predictive reward signal of dopamine neurons. *J Neurophysiol* **80,** 1-27.

Selvaraj S, Sun Y, Watt JA, Wang S, Lei S, Birnbaumer L & Singh BB. (2012). Neurotoxin-induced ER stress in mouse dopaminergic neurons involves downregulation of TRPC1 and inhibition of AKT/mTOR signaling. *J Clin Invest* **122,** 1354-1367.

Selyanko AA, Hadley JK, Wood IC, Abogadie FC, Jentsch TJ & Brown DA. (2000). Inhibition of KCNQ1-4 potassium channels expressed in mammalian cells via M1 muscarinic acetylcholine receptors. *J Physiol* **522 Pt 3,** 349-355.

Shepard PD & Bunney BS. (1991). Repetitive firing properties of putative dopamine-containing neurons in vitro: regulation by an apamin-sensitive Ca(2+)-activated K+ conductance. *Exp Brain Res* **86,** 141-150.

Shin JH, Adrover MF, Wess J & Alvarez VA. (2015). Muscarinic regulation of dopamine and glutamate transmission in the nucleus accumbens. *Proc Natl Acad Sci U S A* **112,** 8124-8129.

Solecki W, Wickham RJ, Behrens S, Wang J, Zwerling B, Mason GF & Addy NA. (2013). Differential role of ventral tegmental area acetylcholine and N-methyl-D-aspartate receptors in cocaine-seeking. *Neuropharmacology* **75,** 9-18.

Song K, Wei M, Guo W, Quan L, Kang Y, Wu JX & Chen L. (2021). Structural basis for human TRPC5 channel inhibition by two distinct inhibitors. *Elife* **10**.

Sotak BN, Hnasko TS, Robinson S, Kremer EJ & Palmiter RD. (2005). Dysregulation of dopamine signaling in the dorsal striatum inhibits feeding. *Brain Res* **1061,** 88-96.

Sotty F, Damgaard T, Montezinho LP, Mork A, Olsen CK, Bundgaard C & Husum H. (2009). Antipsychotic-like effect of retigabine [N-(2-Amino-4-(fluorobenzylamino)-phenyl)carbamic acid ester], a KCNQ potassium channel opener, via modulation of mesolimbic dopaminergic neurotransmission. *J Pharmacol Exp Ther* **328,** 951-962.

Steidl S, Cardiff KM & Wise RA. (2015). Increased latencies to initiate cocaine self-administration following laterodorsal tegmental nucleus lesions. *Behav Brain Res* **287,** 82-88.

Steidl S, Wang H & Wise RA. (2014). Lesions of cholinergic pedunculopontine tegmental nucleus neurons fail to affect cocaine or heroin self-administration or conditioned place preference in rats. *PLoS One* **9,** e84412.

Steidl S & Yeomans JS. (2009). M5 muscarinic receptor knockout mice show reduced morphine-induced locomotion but increased locomotion after cholinergic antagonism in the ventral tegmental area. *J Pharmacol Exp Ther* **328,** 263-275.

Stocker M. (2004). Ca(2+)-activated K+ channels: molecular determinants and function of the SK family. *Nat Rev Neurosci* **5,** 758-770.

Storch U, Forst AL, Pardatscher F, Erdogmus S, Philipp M, Gregoritza M, Mederos YSM & Gudermann T. (2017). Dynamic NHERF interaction with TRPC4/5 proteins is required for channel gating by diacylglycerol. *Proc Natl Acad Sci U S A* **114,** E37-E46.

Storch U, Forst AL, Philipp M, Gudermann T & Mederos y Schnitzler M. (2012). Transient receptor potential channel 1 (TRPC1) reduces calcium permeability in heteromeric channel complexes. *J Biol Chem* **287,** 3530-3540.

Strubing C, Krapivinsky G, Krapivinsky L & Clapham DE. (2001). TRPC1 and TRPC5 form a

novel cation channel in mammalian brain. *Neuron* **29,** 645-655.

Strubing C, Krapivinsky G, Krapivinsky L & Clapham DE. (2003). Formation of novel TRPC channels by complex subunit interactions in embryonic brain. *J Biol Chem* **278,** 39014-39019.

Su W, Song X & Ji JJ. (2010). Functional expression of a large-conductance Ca2+-activated K+ channel in mouse substantia nigra pars compacta dopaminergic neurons. *Neurosci Lett* **471,** 1-5.

Sun Y, Sukumaran P, Selvaraj S, Cilz NI, Schaar A, Lei S & Singh BB. (2018). TRPM2 Promotes Neurotoxin MPP(+)/MPTP-Induced Cell Death. *Mol Neurobiol* **55,** 409-420.

Sun Y, Sukumaran P & Singh BB. (2020). Magnesium-Induced Cell Survival Is Dependent on TRPM7 Expression and Function. *Mol Neurobiol* **57,** 528-538.

Sun Y, Zhang H, Selvaraj S, Sukumaran P, Lei S, Birnbaumer L & Singh BB. (2017). Inhibition of L-Type Ca(2+) Channels by TRPC1-STIM1 Complex Is Essential for the Protection of Dopaminergic Neurons. *J Neurosci* **37,** 3364-3377.

Swanson LW. (1982). The projections of the ventral tegmental area and adjacent regions: a combined fluorescent retrograde tracer and immunofluorescence study in the rat. *Brain Res Bull* **9,** 321-353.

Sylvester JB, Mwanjewe J & Grover AK. (2001). Transient receptor potential protein mRNA expression in rat substantia nigra. *Neurosci Lett* **300,** 83-86.

Szczypka MS, Kwok K, Brot MD, Marck BT, Matsumoto AM, Donahue BA & Palmiter RD. (2001). Dopamine production in the caudate putamen restores feeding in dopamine-deficient mice. *Neuron* **30,** 819-828.

Tai C, Hines DJ, Choi HB & MacVicar BA. (2011). Plasma membrane insertion of TRPC5 channels contributes to the cholinergic plateau potential in hippocampal CA1 pyramidal neurons. *Hippocampus* **21,** 958-967.

Takada M, Kang Y & Imanishi M. (2001). Immunohistochemical localization of voltage-gated calcium channels in substantia nigra dopamine neurons. *Eur J Neurosci* **13,** 757-762.

Takezawa R, Cheng H, Beck A, Ishikawa J, Launay P, Kubota H, Kinet JP, Fleig A, Yamada T & Penner R. (2006). A pyrazole derivative potently inhibits lymphocyte Ca2+ influx and cytokine production by facilitating transient receptor potential melastatin 4 channel activity. *Mol Pharmacol* **69,** 1413-1420.

Tan KR, Rudolph U & Luscher C. (2011). Hooked on benzodiazepines: GABAA receptor subtypes and addiction. *Trends Neurosci* **34,** 188-197.

Tang J, Lin Y, Zhang Z, Tikunova S, Birnbaumer L & Zhu MX. (2001). Identification of common binding sites for calmodulin and inositol 1,4,5-trisphosphate receptors on the carboxyl termini of trp channels. *J Biol Chem* **276,** 21303-21310.

Theile JW, Morikawa H, Gonzales RA & Morrisett RA. (2011). GABAergic transmission modulates ethanol excitation of ventral tegmental area dopamine neurons.

Neuroscience **172,** 94-103.

Thomsen M, Woldbye DP, Wortwein G, Fink-Jensen A, Wess J & Caine SB. (2005). Reduced cocaine self-administration in muscarinic M5 acetylcholine receptor-deficient mice. *J Neurosci* **25,** 8141-8149.

Tolu S, Eddine R, Marti F, David V, Graupner M, Pons S, Baudonnat M, Husson M, Besson M, Reperant C, Zemdegs J, Pages C, Hay YA, Lambolez B, Caboche J, Gutkin B, Gardier AM, Changeux JP, Faure P & Maskos U. (2013). Co-activation of VTA DA and GABA neurons mediates nicotine reinforcement. *Mol Psychiatry* **18,** 382-393.

Tozzi A, Bengtson CP, Longone P, Carignani C, Fusco FR, Bernardi G & Mercuri NB. (2003). Involvement of transient receptor potential-like channels in responses to mGluR-I activation in midbrain dopamine neurons. *Eur J Neurosci* **18,** 2133-2145.

Tracy ME, Tesic V, Stamenic TT, Joksimovic SM, Busquet N, Jevtovic-Todorovic V & Todorovic SM. (2018). CaV3.1 isoform of T-type calcium channels supports excitability of rat and mouse ventral tegmental area neurons. *Neuropharmacology* **135,** 343-354.

Trebak M, Lemonnier L, DeHaven WI, Wedel BJ, Bird GS & Putney JW, Jr. (2009). Complex functions of phosphatidylinositol 4,5-bisphosphate in regulation of TRPC5 cation channels. *Pflugers Arch* **457,** 757-769.

Tucker KR, Huertas MA, Horn JP, Canavier CC & Levitan ES. (2012). Pacemaker rate and depolarization block in nigral dopamine neurons: a somatic sodium channel balancing act. *J Neurosci* **32,** 14519-14531.

Tye KM, Mirzabekov JJ, Warden MR, Ferenczi EA, Tsai HC, Finkelstein J, Kim SY, Adhikari A, Thompson KR, Andalman AS, Gunaydin LA, Witten IB & Deisseroth K. (2013). Dopamine neurons modulate neural encoding and expression of depression-related behaviour. *Nature* **493,** 537-541.

Um KB, Hahn S, Kim SW, Lee YJ, Birnbaumer L, Kim HJ & Park MK. (2021). TRPC3 and NALCN channels drive pacemaking in substantia nigra dopaminergic neurons. *Elife* **10**.

Vandael DH, Marcantoni A, Mahapatra S, Caro A, Ruth P, Zuccotti A, Knipper M & Carbone E. (2010). Ca(v)1.3 and BK channels for timing and regulating cell firing. *Mol Neurobiol* **42,** 185-198.

Vandecasteele M, Deniau JM & Venance L. (2011). Spike frequency adaptation is developmentally regulated in substantia nigra pars compacta dopaminergic neurons. *Neuroscience* **192,** 1-10.

Vanderschuren LJ, Di Ciano P & Everitt BJ. (2005). Involvement of the dorsal striatum in cue-controlled cocaine seeking. *J Neurosci* **25,** 8665-8670.

Vazquez G, Wedel BJ, Trebak M, St John Bird G & Putney JW, Jr. (2003). Expression level of the canonical transient receptor potential 3 (TRPC3) channel determines its mechanism of activation. *J Biol Chem* **278,** 21649-21654.

Velasquez-Martinez MC, Vazquez-Torres R, Rojas LV, Sanabria P & Jimenez-Rivera CA. (2015).

Alpha-1 adrenoreceptors modulate GABA release onto ventral tegmental area dopamine neurons. *Neuropharmacology* **88,** 110-121.

Vilaro MT, Palacios JM & Mengod G. (1990). Localization of m5 muscarinic receptor mRNA in rat brain examined by in situ hybridization histochemistry. *Neurosci Lett* **114,** 154-159.

Volkow ND, Wise RA & Baler R. (2017). The dopamine motive system: implications for drug and food addiction. *Nat Rev Neurosci* **18,** 741-752.

Wanat MJ, Hopf FW, Stuber GD, Phillips PE & Bonci A. (2008). Corticotropin-releasing factor increases mouse ventral tegmental area dopamine neuron firing through a protein kinase C-dependent enhancement of Ih. *J Physiol* **586,** 2157-2170.

Wang H, Cheng X, Tian J, Xiao Y, Tian T, Xu F, Hong X & Zhu MX. (2020). TRPC channels: Structure, function, regulation and recent advances in small molecular probes. *Pharmacol Ther* **209,** 107497.

Wang HL & Morales M. (2009). Pedunculopontine and laterodorsal tegmental nuclei contain distinct populations of cholinergic, glutamatergic and GABAergic neurons in the rat. *Eur J Neurosci* **29,** 340-358.

Weiner DM, Levey AI & Brann MR. (1990). Expression of muscarinic acetylcholine and dopamine receptor mRNAs in rat basal ganglia. *Proc Natl Acad Sci U S A* **87,** 7050-7054.

Westerink BH, Kwint HF & deVries JB. (1996). The pharmacology of mesolimbic dopamine neurons: a dual-probe microdialysis study in the ventral tegmental area and nucleus accumbens of the rat brain. *J Neurosci* **16,** 2605-2611.

Willuhn I, Wanat MJ, Clark JJ & Phillips PE. (2010). Dopamine signaling in the nucleus accumbens of animals self-administering drugs of abuse. *Curr Top Behav Neurosci* **3,** 29-71.

Wise RA. (2009). Roles for nigrostriatal--not just mesocorticolimbic--dopamine in reward and addiction. *Trends Neurosci* **32,** 517-524.

Wise RA & Raptis L. (1986). Effects of naloxone and pimozide on initiation and maintenance measures of free feeding. *Brain Res* **368,** 62-68.

Wolfart J, Neuhoff H, Franz O & Roeper J. (2001). Differential expression of the small-conductance, calcium-activated potassium channel SK3 is critical for pacemaker control in dopaminergic midbrain neurons. *J Neurosci* **21,** 3443-3456.

Wolfart J & Roeper J. (2002). Selective coupling of T-type calcium channels to SK potassium channels prevents intrinsic bursting in dopaminergic midbrain neurons. *J Neurosci* **22,** 3404-3413.

Wooltorton JR, Pidoplichko VI, Broide RS & Dani JA. (2003). Differential desensitization and distribution of nicotinic acetylcholine receptor subtypes in midbrain dopamine areas. *J Neurosci* **23,** 3176-3185.

Xia YF, Margolis EB & Hjelmstad GO. (2010). Substance P inhibits GABAB receptor signalling in the ventral tegmental area. *J Physiol* **588,** 1541-1549.

Xiao C, Cho JR, Zhou C, Treweek JB, Chan K, McKinney SL, Yang B & Gradinaru V. (2016). Cholinergic Mesopontine Signals Govern Locomotion and Reward through Dissociable Midbrain Pathways. *Neuron* **90,** 333-347.

Xu SZ, Sukumar P, Zeng F, Li J, Jairaman A, English A, Naylor J, Ciurtin C, Majeed Y, Milligan CJ, Bahnasi YM, Al-Shawaf E, Porter KE, Jiang LH, Emery P, Sivaprasadarao A & Beech DJ. (2008). TRPC channel activation by extracellular thioredoxin. *Nature* **451,** 69-72.

Xue B, Li C, Chang X, Jiang H, Shi L & Xie J. (2020). Ghrelin Reduces A-Type Potassium Currents in Dopaminergic Nigral Neurons via the PLC/PKCdelta Pathway. *Neurosci Bull* **36,** 947-950.

Yan HD, Villalobos C & Andrade R. (2009). TRPC Channels Mediate a Muscarinic Receptor-Induced Afterdepolarization in Cerebral Cortex. *J Neurosci* **29,** 10038-10046.

Yang J, Xiao Y, Li L, He Q, Li M & Shu Y. (2019). Biophysical Properties of Somatic and Axonal Voltage-Gated Sodium Channels in Midbrain Dopaminergic Neurons. *Front Cell Neurosci* **13,** 317.

You ZB, Wang B, Zitzman D & Wise RA. (2008). Acetylcholine release in the mesocorticolimbic dopamine system during cocaine seeking: conditioned and unconditioned contributions to reward and motivation. *J Neurosci* **28,** 9021-9029.

Yu FH & Catterall WA. (2004). The VGL-chanome: a protein superfamily specialized for electrical signaling and ionic homeostasis. *Sci STKE* **2004,** re15.

Yuan JP, Zeng W, Huang GN, Worley PF & Muallem S. (2007). STIM1 heteromultimerizes TRPC channels to determine their function as store-operated channels. *Nat Cell Biol* **9,** 636-645.

Yuhas WA & Fuchs PA. (1999). Apamin-sensitive, small-conductance, calcium-activated potassium channels mediate cholinergic inhibition of chick auditory hair cells. *J Comp Physiol A* **185,** 455-462.

Zagranichnaya TK, Wu X & Villereal ML. (2005). Endogenous TRPC1, TRPC3, and TRPC7 proteins combine to form native store-operated channels in HEK-293 cells. *J Biol Chem* **280,** 29559-29569.

Zeng C, Tian F & Xiao B. (2016). TRPC Channels: Prominent Candidates of Underlying Mechanism in Neuropsychiatric Diseases. *Mol Neurobiol* **53,** 631-647.

Zhang J, Chiodo LA & Freeman AS. (1994). Influence of excitatory amino acid receptor subtypes on the electrophysiological activity of dopaminergic and nondopaminergic neurons in rat substantia nigra. *J Pharmacol Exp Ther* **269,** 313-321.

Zhang L, Liu Y & Chen X. (2005). Carbachol induces burst firing of dopamine cells in the ventral tegmental area by promoting calcium entry through L-type channels in the rat. *J Physiol* **568,** 469-481.

Zhang W, Yamada M, Gomeza J, Basile AS & Wess J. (2002). Multiple muscarinic acetylcholine receptor subtypes modulate striatal dopamine release, as studied with M1-M5 muscarinic receptor knock-out mice. *J Neurosci* **22,** 6347-6352.

Zhang Z, Reboreda A, Alonso A, Barker PA & Seguela P. (2011). TRPC channels underlie cholinergic plateau potentials and persistent activity in entorhinal cortex. *Hippocampus* **21,** 386-397.

Zhang Z, Tang J, Tikunova S, Johnson JD, Chen Z, Qin N, Dietrich A, Stefani E, Birnbaumer L & Zhu MX. (2001). Activation of Trp3 by inositol 1,4,5-trisphosphate receptors through displacement of inhibitory calmodulin from a common binding domain. *Proc Natl Acad Sci U S A* **98,** 3168-3173.

Zheng J. (2013). Molecular mechanism of TRP channels. *Compr Physiol* **3,** 221-242.

Zholos AV. (2014). Trpc5. *Handb Exp Pharmacol* **222,** 129-156.

Zhou QY & Palmiter RD. (1995). Dopamine-deficient mice are severely hypoactive, adipsic, and aphagic. *Cell* **83,** 1197-1209.

Zhu MH, Chae M, Kim HJ, Lee YM, Kim MJ, Jin NG, Yang DK, So I & Kim KW. (2005). Desensitization of canonical transient receptor potential channel 5 by protein kinase C. *Am J Physiol Cell Physiol* **289,** C591-600.

Zhu X, Ottenheimer D & DiLeone RJ. (2016). Activity of D1/2 Receptor Expressing Neurons in the Nucleus Accumbens Regulates Running, Locomotion, and Food Intake. *Front Behav Neurosci* **10,** 66.

Zitt C, Zobel A, Obukhov AG, Harteneck C, Kalkbrenner F, Luckhoff A & Schultz G. (1996). Cloning and functional expression of a human Ca2+-permeable cation channel activated by calcium store depletion. *Neuron* **16,** 1189-1196.

Zwart R & Vijverberg HP. (1997). Potentiation and inhibition of neuronal nicotinic receptors by atropine: competitive and noncompetitive effects. *Mol Pharmacol* **52,** 886-895.

Zweifel LS, Parker JG, Lobb CJ, Rainwater A, Wall VZ, Fadok JP, Darvas M, Kim MJ, Mizumori SJ, Paladini CA, Phillips PE & Palmiter RD. (2009). Disruption of NMDAR-dependent burst firing by dopamine neurons provides selective assessment of phasic dopamine-dependent behavior. *Proc Natl Acad Sci U S A* **106,** 7281-7288.

CURRICULUM VITAE

"Rita" Yu-Tzu Chen (Ph.D. Student)

PERSONAL INFORMATION

Date and place of birth: November 19, 1991, Taipei, Taiwan
Institute name: Virginia Commonwealth University
Address: VCU School of Medicine
Rm 3-038, 1101 E. Marshall St.
Richmond, VA 23298-0551
Phone: (804) 874-1523
E-mail: chenr6@vcu.edu; ritachen@uwalumni.com

EDUCATION

2016 – present   **Ph.D. student in Neuroscience**
Virginia Commonwealth University, Richmond, Virginia, USA
Advisor: Jose M. Eltit, Ph.D.
Co-advisor: A. Rory McQuiston, Ph.D.

Relevant coursework: Cellular and Molecular Neuroscience, Systems Neuroscience, Biochemistry, Ion Channels in Membranes, Principles of Pharmacology, Cellular Signaling

2010 – 2014   **B.Sc. in Biology, honors in research**
University of Wisconsin-Madison, Madison, Wisconsin, USA

RESEARCH EXPERIENCES

2017 – present   **Ph.D. dissertation research**

Electrophysiological characterization of muscarinic excitation of VTA dopaminergic neurons
(PI: Jose M. Eltit, Ph.D., Virginia Commonwealth University, Richmond, VA)
This project aims to identify new molecular mechanisms involved in the regulation of ventral tegmental area (VTA) dopaminergic (DA) neuron excitability downstream of cholinergic signaling, which promotes reward and motivational behaviors. Whole-cell and cell-attached patch-clamp experiments are performed on mouse acute brain slices to determine the effects of muscarinic agonism and antagonism on the intrinsic membrane properties, firing patterns, action potential kinetics, and synaptic inputs in VTA DA neurons. The pharmacology of the muscarinic receptor-induced current is also being characterized.

2016 – 2017   **Ph.D. laboratory rotations and other lab experiences**

Identification of novel dopamine and serotonin transporter bivalent inhibitors
(PI: Jose M. Eltit, Ph.D., Virginia Commonwealth University, Richmond, VA)
This project was to determine the *in vitro* efficacy of novel bivalent inhibitors of the dopamine and serotonin transporters, which are targets of psychostimulants and antidepressants. Fluorescent calcium imaging assay was performed on a HEK293 cell system co-expressing

the monoamine transporters and voltage-gated calcium channels. Dose-response relationships were determined by as the inhibition efficacy of transporter-mediated inward current and depolarization-induced calcium entry.

2015 – 2016   Laboratory technician

Spreading depression enhances gliotransmission to hippocampal neurons
(PI: Ning Zhou, Ph.D., China Medical University, Taichung, Taiwan)
This project was to investigate the role of gliotransmission in the pathogenesis of spreading depression (SD). SD was induced in a mouse acute brain slice model. Whole-cell patch-clamp was used to record NMDAR-mediated currents in hippocampal neurons and dialyze astrocytes with calcium-chelating agents with the aim to determine the relationship between astrocytic calcium oscillations and SD-induced neuronal hyperexcitability.

2012 – 2014   Undergraduate independent research

Production and purification of Manduca juvenile hormone binding protein (JHBP)
(PI: Walter G. Goodman, Ph.D., University of Wisconsin-Madison, Madison, WI)
This project was to establish and standardize a protein production and purification protocol for the hemolymph JHBP of the moth *Manduca sexta* through a bacterial expression system. The insect protein was expressed in *E. coli* culture, purified using affinity chromatography, and detected with Western blotting. The goal was to artificially produce JHBP for future studies on insect endocrinology and pest control.

HONORS & AWARDS

2021   Charles C. Clayton Award, School of Medicine, Virginia Commonwealth University

2021   Robert W. Ramsey Departmental Award, Department of Physiology & Biophysics, Virginia Commonwealth University

2014   Graduated with Honors Degree, Dean's List (7 semesters), University of Wisconsin-Madison

2013   Hilldale Undergraduate/Faculty Research Fellowships, University of Wisconsin-Madison

PUBLICATIONS

1. Ruchala, I., Battisti, U.M., Nguyen, V.T., **Chen, R.Y.**, Glennon, R.A., Eltit, J.M. (2021). Functional characterization of N-octyl-4-methylamphetamine variants and related bivalent compounds at the dopamine and serotonin transporters using Ca^{2+} channels as sensors. *Toxicology and Applied Pharmacology, 419,* 115513. DOI: 10.1016/j.taap.2021.115513.

2. Bagdas, D., Jackson, A., Carper, M., **Chen, R.Y.**, Akinola, L.S., & Damaj, M.I. (2020). Impact of menthol on nicotine intake and preference in mice: Concentration, sex, and age differences. *Neuropharmacology*, 108274. DOI:10.1016/j.neuropharm.2020.108274.

3. Wu, D.C., **Chen, R.Y.**, Cheng, T.C., Chiang, Y.C., Shen, M.L., Hsu, L.L., Zhou, N. (2018). Spreading depression promotes astrocytic calcium oscillations and enhances gliotransmission to hippocampal neurons. *Cerebral Cortex, 28(9),* 3204-3216. DOI: 10.1093/cercor/bhx192.

4. Shen, M.L., Wang, C.H., **Chen, R.Y.**, Zhou, N., Kao, S.T., Wu, D.C. (2016). Luteolin inhibits GABAA receptors in HEK cells and brain slices. *Scientific Reports, 6,* 27695. DOI: 10.1038/srep27695.

CONFERENCE PRESENTATIONS

Chen, R.Y., Eltit, J.M., McQuiston, A.R. Electrophysiological characterization of muscarinic excitation of dopamine neurons in the ventral tegmental area. Society for Neuroscience, Global Connectome Virtual Conference, 2021.

PROFESSIONAL AFFILIATIONS

Society for Neuroscience (SfN)

COMMUNITY OUTREACH

Science blogging: writing scientific commentaries on a wide range of neuroscience and physiology topics and posting biweekly on social media for a popular audience.

Neuroscience outreach: leading hand-on activities and giving oral presentations to local middle and high school students with the VCU Neuroscience Interest Group.

Entomology outreach: assisting at booths sponsored by entomology labs, handling live insects, and educating the public at both UW-Madison and VCU.